The receptor guanylyl cyclase Npr2 regulates the bifurcation of cranial sensory axons

Inaugural-Dissertation
to obtain the academic degree
Doctor rerum naturalium (Dr. rer. nat.)

Submitted to the Department of Biology, Chemistry and Pharmacy
of Freie Universität Berlin

by

Gohar Ter-Avetisyan

from Gyumri, Armenia

Berlin, 2013

This thesis was prepared between July 2009 and November 2012 at the Max Delbrück Center for Molecular Medicine, Department of Developmental Neurobiology, under the supervision of Prof. Dr. Fritz G. Rathjen.

1st Reviewer: Prof. Dr. Fritz G. Rathjen

2nd Reviewer: Prof. Dr. Carmen Birchmeier-Kohler

Disputation on __06.02.2013__

In honor of my grandparents

Hakob Ter-Avetisyan

Zina Ter-Avetisyan

Hovhannes Manukyan

Kalipse Manukyan

Acknowledgments

Իմ կարոտած սրտի համար ո՛չ մի ուրիշ հեքիաթ չկա .

Նարեկացու, Քուչակի պես լուսապսակ ճակատ չկա .

Աշխա՛րհի անցի՛ր, Արարատի նման ճերմակ զագաթ չկա .

Ինչպես անհաս փառքի ճամփա՝ Ես իմ Մասիս սա՛րն եմ սիրում .

Եղիշե Չարենց

Table of Contents

List of Abbreviations

aa	amino acid
ANP	arterial natriuretic peptide
AON	anterior olfactory nucleus
AP	alkaline phosphatase
APS	ammonium persulfate
ATP	adenosine-5'-triphosphate
B	bone
BABB	benzyl alcohol/benzyl benzoate
BAC	bacterial artificial chromosome
Bc	basicranium
BCIP	5-bromo-4-chloro-3-indolyl phosphate p-toluidine salt
β-gal	β-galactosidase
BNP	brain natriuretic peptide
bp	base pairs
Bq	becquerel
BSA	bovine serum albumin
Cb	cerebellum
CD	catalytic domain
CHAPS	3[(3-cholamidopropyl)dimethylammonio]-propanesulfonate
cGKI	cGMP-dependent kinase I
cGMP	cyclic guanosine monophosphate
cn	autosomal recessive gene for achondroplasia
CNP	C-type natriuretic peptide
CNS	central nervous system
CPd	cerebral peduncle
Cre	cyclization recombination
CRMP2	collapsin response mediator protein 2
DAB	3,3'-diaminobenzidine
DAPI	4',6-diamidino-2-phenylindole
dCTP	deoxycytidine triphosphate
DD	dimerization domain
ddH$_2$0	distilled deionized water
DG	dentate gyrus
DMEM	Dulbecco`s modified Eagle medium

DMF	dimethylformamide
DMSO	dimethyl sulfoxide
DNA	deoxyribonucleic acid
dNTPs	deoxyribonucleoside triphosphates
DPa	dental papilla
DREZ	dorsal root entry zone
DRG	dorsal root ganglion/ganglia
E	embryonic day
E.coli	Escherichia coli
EDTA	ethylenediaminetetraacetic acid
eGFP	enhanced green fluorescent protein
EGTA	ethylene glycol tetraacetic acid
ERT2	estrogen receptor T2
ES	embryonic stem
EtBr	ethidium bromide
Ey	eye
FCS	fetal calf serum
Flp	flippase
FRT	flippase recognition target
g	ganglion
gcFL	granule cell layer of flocculus
gSC	genomic subclone
GSK-3	glycogen synthase kinase 3
GTP	guanosinetriphosphate
G418	geneticin
gV	trigeminal ganglion
Hb	hindbrain
Hbl	habenula
het	heterozygous
Hi	hippocampus
hPLAP	human placental alkaline phosphatase
HRP	horseradish peroxidase
Hsp90	heat shock protein 90
inf	inferior
Kan	kanamycin
kb	kilobase pairs

kDa	kilodalton
KHD	kinase homology domain
KIF2A	kinesin heavy chain member 2A
KO	knockout
LB	lysogeny broth
LBD	ligand binding domain
LIF	leukemia inhibitory factor
loxP	locus of crossover [x] in P1
LTN	lateral tegmental nucleus
MAP1b	microtubule-associated protein 1b
MB	mammilary body
MCPd	middle cerebellar peduncle
Me	mesencephalon
MeT	mesencephalic tegmentum
mGFP	membrane-tethered axonally transported form of GFP
MHb	midbrain-hindbrain boundary
MNTN	mesencephalic nucleus of trigeminal nerve
MOPS	3-(N-morpholino) propanesulfonic acid
MSN	medial septal nucleus
MTN	mesencephalic trigeminal nucleus
NBT	nitro-blue tetrazolium chloride
NC	nasal cavity
Neo	neomycin
NF-M	neurofilament-M
NFN	nucleus of facial nerve
NLS	nuclear localization sequence
Npr1,2,3	natriuretic peptide receptor 1,2,3
NP-40	nonidet P-40
NS	nasal septum
OD	optical density
OE	olfactory epithelium
OHT	4-hydroxytamoxifen
P	postnatal day
pBlu	pBluescript II SK+ (SacI->KpnI polylinker orientation)
PBS	phosphate buffered saline
PCR	polymerase chain reaction

pDTA	plasmid diptheria toxin A
PFA	paraformaldehyde
PMSF	phenylmethylsulfonyl fluoride
PN	pontine nuclei
rec	recombinant
RT	room temperature
SC	spinal cord
SCPd	superior cerebellar peduncle
SDS-PAGE	sodium dodecyl sulfate - polyacrylamide gel electrophoresis
SOB	super optimal broth
SOC	super optimal broth with catabolic repressor
SSC	saline-sodium citrate
sup	superior
TAE	tris-acetate-EDTA
TBS	tris-buffered saline
TEMED	N',N'-tetramethylendiamine
TFB	transformation buffer
TMD	transmembrane domain
TN	thamalic nulei
Tris	tris(hydroxymethyl)aminomethane
UV	ultraviolet
V	volt
VN	vestibular nuclei
v/v	volume/volume
VTN	ventral tegmental nucleus
WGA	wheat germ agglutinin
wt	wildtype
w/v	weight/volume
X-Gal	5-bromo-4-chloro-indolyl-β-D-galactopyranoside
Z/AP	lacZ/human placental alkaline phosphatase
^{32}P	phosphorous 32
8-pCPT-cGMP	8-(4-chlorophenylthio) guanosine-3', 5'-cyclic monophosphate

Abstract

Axonal branching is a key mechanism to form complex circuits in the mature nervous system. Depending on their functions, axons can branch extensively to send information to their distinct targets and establish a unique pattern of connectivity. However, signaling mechanisms regulating axonal branching during the development of the nervous system are still poorly understood.

The cGMP signaling pathway including the secreted C-type natriuretic peptide (CNP), its receptor natriuretic peptide receptor 2 (Npr2) and the cGMP-dependent protein kinase Iα (cGKIα) has been shown to control the bifurcation of DRG (dorsal root ganglion) sensory neurons within the spinal cord. Using mutant mouse models it has been demonstrated that in the absence of one of these components, the sensory axons are unable to bifurcate at the entry zone of the spinal cord.

Based on these findings, it is intriguing to ask whether other neuronal subpopulations besides the DRG neurons exist and if they use the above mentioned cGMP signaling pathway to form branches emerging from the bifurcating growth cone.

To investigate the role of Npr2-dependent axonal branching in other neural systems than DRG neurons, a genetic strategy was used and two mouse models (Npr2LacZ and Npr2CreERT2) were generated, which allow studies on the expression pattern of Npr2 and its influence on axonal branching of single Npr2-expressing axons in the mouse nervous system. While the Npr2LacZ reporter mouse enabled detailed analysis of the localization of the signaling pathway components, the Npr2CreERT2 mouse is a valuable tool for visualizing single axonal projections after crossing with reporter strains.

A prominent Npr2 expression was found not only in the DRG, but also in the cranial sensory ganglia of the developing mouse. Using immunohistochemistry, a co-localization of the receptor Npr2 and the kinase cGKIα was detected in neurons of cranial sensory ganglia. To follow the single projections of sensory axons from cranial sensory ganglia and study their branching behavior, the Npr2CreERT2 mouse was crossed with two different reporter strains (Z/AP and mGFP). After induction of Cre recombinase with tamoxifen or 4-hydroxytamoxifen at embryonic day 9.5 or 10.5, single axonal projections could be visualized at embryonic day 12.5 or 13.5, respectively. This genetic approach uncovered two new aspects about central projections of cranial sensory ganglia: (i) almost all central projections of cranial sensory ganglia bifurcate at the entry zone of the hindbrain and (ii) in the absence of Npr2 the sensory axons lose their bifurcational behavior when entering the hindbrain. Hence, the neurons of all cranial sensory ganglia - similar to DRG neurons - use cGMP signaling to bifurcate as soon as they enter the hindbrain.

Zusammenfassung

Die axonale Verzweigung ist ein wichtiger Mechanismus, um die komplexen Verschaltungen des Nervensystems zu bilden. Je nach ihrer Funktion können sich Axone weitläufig verzweigen, um die Informationen an ihre verschiedenen Ziele zu senden und ein einzigartiges Muster der Verschaltung zu etablieren. Allerdings sind die Signalmechanismen, die die axonale Verzweigung während der Entwicklung des Nervensystems regulieren, noch weitgehend unverstanden. Ein cGMP-Signalweg kontrolliert die Bifurkation der sensorischen DRG-Neurone (Dorsal root ganglia; Spinalganglien) im Rückenmark und besteht aus folgenden Komponenten: dem C-Typ natriuretischen Peptid (CNP), dem natriuretischen Peptid-Rezeptor-2 (Npr2) und der cGMP-abhängigen Proteinkinase Iα (cGKIα). In Mausmodellen konnte gezeigt werden, dass in Abwesenheit einer dieser Komponenten die sensorischen DRG-Neurone an der Eintrittszone des Rückenmarks nicht bifurkieren. Offen ist, ob es neben den DRG-Neuronen andere neuronale Subpopulationen gibt, die den cGMP-Signalweg im Rahmen der axonalen Verzweigung nutzen. Um die Rolle der Npr2-abhängigen axonalen Verzweigung in anderen Systemen als DRG-Neuronen zu untersuchen, wurden zwei transgene knock-in-Mausmodelle (Npr2LacZ und Npr2CreERT2) generiert, die es erlauben, das Expressionsmuster von Npr2 und die axonale Verzweigung einzelner Npr2-exprimierender Axone in der Maus zu studieren. Während die Npr2LacZ-Reportermaus es ermöglichte, eine detaillierte Analyse der Lokalisation der cGMP-Komponenten durchzuführen, stellte die Npr2CreERT2-Maus nach Kreuzung mit Reporter-Stämmen (Z/AP und mGFP) ein wertvolles Werkzeug für die Visualisierung einzelner axonaler Verzweigungen dar. Eine starke Npr2-Expression wurde nicht nur in den DRG-Neuronen gefunden, sondern auch in den kranialen sensorischen Ganglien. In Neuronen der kranialen sensorischen Ganglien wurde immunhistochemisch eine Ko-Expression des Rezeptors Npr2 und der Kinase cGKIα detektiert. Um das Bifurkationsverhalten einzelner Axone der kranialen sensorischen Neurone zu verfolgen, wurde die Npr2CreERT2-Maus mit den zwei Reporter-Stämmen gekreuzt. Nach Induktion der Cre-Rekombinase mit Tamoxifen am embryonalen Tag 9.5 bzw. 10.5 konnten einzelne axonalen Verweigungen am embryonalen Tag 12.5 bzw. 13.5 visualisiert werden. Dieser genetische Ansatz deckte zwei neue Aspekte der axonalen Bifurkation auf: (i) fast alle zentralen Projektionen der kranialen sensorischen Axone verzweigen an der Eingangszone des Hinterhirns und (ii) in Abwesenheit von Npr2 verlieren die sensorischen Axone ihre Fähigkeit beim Eintritt ins Hinterhirn zu bifurkieren. Zusammenfassend zeigen diese Untersuchungen, dass die kranialen sensorischen Neurone den cGMP-Signalweg nutzen, um beim Erreichen des Hinterhirns zu bifurkieren.

1. Introduction

1.1 Axonal pathfinding

The mature nervous system is composed of a complex web of entangled neuronal circuits framed by axonal and dendritic arbors. In 1890 Ramón y Cajal has visualized for the first time the complexity of the neuron arborization and recognized the growth cone as important structure in axon pathfinding to targets (Garcia-Marin et al. 2009). This key feature of the developing axons to outgrow in a directed manner is crucial for functionality of the nerves and neuronal networks. In the last three decades the molecular mechanisms involved in axonal outgrowth and morphology have been extensively studied. Numerous *in vitro* and *in vivo* studies have been performed revealing that the growth cone responds to the environmental cues and control the growth cone guidance. The identification of guidance factors opened a broad field of study on signaling cascades underlying growth cone motility and axon guidance. Guidance factors can promote attraction and repulsion resulting in growth cone protrusion or collapse (Tessier-Lavigne and Goodman 1996). The chemoattractive and chemorepulsive functionality of the guidance factors is specific for a particular axon population. Guidance factors are not specialized for one mechanism and can have different effects dependent on their functional context. Netrins, for example, were first identified as chemoattractive guidance factors for the commissural axons in the floor plate of the spinal cord (Kennedy et al. 1994; Tessier-Lavigne et al. 1988). However, later it was shown that they can also serve as chemorepulsive guidance factors for the trochlear motor axons (Colamarino and Tessier-Lavigne 1995). It is widely accepted that specific guidance factors mediate cytoskeleton rearrangements in order to steer the growth cone to its target region (Dent and Gertler 2003; Huber et al. 2003; Lowery and Van 2009).

The axonal outgrowth and pathfinding behavior includes axonal branching. Axons form branches to innervate multiple targets and almost all axons branch in specific target locations to reach their destinations in different regions of the nervous system (Acebes and Ferrus 2000; Gibson and Ma 2011; Schmidt and Rathjen 2010; Ter-Avetisyan et al. 2012). The interrelation of guidance factors and axonal branching conduce to the establishment of the precise patterns of neuronal connectivity, since its geometry influences the functional properties of neurons. Over the past decades, cellular mechanisms and molecular signaling pathways underlying the axonal pathfinding were characterized in various studies. However, the detailed molecular mechanisms required for both correct axon navigation during development and formation of axonal branches remain poorly understood.

1.2 Axonal branching

During development axons form branches allowing them to reach multiple targets, establish synaptic contacts and assemble neuronal networks with defined innervation patterns. There are at least three modes of axonal branching (Figure 1.1) : (i) bifurcation of a growth cone by cytoskeletal reorganization and splitting of the outgrowing growth cone resulting in the formation of the second active growth cone, (ii) collateral branching, also referred to as interstitial branching in which the neuron initially extends an axon to reach its primary target and then projects collaterals along the axon shaft to innervate secondary targets and (iii) axonal branching in the termination zone generated by the growth cone or by the axon segment adjacent to the growth cone.
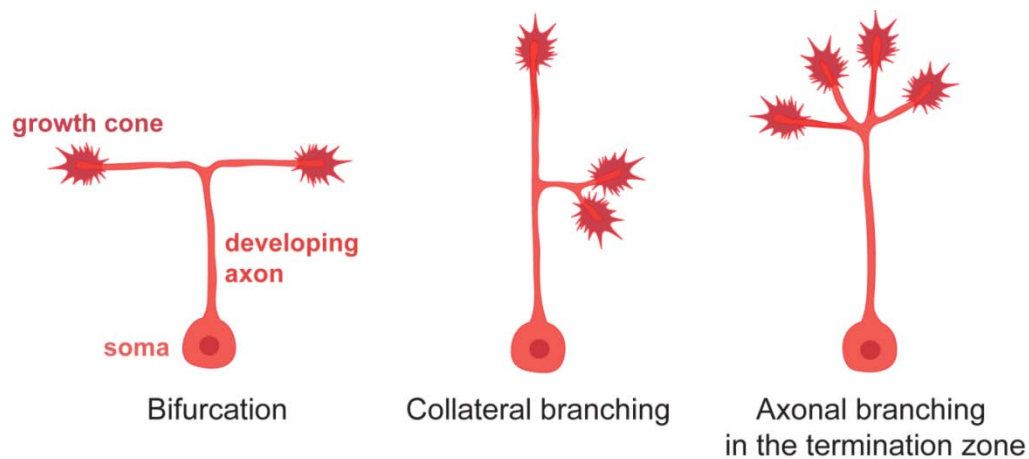
Figure 1.1: Three axonal branching modes: (i) branching initiated by the bifurcating growth cone (ii) collateral branching, also termed interstitial branching, initiated at the axon shaft and (iii) axonal branching at the termination zone initiated by the growth cone or by the axon segment adjacent to the growth cone. Adapted from (Ter-Avetisyan et al. 2012).

Investigations on corticospinal and thalamocortical axons have shown that interstitial branching mediated by axon shaft is the dominating branching mode (Bastmeyer and O'Leary 1996; Heffner et al. 1990; O'Leary and Terashima 1988; Portera-Cailliau et al. 2005). Although different modes of axonal branching have been identified, the underlying mechanisms remain unclear.

The highly dynamic growth cone rapidly responds to extracellular and intracellular cues. The identification of extrinsic and intrinsic factors controlling axonal branching was essential for the understanding of the formation of neuronal circuits. Known branching factors comprise the neurotrophins (Cohen-Cory and Fraser 1995), semaphorins (Bagri et al. 2003), ephrins (O'Leary and McLaughlin, 2005), slit2 (Wang et al. 1999), secreted glycoprotein Wnt (Bodmer et al. 2009), cell-adhesion molecules (Colavita and Tessier-Lavigne 2003; Zhu and Luo 2004) and the extracellular matrix protein anosmin-1 (Gianola et al. 2009). Besides these extrinsic regulators of axonal branching, a number of

intracellular factors have been identified. These include members of the Rho family of GTPases as well as several microtubule-associated proteins like KIF2A, MAP1b, CRMP2 and the E3 ubiquitin ligase Nedd4 (Bouquet et al. 2004; Drinjakovic et al. 2010; Govek et al. 2011; Hall and Lalli 2010; Homma et al. 2003; Kawabe et al. 2010). In addition, transcription factors like Pea3 and Er81 have been shown to be involved in axonal branching (Dasen 2009). Other factors, which affect the axonal branch formation include neuronal activity (Ruthazer et al. 2003) and injuries (Dancause et al. 2005). Whereas *in vitro* experiments can shed light on molecules affecting axonal branching morphology (Gallo 2011), *in vivo* studies are instrumental for the understanding of molecular mechanisms underlying axonal branching (Schmidt and Rathjen 2010).

1.3 Axonal projections of dorsal root ganglion (DRG) neurons

The sensory neurons of DRG convey the sensory information from the periphery to the central nervous system (CNS). Their cell bodies reside in dorsal root ganglia. The DRG sensory neurons project their axons into the spinal cord where they constitute most likely the simplest axonal branching, which is easily accessible. The simplicity and accessibility of the axonal branching in the spinal cord allows examination of axonal projections as well as investigation of regulatory and developmental processes conducting the axonal branching.

In mammals the central projections of DRG neurons extend via the dorsal root toward the dorsal root entry zone (DREZ) of the spinal cord. In mice the first axons arrive at the DREZ at around embryonic day 10 (E10). DRG axons then bifurcate into two arms in a manner of a **T** or **Y** and without penetrating the dorsal mantle layer, extend their two branches in caudal and rostral directions over several segments within the dorsal funiculus. By embryonic day 12.5 the first collateral branches sprout from the stem axons to penetrate the mantle layer (Ozaki and Snider 1997). Finally, collaterals terminate in distinct laminae of the spinal cord where they further branch out to establish specific synaptic contacts (Figure 1.2).

Depending on their termination zone and sensory specification, DRG neurons are classified as nociceptive, mechanoreceptive and proprioceptive neurons (Marmigere and Ernfors 2007). Nociceptive and mechanoreceptive collaterals terminate in the dorsal spinal cord while proprioceptive collaterals end on motor neurons in the ventral spinal cord (Figure 1.2). The formation of collateral axon branches and the growing towards a precise target region has been subject of intense studies. However, the underlying molecular mechanisms are not fully understood. Since the three types of axonal branching in the

spinal cord are spatiotemporally separated, they are easily accessible and represent an ideal system for a molecular analysis.
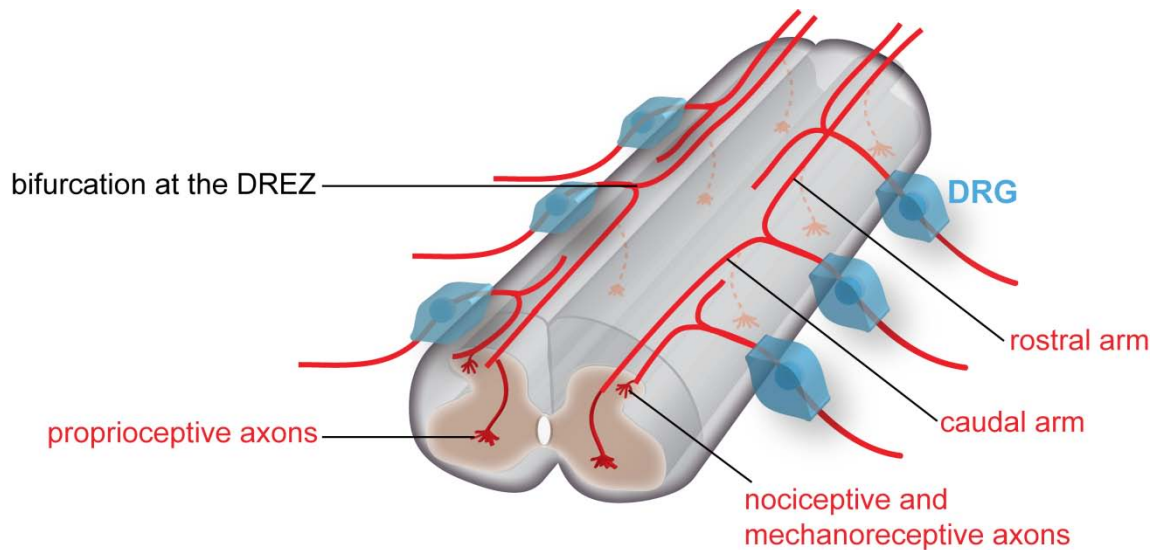
Figure 1.2: Scheme of the three branching modes of DRG axons within the spinal cord. An axon of a DRG neuron enters the spinal cord at the DREZ where it bifurcates into two daughter axons resulting in longitudinally growing rostral or caudal arms. Collaterals are then generated from these stem axons that terminate in the dorsal or ventral sublaminae of the spinal cord where terminal arbors are formed. Nociceptive and mechanoreceptive axons terminate in dorsal layers, while proprioceptive axons end on motor neurons in the ventral part of the spinal cord. Adapted from (Ter-Avetisyan et al. 2012). DREZ, dorsal root entry zone; DRG, dorsal root ganglion.

1.4 The cGMP-dependent signaling pathway in axonal branching

Previous investigations on axonal projections of DRG sensory neurons have demonstrated a strong expression of cGMP-dependent kinase I (cGKI) at the DREZ of the spinal cord indicating an involvement of cGKI in the bifurcation mode of axonal branching (Schmidt et al. 2002). It was furthermore shown that only one of the two known forms of cGKI (Hofmann et al. 2009), the α-form is expressed in DRG sensory axons (Schmidt et al. 2002). Using the cGKI-deficient mice and labeling individual DRG neurons with the lipophilic tracer DiI, it was shown that in the absence of cGKIα the branching of sensory DRG axons is impaired: all sensory axons turn without bifurcation only either in caudal or rostral direction, while a small percentage of axons directly enters the gray matter growing towards the central canal (Schmidt et al. 2007; Schmidt et al. 2002; Zhao et al. 2009).

The identification of the cGMP and its kinase cGKIα as essential factors for axonal branching yielded the finding of the protein, which is responsible for the generation of cGMP in embryonic DRG during development: the guanylyl cyclase natriuretic peptide receptor 2 (Npr2; also termed Npr-B or GC-B) (Schmidt et al. 2007). Mice carrying a spontaneous loss-of-function mutation in the Npr2 gene demonstrated an impaired axonal

bifurcation identical to that observed in cGKI-deficient mice. Thus, Npr2 is another significant factor besides the cGMP and its kinase cGKIα that enables the sensory DRG neurons to bifurcate at the DREZ. Further investigations on this signaling pathway led to the identification of the Npr2 ligand, which induces bifurcation: the C-type natriuretic peptide (CNP) (Schmidt et al. 2009; Zhao and Ma 2009). Schmidt et al. have generated a CNP-deficient mouse strain with a LacZ reporter cassette insertion. Using the CNPLacZ mice, the expression pattern of CNP was determined in the developing nervous system and its role in sensory axon bifurcation was elucidated by DiI-labeling of DRG sensory axons. As already seen in the mouse models with knockout cGKI and spontaneous loss-of-function mutation in the Npr2 gene, the sensory axons in CNP knockout mice are not able to bifurcate and make turns in one direction, instead (Figure 1.3).
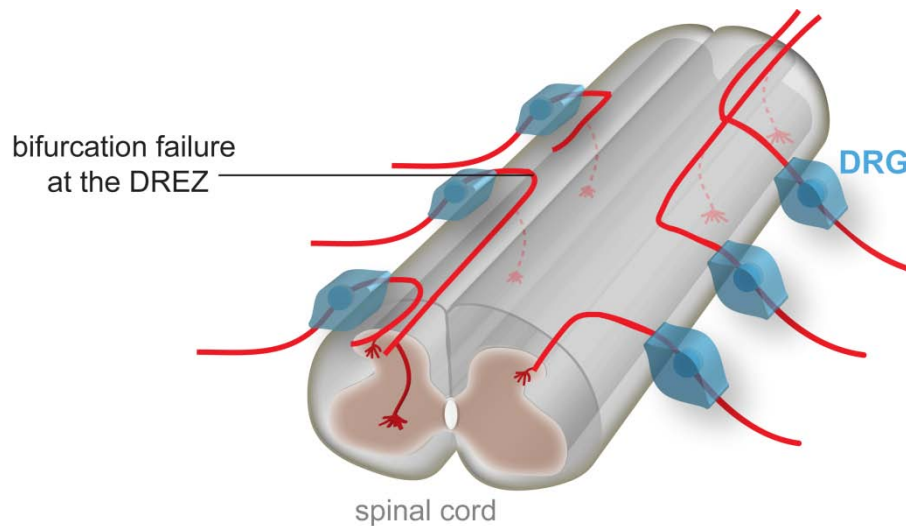
Figure 1.3: Schematic representation of the branching errors in the absence of cGMP signaling within the spinal cord. Sensory axons form only turns in the absence of C-type natriuretic peptide (CNP), Natriuretic peptide receptor 2 (Npr2) or cGMP-dependent kinase Iα (cGKIα) and do not bifurcate. Adapted from (Ter-Avetisyan et al. 2012).

Currently, three components of this signaling cascade are known to be important for sensory axon branching at the DREZ of the spinal cord (Figure 1.2). CNP, which is released by precursor cells and neurons of the dorsal horn, activates Npr2 on the growth cones of incoming sensory axons. Activation of Npr2 causes the generation of cGMP from GTP in the sensory neurons. cGMP then activates cGKIα, which thereupon phosphorylates serine or threonine residues in so far unknown intracellular targets. In the absence of either CNP, Npr2 or cGKIα sensory axons are unable to bifurcation at the DREZ, suggesting that these components act together in a signaling cascade (Figure 1.4).
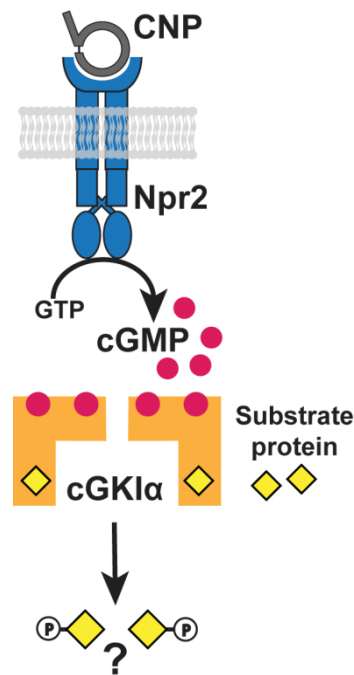
Figure 1.4: Schematic representation of the CNP-Npr2-cGKIα signaling pathway: the binding of CNP by the particulate guanylyl cyclase Npr2 results in the generation of cGMP from GTP through the intracellular guanylyl cyclase domain of Npr2. The second messenger cGMP activates cGKIα, which elicits the phosphorylation of its hitherto unknown substrates.

To understand the cell biology of the branching process and to broaden the knowledge of cGMP signaling, it is important to characterize the phosphorylation target(s) of cGKIα. Axonal branching involves the rearrangement of cytoskeletal structures including reorganization of actin assembly, microtubule polymerization and microtubule transport (Acebes and Ferrus 2000; Baas et al. 2006; Dent and Kalil 2001). Regulators of actin and microtubule dynamics are therefore essential for axonal branching.

Glycogen synthase kinase-3 (GSK-3) with its two isoforms GSK-3α and GSK-3β is a well-known regulator involved in axonal growth and branching (Garrido et al. 2007; Kim et al. 2011). It regulates microtubule assembly by phosphorylating cytoskeletal proteins such as Tau, microtubule-associated protein (MAP1b), collapse-response mediator protein 2 (CRMP2), CLIP-associated proteins (CLASP), adenomatous polyposis coli (APC) and stathmin (Hur and Zhou 2010; Kim et al. 2006; Kumar et al. 2009; Moreno and Avila 1998). *In vitro* studies on cultured rat DRG neurons have shown that GSK-3 becomes phosphorylated by cGKI (Zhao et al. 2009). However, GSK-3 mutant mice showed no obvious deficits in dendritic or axonal projections suggesting that phosphorylation of GSK-3 by cGKI is not essential for sensory axon bifurcation (Gartner et al. 2006; McManus et al. 2005). Thus, the cGKI-dependent phosphorylation event, which is crucial for sensory axon bifurcation remains to be identified.

1.5 Characterization of CNP, Npr2 and cGKI

At the beginning of the 1980s the first natriuretic peptide, the arterial natriuretic peptide (ANP) has been isolated and described. A few years later the receptor for ANP, the atrial natriuretic peptide receptor (Npr1; also termed NPR-A or GC-A) has been identified. Two other natriuretic peptides have been discovered: the brain (BNP) and C-type (CNP) natriuretic peptides. Apart from Npr1, there are two more receptors that bind the natriuretic peptides: the natriuretic peptide receptor 2 (Npr2, also termed as NPR-B or GC-B) and the clearance receptor (Npr3, also termed as Npr-C) (Potter et al. 2006).

The members of the natriuretic peptide family share a common ring structure that is formed by 17aa residues linked by disulphide bonds (Figure 1.5A). The CNP-encoding gene Nppc gene is located on murine chromosome 1 and contains two exons and one intron. CNP is a polypeptide of 126aa residues that gets cleaved into a biologically active form. After cleavage, this biologically active form CNP-53 (53 C-terminal aa residues of CNP) is further processed to CNP-22 by an extracellular protease (Potter et al. 2009).

The natriuretic peptide receptors belong to the family of particulate guanylyl cyclases. Until now,seven members have been identified in mammals (Potter 2011). The particulate guanylyl cyclases form homodimers and share, excluding Npr3, a unique topology that consists of extracellular ligand-binding (LBD), transmembrane (TMD), kinase homology (KHD), dimerization (DD) and carboxyl-terminal catalytic domains (CD) (Figure 1.5B). In contrast, Npr3 has a short intracellular domain that bears no homology to the intracellular domain of the other particulate guanylyl cyclases and no cyclase activity. The guanylyl cyclases with their catalytic domain serve as receptors that produce cyclic GMP (cGMP) in response to ligand binding. Npr1, Npr2 and Npr3 serve as receptors for the natriuretic peptides. The ligands for the other receptors include guanylin, uroguanylin and the endotoxin Sta activating GC-C and bicarbonate activating GC-D and GC-G. Until now, the GC-E and GC-F orphan receptors are poorly characterized (Potter 2011). The natriuretic peptide receptors differ in their relative affinities for the natriuretic peptides (Lucas et al. 2000). While Npr1 binds ANP and BNP with high affinity, it binds CNP with very low affinity. On the other hand, Npr2 is specific for CNP, whereas Npr3 binds all natriuretic peptides with relative high affinity. The natriuretic peptide receptors are expressed in a variety of tissues and therefore this ligand-receptor system is implicated in numerous regulatory, developmental and functional activities. Npr2, a protein of 1047aa residues, is selectively expressed in DRG, where it is involved in the CNP-Npr2-cGKIα signaling pathway (Schmidt et al. 2007; Zhao and Ma 2009). The Npr2 gene, which encodes Npr2, contains 22 exons and is located on murine chromosome 4.

cGMP-dependent kinases (cGKs) are serine/threonine kinases. The functional and structural properties as well as tissue distribution pattern of known cGKs are reviewed in (Hofmann et al. 2009). cGKs are composed of an NH_2-terminal domain with dimerization-mediating and inhibitory regions, a regulatory domain with two cGMP binding sites and a catalytic domain with ATP and substrate binding sites (Figure 1.5C).
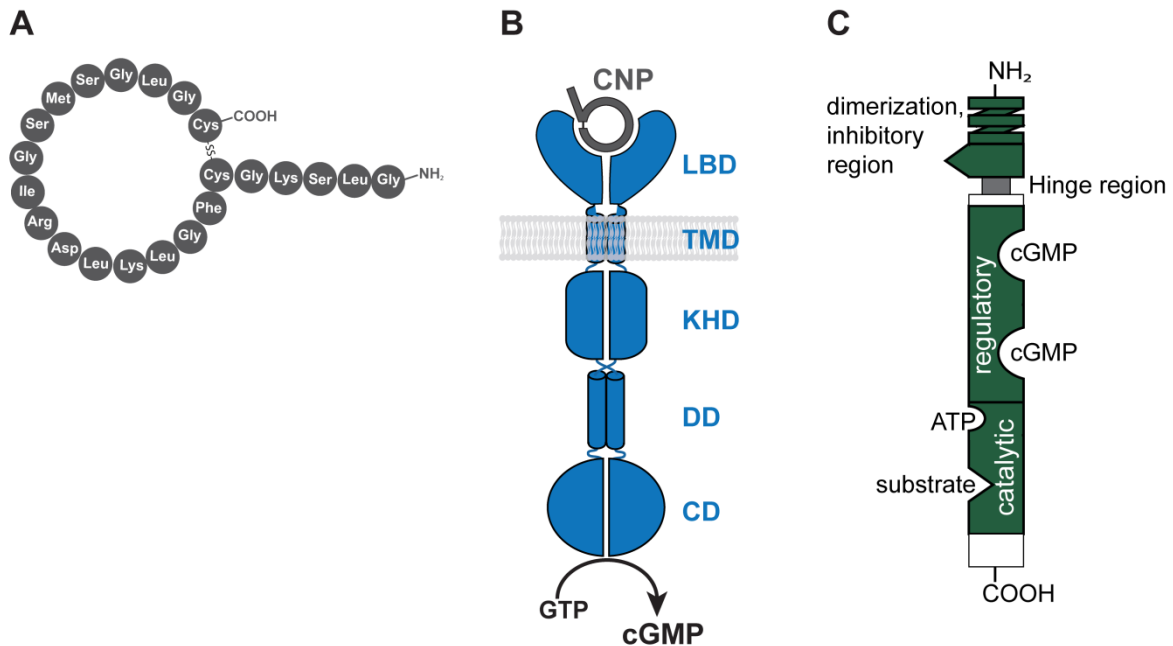
Figure 1.5: Schematic representations of **(A)** C-type natriuretic peptide (CNP-22), **(B)** the homodimeric receptor guanylyl cyclase Npr2 that produces cyclic GMP (cGMP) from GTP in response to ligand CNP binding and **(C)** cGMP-dependent protein kinase (cGK). Adapted from (Ter-Avetisyan et al. 2012). LBD, ligand-binding domain; TMD, transmembrane domain; KHD, kinase homology domain; DD, dimerization domain; CD, catalytic domain.

There are two types of cGKs: type I and type II (cGKI and cGKII) encoded by the genes Prkg1 and 2, respectively. cGKI with its two isoforms cGKIα and cGKIβ is a soluble enzyme, whereas cGKII is attached to the membrane. cGKIα is specifically expressed in DRG, where the CNP-Npr2-cGKIα signaling cascade regulates the sensory axon bifurcation at the DREZ (Schmidt et al. 2002). cGKI contains a consensus phosphorylation motif with the amino acid sequence K/R-K/R-X-pS/pT.

1.6 Cre and Flp recombination in gene targeting

Gene targeting in mice is a powerful tool to investigate individual gene functions. The combination of gene targeting and site-specific recombination allows the exploration of gene functions in a cell- and tissue-specific manner (spatially regulated). Additionally, activation of the mutation by drug administration (inducible mutation) at a particular time

(time-regulated) increases the number and variety of genetic manipulations that can be introduced in mice (Metzger and Chambon 2001; Metzger and Feil 1999; Nagy 2000).

Most commonly used site-specific recombinases are Cre (cyclization recombination) and Flp (Flippase). Both are tyrosine recombinases, which belong to the λ superfamily of site-specific recombinases. Cre is a 38kDa protein encoded by bacteriophage P1 and Flp is a 45kDa protein encoded by *Saccharomyces cerevisiae* (Babineau et al. 1985; Nagy 2000; Sadowski 1995). Both Cre and Flp have a minimal DNA recognition sequence of 34 base pairs (bp). The 34bp recognition sequence for Cre is termed loxP (locus of crossover [x] in P1) and for Flp is termed FRT (Flippase Recognition Target). Both loxP- and FRT-sites consist of two 13bp inverted repeats (palindromes) that flank an 8bp core sequence. The orientations of the core sequences give directionality to the target site and govern the crossover reaction catalyzed by the recombinase. Dependent on the relative orientation of the recognition sequences, the site-specific recombinases bind to the target DNA sequence and induce DNA deletion, insertion and exchange at the desired gene locus (Joyner A.L. 1993). If the FRT/loxP-sites are orientated identically, the recombinase catalyzes the excision of the flanked DNA, while it catalyzes the inversion of the flanked DNA, whenever the FRT/loxP-sites are orientated oppositely. If two DNA sequences contain a single FRT/loxP-site, the recombinase catalyzes a translocation reaction (Nagy 2000; Rodriguez et al. 2000; Sauer and Henderson 1988).

Site-specific recombinases are commonly used to create mouse models carrying a desired DNA sequence. Once the gene targeting is accomplished, Cre and Flp recombinases are used in order to remove for example positive selection markers (usually a neomycin (Neo)-cassette). Therefore the selection marker is flanked by either loxP-sites (floxed) or FRT-sites (flirted). Chimeric mice with a desired gene mutation and floxed or flIrted selection marker are mated with the respective Cre- or Flp-deleter mouse strain, which ubiquitously expresses Cre or Flp recombinase. This crossing step results in excision of the selection marker in the offspring (Fig. 1.6A and B).

For the removal of the Neo-cassette another strategy has been described using the introduction of the Cre/loxP recombination system in the same mouse, in which the self-excising Cre recombinase is expressed under the control of a testis-specific promoter (Bunting et al. 1999). Upon backcrossing of the chimera with the wildtype mice, the selection marker is removed during germline transmission of the targeted gene (Fig 1.6C).

An additional example for the spatial gene regulation is the combination of the Cre/loxP recombination system with reporter gene detection. A reporter gene [e.g. Alkaline Phosphatase (AP) or enhanced Green Fluorescent Protein (eGFP)] can be selectively activated after crossing a Cre-expressing line with the reporter lines. A floxed STOP-cassette is placed in front of the reporter expression cassette, so that the reporter gene

expression does not proceed until Cre excises the STOP-sequence (Fig 1.6D). This approach allows the selective expression of a reporter gene in the conditional knockout tissues.
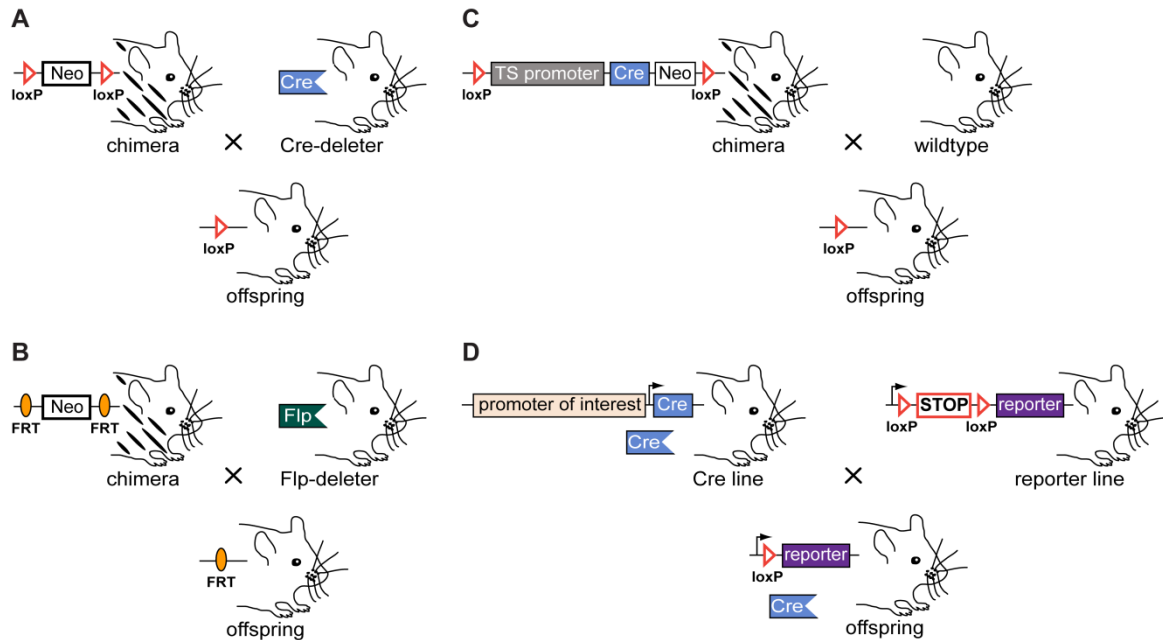
Figure 1.6: Schematic representation of the Cre/loxP and Flp/FRT recombination systems. **(A, B)** The removal of the floxed or flirted Neo-cassette by crossbreeding of chimeric mice and Cre- or Flp-deleter strains, respectively. **(C)** The self-excising Cre recombinase is expressed under the control of the testis promoter (TS promoter). It removes the Neo-cassette upon backcrossing of the chimeric mice with the wildtype mice. **(D)** The Cre expression under the control of the promoter of interest removes the STOP-cassette upstream of the reporter gene. This results in the expression of the reporter gene specifically in cells expressing Cre driven by promoter of interest.

1.6.1 The inducible Cre recombination system

The first system designed to provide a temporal control of gene expression made use of an inducible promoter to express the Cre recombinase (Kuhn et al. 1995). Nowadays an established method for the temporal control of gene expression is the activation of the Cre recombinase by an exogenous inducer that is introduced at a chosen time. In this system the coding region of the C̲re recombinase is fused to a mutated e̲strogen r̲eceptor (ER) ligand binding domain (LBD), which binds the synthetic antagonist t̲amoxifen or 4-hydroxytamoxifen (named as CreERT) (Brocard et al. 1998; Danielian et al. 1998; Feil et al. 1996; Feil et al. 1997; Metzger et al. 1995). At least three different mutant human-derived and two mouse-derived CreERTs are known (Birling et al. 2009). The modification(s) in CreERT prevents the interaction with endogenous ligand 17β-estradiol and allows the use of exogenous synthetic ligands such as tamoxifen or 4-hydroxytamoxifen. Additionally the CreERT fusion protein ensures that Cre is trapped in the cytoplasm by heat-shock protein 90 (HSP90) and is therefore initially inactive. The

CreERT fusion protein only becomes active in the presence of the external synthetic ligand. A specific triple amino acid mutation (G400V/M543A/L544A) in the human ER-LBD rendered Cre (named CreERT2) more sensitive to tamoxifen and 4-hydroxytamoxifen compared to an earlier version of the LBD, harboring only one amino acid mutation (Feil et al. 1997; Indra et al. 1999; Metzger and Chambon 2001). Binding of tamoxifen or 4-hydroxytamoxifen to the ERT/ERT2 domain leads to a release of CreERT/CreERT2 from HSP90. CreERT/CreERT2 then translocates into the nucleus where it mediates the site-specific recombination (Hayashi and McMahon 2002) (Figure 1.7). CreERT2 is preferred for the generation of inducible tissue-specific Cre mouse lines and has been successfully used in spatially and temporally regulated mutagenic experiments (Feil 2007; Gaveriaux-Ruff and Kieffer 2007).
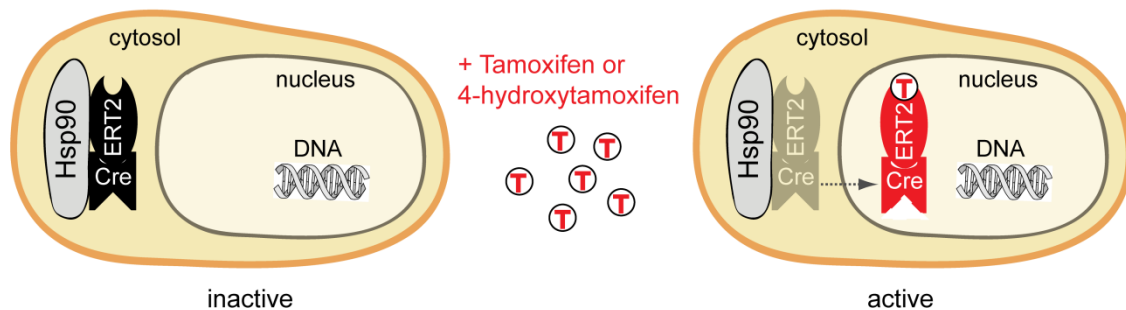
Figure 1.7: Schematic illustration of the Cre induction by tamoxifen or 4-hydroxytamoxifen. The Cre recombinase in the cytosol is bound to Hsp90 (inactive, on the left). Binding of tamoxifen or 4-hydroxytamoxifen to the ERT2 domain frees the Cre recombinase whereupon Cre translocates into the nucleus and mediates the site-specific recombination (active, on the right). CreERT2, Cre recombinase fused to estrogen receptor T2; Hsp90, heat shock protein 90; T, Tamoxifen/4-hydroxytamoxifen.

1.6.2 Inducible Cre-mediated reporter gene expression

One of the many strategies to monitor Cre-mediated recombination makes use of Cre-dependent reporter mouse strains that express the reporter gene (AP, eGFP) after Cre-mediated recombination. Here, the reporter gene is placed behind the STOP-cassette, which is flanked by loxP-sites (loxP-STOP-loxP). Consequently, the reporter mouse strain does not express the reporter gene until Cre is expressed, leading to excision of the floxed STOP-cassette. The reporter genes can be expressed under the control of ubiquitous or tissue-specific gene promoters. Examples for reporter mouse strains are: the Z/AP (lacZ/AP) reporter line, which contains the ubiquitously expressed pCCAG promoter and produces human placental alkaline phosphatase (hPLAP) upon excision of the loxP-flanked STOP-cassette (Lobe et al. 1999) and the mGFP reporter line, which contains the

Tau gene promoter and produces membrane-targeted GFP after Cre-mediated recombination (Hippenmeyer et al. 2005) (Figure 1.8 A).

By placing the Cre recombinase under the control of the promoter of interest, only the Cre-expressing cells will be labeled. Moreover, introduction of a tamoxifen- or 4-hydroxytamoxifen-inducible Cre recombinase under the control of the promoter of interest provides a controlled recombination process with spatially and temporally regulated labeling of cell populations (Fig 1.8B).
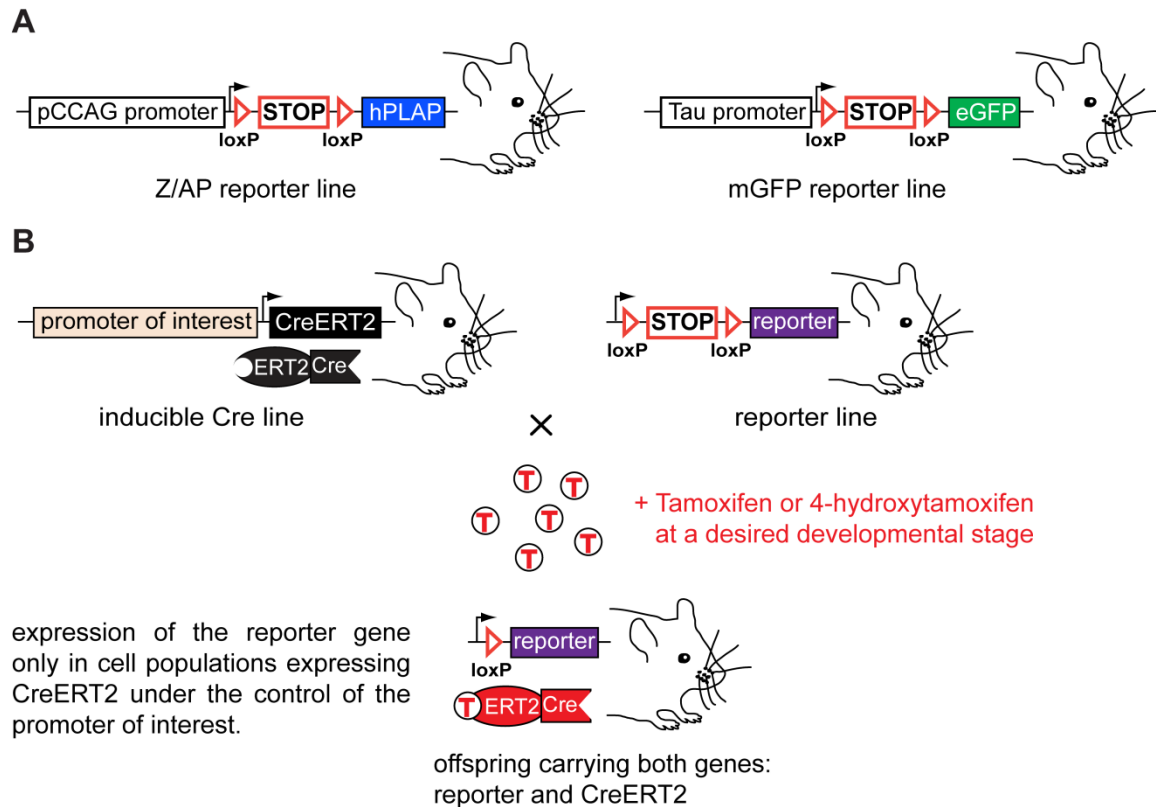
Figure 1.8: (A) Schematic illustration of the Z/AP and mGFP reporter lines. **(B)** The inducible Cre-mediated reporter gene expression. After crossing of a mouse strain expressing the CreERT2 under the control of the promoter of interest with a reporter strain containing a loxP-STOP-loxP cassette, the induction of the Cre recombinase by tamoxifen or 4-hydroxytamoxifen allows cell-specific labeling at a desired developmental stage.

1.6.3 Single neuron labeling using inducible Cre reporter lines

The controlled temporal and spatial labeling of selective cell populations using gene-specific promoters for inducible Cre-dependent reporter gene expression has become a popular method to study distinct cell types, particular genes and cellular properties (Branda and Dymecki 2004). This approach as well as the ability to induce the Cre recombinase in a dose-dependent manner allow single cell labeling (Dymecki and Kim

2007). The latter is instrumental in studying single neuron morphology in complex neuronal networks (Buffelli et al. 2003; Li et al. 2010; Miyoshi et al. 2010).

Resolving individual neurons is essential to elucidate their function and organization and to understand the developmental principles of neuronal circuits. Historically, the Golgi staining method developed in the 19th century was the first technique used to label small populations of neurons and to study their morphology. Since then many labeling methods have been developed that allow a more detailed study of neuronal structure and connectivity. Carbocyanine dyes, for example DiI (1,1'-dioctadecyl-3,3,3',3'-tetramethylindocarbocyanine perchlorate) are lipophilic fluorescent tracers that are used to label neuronal plasma membranes with high specificity (Honig and Hume 1989). Despite many advantages of carbocyanine dyes, they do not allow analysis of individual neuron morphology in complex neuronal circuits. In the last decade sophisticated strategies have been developed to label and image individual neurons. The approach of genetically encoded labeling of neurons is a powerful tool that offers new opportunities to characterize neuronal circuits *in vivo*, to understand the impact of cellular components on the lineage and function of individual neurons. Such an approach is the CreERT2-system with inducible Cre-mediated reporter gene expression. It provides the following substantial advantages 1) temporal control of the gene excision by Cre-mediated site-specific recombination 2) restriction of the mutation to distinct neuronal populations 3) sparse labeling of neurons in a dose-dependent manner. Several studies utilizing this strategy succeeded in the analysis of single neuron morphology (Badea et al. 2009; Badea and Nathans 2004; Badea et al. 2003; Koundakjian et al. 2004; Madisen et al. 2010; Rotolo et al. 2008; Young et al. 2008). Remarkably, the CreERT2 genetic sparse labeling approach allows targeting and manipulation of specific neuron subpopulations during development. This is fundamental for the understanding of developmental processes leading to the formation of complex neuronal circuits with their individual pattern of connections.

2. Preface and Objective

The functionally important cGMP signaling pathway controls sensory axon bifurcation within the spinal cord via activation of cGMP-dependent protein kinase Iα (cGKIα). It is therefore compelling to deal with the question whether other neuronal subpopulations besides the DRG neurons use the CNP-Npr2-cGKIα signaling pathway to form branches emerging from the bifurcating growth cone.

To study the signaling pathway in other neuronal subpopulations, it was first important to describe the localization of the receptor Npr2. Therefore, a versatile system for gene expression studies was used by generating an Npr2LacZ reporter mouse. In this mouse model the introduction of a LacZ-cassette with a nuclear localization sequence (NLS) in frame with exon 1 of the Npr2 gene locus enabled the identification of Npr2-expressing neuronal cell bodies in developing heterozygous offspring. By analyzing the X-Gal staining of embryonic whole mounts and cryosections the localization of Npr2 was exactly determined. Furthermore, by means of immunohistochemical analysis using antibodies against cGKIα, β-gal and neurofilament-M it was possible to demonstrate the presence of components of the CNP-Npr2-cGKIα signaling pathway in distinct neuronal subpopulations identified by X-Gal staining.

After identification of Npr2-expressing neurons, the next objective was to study single axonal projections of Npr2-positive neurons and their branching pattern. To address this question, it was essential to generate an Npr2CreERT2 mouse line. In this mouse model the Npr2 allele was replaced by tamoxifen-inducible Cre recombinase (CreERT2) resulting in the expression of CreERT2 in Npr2-positive cells. After crossbreeding of Npr2CreERT2 mice with different reporter strains (Z/AP, mGFP) the induction of Cre recombinase with limited amounts of tamoxifen or 4-hydroxytamoxifen allowed the visualization of single axonal projections. Using this time- and tissue-specific induction method the axonal branching and branching errors of Npr2-positive axons were identified and investigated at different developmental stages in murine brains.

In addition to the above studies, the phosphorylation target(s) of cGKI was searched in embryonic DRG in order to further understand the CNP-Npr2-cGKIα signaling pathway. Distinct phospho-motif specific antibodies directed against the consensus phosphorylation site of cGKI K/RK/RXpS/pT (anti-RRXpS/pT; anti-RKVpS; anti-RKRpSV; anti-GKKKpS; anti-RRMpS) as well as diverse phopsho-specific antibodies directed against phosphorylation targets of cGKIα in embryonic DRG were used to perform Western blot analysis. Furthermore, to analyze the role of a phosphorylation target in the sensory axon bifurcation at the dorsal root entry zone genetically, knockout mouse models were analyzed by DiI-labeling of the embryonic DRG sensory axons.

During this work, the generation of Npr2LacZ and Npr2CreERT2 mouse lines was successfully accomplished. The mouse lines were verified besides genetic verification by Southern blot, immunohistochemical analysis and PCR genotyping, by examination of sensory axons of DRG neurons – an established neuronal system to study the co-expression of Npr2 and cGKIα in sensory neurons and their implication in the bifurcation of sensory axons at the dorsal root entry zone. The purpose to identify novel Npr2-positive neuronal subpopulations and to analyze their central projections culminated in the following findings:

- The expression of Npr2 is most striking in the developing cranial sensory ganglia on the basis of nuclear localized β-gal expression in the heterozygous Npr2LacZ mice.
- In the cranial sensory axons Npr2 and cGKIα exhibit co-localization.
- The Npr2CreERT2 mouse model revealed at the single axon level that in the absence of Npr2 the central projections of cranial sensory axons fail to bifurcate when they enter the hindbrain.

.

3. Materials

3.1 Buffers, solutions and media

Table 3.1

Name	Composition and preparation
ABS (3x)	12g BSA, 3ml Tween-20 diluted in 1xTBS to a total volume of 200ml and stored at -20°C. The 1xABS was prepared freshly before the use by diluting the 3xABS in 1xTBS.
Agarose gel	0.7-2.5% (w/v) agarose was dissolved in 1xTAE by boiling. After chilling for 2min at RT, 0.01% (v/v) ethidium bromide was added, mixed gently and poured into a gel tray avoiding air bubbles.
Anesthetic mixture	12% (v/v) Rhompon, 34% (v/v) Ketanest, 54% NaCl from 0.9% stock solution were mixed before use.
AP fixative	2% (v/v) PFA from 4% stock solution, 0.2% (v/v) glutaraldehyde from 25% stock, 100mM $MgCl_2$ were prepared freshly in 1xPBS before use.
AP staining solution	100mM Tris-HCl pH 9.5, 100mM NaCl, 50mM $MgCl_2$, 0.02% (v/v) NP-40, 0.01%(w/v) sodium deoxycholate, 337µg/ml NBT, 175µg/ml BCIP; prepared freshly before use.
AP washing buffer	100mM Tris-HCl pH 9.5, 100mM NaCl, 10mM $MgCl_2$; stored at RT.
CHAPS +protease inhibitors	1% (w/v) CHAPS was dissolved in 1xTBS and the following protease inhibitors were added: leupeptin hemisulfate salt, pepstatin A, aprotinin to a final concentration of 10µM and PMSF to a final concentration of 0.1µM; the 2ml aliquots were stored at -20°C.
Church buffer (200ml)	0.5M NaH_2PO_4, 1mM EDTA from 0.5M stock solution, filled up to 190ml with ddH_2O and the pH adjusted to 7.2 with 0.1M NaOH. 1% (w/v) BSA was added and dissolved at 68°C. After cooling, 7% (w/v) SDS was added and filled up to 200ml. The buffer was filtered and aliquots were stored at -20°C.
Denaturation buffer	0.5M NaOH and 1M HCl; was prepared freshly by 1:4 dilution of the stock solution of 2M NaOH and 4M HCl.
Depurination buffer	250mM HCl; was prepared freshly by 1:10 dilution of the 2.5M HCl stock solution.
DNA loading buffer (10x)	25% (v/v) Ficoll, 100mM Tris-HCl pH 7.4, 100mM EDTA was heated to 65°C to dissolve. Then 0.25% (w/v) Xylen cyanol was added.
ES cell medium	DMEM (500ml), 90ml FCS, 6ml non essential amino acids, 6ml Penicillin/Streptomycin, 1.2ml 2-mercaptoethanol, 180µl LIF and 400µg/ml G418; stored at 4°C.
ES freezing medium	The same as the ES medium. 25% (v/v) FCS and 10% (v/v) DMSO were added freshly before use.
ES lysis buffer	10mM Tris-HCL pH 7.5, 10mM EDTA, 10mM NaCl, 0.5% (w/v) N-lauroylsarcosine; stored at RT.
Feeder medium	The same as the ES medium but with 60ml FCS, without LIF and G418; stored at 4°C.
Flushing solution	1mM $CaCl_2$, 1mM $MgCl_2$ dissolved in 1xPBS; prepared freshly before use.

Immuno-blocking buffer	1% (v/v) heat inactivated goat serum and 0.1% (v/v) Triton X-100 diluted in 1xPBS; stored at 4°C.
Immuno-washing buffer	0.1% (v/v) Triton X-100 diluted in 1xPBS; stored at RT.
Laemmli sample buffer (5x)	50mM Tris–HCl pH 6.8; 12.5% (v/v) glycerol; 1% (v/v) SDS; 0.01% (w/v) bromophenol blue, 5% (v/v) 2-mercaptoethanol; aliquots stored at -20°C.
LB medium	1% (w/v) Bacto-Tryptone, 0.5% (w/v) Bacto-Yeast-Extract, 1% (w/v) NaCl dissolved in ddH$_2$O. The LB medium was autoclaved and stored at 4°C.
LB medium + antibiotics	The antibiotic stock solution was added to the autoclaved and cooled LB medium freshly before use.
LB agar	1.5% (w/v) agar was added to LB-medium, autoclaved and stored at 4°C.
LB agar plates+ antibiotics	The chilled LB-agar was dissolved in a microwave, tempered to 50°C in water bath and antibiotic(s) in appropriate concentration(s) were added. The solution was then poured into sterile Petri dishes under the sterile hood, left to dry under UV light and stored at 4°C up to 4 weeks.
PFA solution 4% (500ml)	350ml ddH$_2$O was heated to 60°C and 20g PFA was added. A few drops of 4M NaOH were pipetted until the solution became clear. After cooling, 50ml 10xPBS was added to the solution. After filling up to 500ml and adjusting the pH to 7.2, the solution was filtered and aliquots of 50ml were stored at -20°C.
SOB medium	2% (w/v) Bacto-Tryptone, 0.5% (w/v) Bacto-Yeast-Extract, 10mM NaCl, 2.5mM KCl in ddH$_2$O was autoclaved. Then a 2M stock solution of 1M MgCl$_2$ and 1M MgSO$_4$ was added to a final concentration of Mg^{2+} of 20mM. The medium was sterile filtered and stored at 4°C.
SOC medium	The same as the SOB medium containing 20mM glucose using sterile filtered 2M stock solution. After addition of glucose, the SOC medium was sterile filtered and stored at 4°C.
Sodium acetate (3M)	12.3g sodium acetate was diluted in 30ml ddH$_2$O, the pH was adjusted to 5.2 using acetic acid and filled up to 50ml.
Sodium phosphate buffer (0.5M)	The prepared solution of 1l 0.5M dihydrogen sodium phosphate (NaH$_2$PO4) was added to the prepared solution of 2l 0.5M disodium hydrogen phosphate (Na$_2$HPO$_4$) until the pH was 7.0.
SSC buffer (20x)	3M NaCl and 0.3M sodium citrate were dissolved in ddH$_2$O and the pH was adjusted to 7.0 with 0.1M HCl. The buffer was sterile filtered.
Southern washing buffer I	1xSSC, 1% (v/v) SDS
Southern washing buffer II	1xSSC, 0.1% (v/v) SDS.
Southern washing buffer III	0.5xSSC, 0.1%(v/v) SDS
Southern washing buffer IV	0.2xSSC, 0.1% (v/v) SDS.
Southern washing buffer V	0.1xSSC, 0.1% (v/v) SDS
TAE (50x)	121g Tris, 28.6ml acetic acid and 50ml EDTA (from 0.5M stock solution with pH 8.0) were filled up to 500ml with ddH$_2$O.

TBS (10x)	1.5M NaCl and 0.5M Tris; pH was adjusted to 7.4 using 32% HCl.
TFB1 buffer	100mM $RbCl_2$, 50mM $MnCl_2$, 30mM potassium acetate, 10mM $CaCl_2$. The pH was adjusted to 5.8 with 0.2N acetic acid, then 15% (v/v) glycerol was added, sterile filtered and stored at 4°C.
TFB2 buffer	10mM MOPS, 10mM $RbCl_2$, 75mM $CaCl_2$. The pH was adjusted to 7.0 with NaOH, then 15% (v/v) glycerol was added, sterile filtered and stored at 4°C.
Western blocking buffer	5% (w/v) BSA and 0.5% (v/v) Tween-20 diluted in 1xTBS; aliquots were stored at -20°C.
Western washing buffer	0.5% (v/v) Tween-20 diluted in 1xTBS.
X-Gal (20mg/ml)	0.1g X-Gal was dissolved in 5ml DMF; stored at -20°C protected from light.
X- Gal fixative	2% (v/v) PFA from 4% stock solution, 0.2% (v/v) glutaraldehyde from 25% stock solution, 50mM EGTA from 0.5M stock solution with pH 7.4 and 100mM sodium phosphate buffer with pH 7.0; prepared freshly before use.
X- Gal staining solution	5mM potassium ferrocyanide and 5mM potassium ferricyanide were dissolved in the X-Gal washing buffer and stored at 4°C. 0.5mg/ml X-Gal from 20mg/ml stock solution was added freshly before use.
X- Gal washing buffer	20mM $MgCl_2$, 0.01% (w/v) sodium deoxycholate and 0.02% (v/v) NP-40 diluted in 1xPBS.
Zamboni's fixative (1000ml)	350ml ddH_2O was heated to 60°C and 20g PFA was added. Under stirring 20µl 4M NaOH was pipetted until the solution became clear. 150ml saturated picric acid was added to the cooled solution and filled up to 1000ml with 0.2M Na-phosphate buffer. The solution was filtered and aliquots were stored at 4°C.
1kb DNA ladder	100µl Gibco/BRL ladder (1mg/ml), 100µl 10xTAE, 250µl 6xDNA sample buffer, ddH_2O to 1ml.

3.2 Restriction enzymes

Table 3.2

Name	Company		Name	Company
AflIII	New England Biolabs		NcoI	Fermentas
AvaII	New England Biolabs		NotI	Fermentas
BamHI	Fermentas		PacI	Fermentas
BamHI-HF	New England Biolabs		PspOMI	New England Biolabs
BcuI	Fermentas		PstI	Fermentas
BstXI	Fermentas		PstI-HF	New England Biolabs
ClaI	New England Biolabs		PvuII	Fermentas
EcoRI	Fermentas		SacI	Fermentas
EcoRV	Fermentas		SalI	Fermentas
FspI	New England Biolabs		SmaI	Fermentas
HindIII	Fermentas		SpeI	New England Biolabs
KpnI	Fermentas		XapI	Fermentas
MluI	Fermentas		XbaI	Fermentas
NheI-HF	New England Biolabs		XhoI	Fermentas

3.3 Polymerases

Table 3.3

Name	Company
Cloned Pfu DNA polymerase	Fermentas
Klenow fragment exo⁻	Fermentas
LA Taq polymerase	TAKARA
Taq DNA Polymerase recombinant	Invitrogen
T4 DNA Ligase	Fermentas
T4 Polynucleotide kinase	Fermentas

3.4 Embryonic stem (ES) cells

Table 3.4

ES cell line	Provided by
AB 2.1	the group of Prof. Dr. Thomas Willnow
E14.1	the group of Prof. Dr. Carmen Birchmeier-Kohler
R1	the group of Prof. Dr. Thomas Jentsch

3.5 Kits

Table 3.5

Name	Company
Genomic DNA buffer Set	Qiagen
Genomic-tip 500/G	Qiagen
High Pure PCR Template Preparation Kit	Roche
Invisorb® DNA CleanUp	Invitek
MicroSpin™ G-50 Columns	GE Healthcare Life Sciences
Plasmid Mini/Midi/Maxi Kit	Qiagen
Prime-IT® RmT Random Primer Labeling Kit	Stratagene
SuperSignal West Dura Chemiluminescent Substrate	Thermo Scientific

3.6 Antibiotics

Table 3.6

Name	Stock solution and storage	Company
Ampicillin	100mg/ml dissolved in ddH$_2$O, at -20°C	Sigma-Aldrich
Chloramphenicol	34mg/ml dissolved in 100% ethanol, at -20°C	Sigma-Aldrich
Geneticin (G418)	100mg/ml dissolved in ddH$_2$O, at -20°C	Invitrogen
Kanamycin	10mg/ml dissolved in ddH$_2$O, at -20°C	Sigma-Aldrich
Penicillin/streptomycin	100x concentrated liquid	Invitrogen
Tetracycline hydrochloride	5mg/ml dissolved in 50% ethanol, at -20°C	Boehringer

3.7 Bacterial strains

Table 3.7

Name	From
Escherichia coli DH5α	Invitrogen
Escherichia coli DH10B	Invitrogen
Escherichia coli DY380	the group of Prof Dr. Carmen Birchmeier-Kohler
Escherichia coli EL350	the group of Prof Dr. Carmen Birchmeier-Kohler
Escherichia coli EL250	the group of Prof Dr. Carmen Birchmeier-Kohler

3.8 Antibodies for immunohistochemistry

Table 3.8

Name	Used dilution/concentration	From
Chicken-α-β-gal	1:5000	Jackson ImmunoResearch
Donkey-α-Chicken-Cy3	1:400	Jackson ImmunoResearch
Goat-α-Mouse-NF-M	7.5µg/ml	BioTrend
Goat-α-Mouse-NeuN	1:500	Millipore
Goat-α-Mouse-647	1:400	Jackson ImmunoResearch
Goat-α-Rabbit-Alexa488	1:300	Jackson ImmunoResearch
Guinea pig-α-cGKIα	1:10.000	AG Rathjen
Guinea pig-α-Npr2	1:10.000	AG Rathjen
Rabbit-α-Cre	1:10.000	Millipore
Rabbit-α-cGKIα	7.5µg/ml	AG Rathjen

3.9 Chemicals

Table 3.9

Name	Company
Acetic acid	Merck
Acryl amide	Bio-Rad
Agarose NEEO Ultra-Qualität	Carl Roth
Aprotinin	Carl Roth
APS	GE Healthcare
L-(+)-Arabinose	Sigma-Aldrich
Bacto™-Tryptone	Becton, Dickinson Company
Bacto™-Yeast-Extract	Becton, Dickinson Company
BCIP	Carl Roth
Benzyl alcohol	Sigma-Aldrich
Benzyl benzoate	Sigma-Aldrich
Bromophenol blue	Sigma-Aldrich
BSA fraction V	Biomol
Calcium chloride	Merck
Calyculin A	New England Biolabs
CHAPS	Merck
CNP-22	Biomol
Corn oil C8267	Sigma-Aldrich

DAPI	Dianova
Dihydrogen sodium phosphate	Sigma-Aldrich
Dimethylformamide	Chemika Fluka
DMSO	Merck
dNTPs Mix (2.5mM each)	Invitrogen
DMEM	Invitrogen (31966-047)
EDTA	Merck
EGTA	Merck
Ethanol	Merck
EtBr	AppliChem
Ficoll	Pharmacia Biotech
Gelatin solution (2%)	Sigma-Aldrich
Glucose	Merck
Glutaraldehyde solution 25%	Polysciences
Glycerol	Merck
Hydrochloride acid 32% solution	Merck
Immu-mount™	Thermo Scientific
Isopropanol	Merck
Ketanest	WDT
Lauroylsarcosine	Sigma-Aldrich
Leupeptin hemisulfate salt	Sigma-Aldrich
LIF	Invitrogen
Magnesium chloride	Merck
Magnesium sulfate heptahydrate	Merck
Manganese chloride	Merck
Methanol	Merck
Mitomycine C	Sigma-Aldrich
Molecular mass standards for SDS-PAGE	BioRad
Monosodium phosphate	Merck
MOPS	Merck
NBT	Carl Roth
Non-essential amino acids solution	Invitrogen
NP-40	Biological
Okadaic acid	Enzo Life Sciences
PBS	Biochrom (L182-50)
Pepstatin A	Sigma-Aldrich
PFA	Merck
Phenol-Chloroform-Isoamyl (25:24:1)	Sigma-Aldrich
Picric acid (≥98%)	Sigma-Aldrich
PMSF	Enzo Life Sciences
Potassium acetate	Sigma-Aldrich
Proteinase K	Roche
Rhompun	Bayer
Rubidium chloride	Sigma-Aldrich
SDS solution	Bio-Rad
SeaKem® LE Agarose	Lonza
Sodium acetate	Merck
Sodium chloride	Merck
Sodium citrate	Merck

Sodium deoxycholat	Sigma-Aldrich
Sodium hydroxide	Merck
Sucrose	Merck
Tamoxifen free base	Sigma-Aldrich (T5648)
TEMED	GE Healthcare
Tissue-Tek® O.C.T compound	Sakura
Tris	Merck
Triton X-100	Merck
Trypsin	Invitrogen
Tween-20	Sigma-Aldrich
Urea	Sigma-Aldrich
Xylencyanol	Merck
X-Gal	Sigma- Aldrich (B4252)
4-hydroxytamoxifen (≥98% Z-isomer)	Sigma-Aldrich
2-mercaptoethanol	Sigma-Aldrich
8-pCPT-cGMP	BioLog
^{32}P-dCTP	PerkinElmer (312H)

3.10 Special equipment

Table 3.10

Name	Company
Axiovert135	Zeiss
BioPhotometer	Eppendorf
BioMax MP1015	Kodak
Chemi Doc	Bio-Rad
Centrifuge 5804	Eppendorf
CM1950 cryostat	Leica
Contamat FH111M contamination monitor	Thermo Scientific
Fluorescence microscope BZ8000	Keyence
Gene Pulser Xcell System	Bio-Rad
Hybridisation oven	Peqlab
KL1500 electronic light source	Schott
LSM710 confocal microscope	Zeiss
MicroPulser Electroporator	Bio-Rad
Mastercycler Gradient	Eppendorf
Maxigel M system PerfectBlue™	Peqlab
Multi-channel pump with variable speed	Ismatec
Powerpac 300	Bio-Rad
Sorvall M150 centrifuge	Thermo Scientific
Sorvall RC6+centrifuge	Thermo Scientific
Stemi DRC stereomicroscope	Zeiss
Stemi SV11 stereomicroscope	Zeiss
UV crosslinker	Fisher Scientific
Vibratome VT1000S	Leica

4. Methods

4.1 Molecular biology

The standard molecular biological and microbiological methods were performed according to protocols from *Molecular Cloning: A Laboratory Manual* (Sambrook J. 2001), *Current Protocols in Molecular Biology* (Wiley online library) and, in case of kits, instructions provided by the manufacturer. Detailed descriptions of other specific techniques or slight modifications from protocols and instructions are provided in the following sections.

4.1.1 Bacterial culture

The bacterial strains used in this study are listed in Table 3.7 and were received as glycerol stocks. Generally, after streaking (in case of a glycerol stock) or plating (after transformation) the bacteria onto an LB agar plate of choice (see Table 4.1) the bacteria were grown overnight at the indicated temperature. The next day, 2-3ml LB medium containing the same antibiotics as the LB agar plate, was inoculated with a single bacterial colony and incubated overnight at 37°C or 32°C with shaking. On the following day the plasmid DNA was isolated employing Mini prep and used for downstream applications. Table 4.1 summarizes the usage, the specific antibiotic resistance and growth conditions of individual bacterial strains used in this study.

Table 4.1

Bacterial strain	Usage	Growth terms and conditions
DH5α	For chemical transformation	No antibiotic selection, at 37°C.
	Amplification of pBluescript II SK+ plasmid DNA	In the presence of 100µg/ml ampicillin, at 37°C.
DH10B	For chemical transformation	No antibiotic selection, at 37°C.
	Amplification of the BAC DNA	In the presence of 20µg/ml chloramphenicol, at 37°C.
	Electroporation of the induced mini-λ into the BAC DNA	In the presence of tetracycline, chloramphenicol each 12.5µg/ml, at 32°C.
	Electroporation of the pDTA plasmid flanked with homology arms into the induced mini-λ-BAC DNA	In the presence of 100µg/ml ampicillin, at 32°C.
DY380	Amplification of the mini-λ DNA	In the presence of 12.5µg/ml tetracycline, at 32°C.
	Electroporation of the pDTA plasmid with integrated Npr2 locus to amplify it.	In the presence of 100µg/ml ampicillin, at 32°C.
	Electroporation of the DNA construct for the site-specific homologies recombination with pDTA plasmid integrating the Npr2 locus.	In the presence of 30µg/ml kanamycin, at 32°C.
EL250	Confirmation of functional Flp target sites	Growth at 32°C.
EL350	Confirmation of functional Cre target sites	Growth at 32°C.

4.1.2 Transformation of *E. coli*

In order to amplify plasmids based on their antibiotic resistance, plasmids of interest were introduced into bacteria in two ways: by chemical transformation and by electroporation. These two methods and the preparation of the respective competent bacteria are described in the following chapters.

4.1.3 Chemical transformation of *E. coli*

To prepare chemo-competent bacteria, the bacterial strains DH5α and DH10B were grown and treated in a way as described in chapter 4.1.1. 100ml LB medium were inoculated with 1ml of the overnight bacterial culture and incubated at 37°C with shaking until the OD_{600} reached 0.4 to 0.5. The culture was transferred into a pre-chilled 50ml Falcon tube and cooled on ice for 10min. Then the culture was centrifuged for 10min at 1500g and 4°C. The pellet was resuspended in 30ml pre-chilled TFB1 buffer, cooled on ice for 10min and centrifuged again for 10min at 1500g and 4°C. The pellet was resuspended in 4ml pre-chilled TFB2 buffer and cooled again on ice for 10min. To aliquot the competent bacteria, 1.5ml pre-chilled microcentrifuge tubes were used and aliquots of 100µl were stored at -80°C. The transformation of chemo-competent bacteria with a plasmid of interest was performed as follows:

1. *Thawing of the chemo-competent bacteria on ice for 20min.*
2. *Addition of 10µl ligation product or other plasmid.*
3. *Incubation on ice for 20min.*
4. *Heating at 42°C for 2min.*
5. *Incubation on ice for 90sec.*
6. *Addition of 390µl pre-warmed LB medium.*
7. *Incubation for 1h at 37°C with shaking.*
8. *Centrifugation at 5500g for 1min and aspiration of the supernatant.*
9. *Resuspension of the pellet in 150µl LB medium.*
10. *Plating on LB agar plate with appropriate antibiotic.*

4.1.4 Transformation of *E. coli* by electroporation

To prepare electro-competent bacteria (both DH10B hosting BAC and its derivative DY380), a single colony was inoculated into 2ml LB medium with appropriate antibiotic(s) and grown overnight with shaking at 32°C (see Table 4.1). From the overnight culture 0.1ml was transferred into 50ml LB medium containing appropriate antibiotic(s) and incubated with shaking at 32°C until the OD_{600} reached 0.4 to 0.5. Then the culture was transferred into a pre-chilled 50ml Falcon tube and cooled on ice for 10min with occasional shaking. The culture was then centrifuged for 10min at 1500g and 4°C. The

pellet was resuspended in 50ml of 10% (v/v) ice-cold glycerol. This step was repeated. Thereafter the pellet was resuspended in 200µl of 10% ice-cold glycerol. 50µl aliquots were dispensed in pre-chilled 1.5ml microcentrifuge tubes and stored at -80°C. The electroporation of the bacteria was performed as follows:

1. *Chilling of the electroporation cuvette with 0.1cm gap width, 1.5ml tube, electro-competent bacteria and the DNA to be electroporated on ice.*
2. *Pipetting of the DNA and 50µl electro-competent bacteria into the 1.5ml tube.*
3. *Transfer of the mixture into the cuvette.*
4. *Placement of the cuvette into the MicroPulser Electroporator and electroporation at 1660V.*
5. *Addition of 1ml SOC medium to the cuvette and transfer of the bacteria into a 1.5ml tube.*
6. *Incubation for 1h at 32°C (at 37°C for non-recombinogenic bacteria) with shaking.*
7. *Plating of 100 to 300µl culture onto a LB agarose plate containing appropriate antibiotic(s).*

4.1.5 Homologous recombination in *E. coli*

The recombination method used in this study to generate BAC based constructs for transgenesis is based on homologous recombination in *E. coli* using the mobile recombination system mini-λ (Court DL et al. 2003). Mini-λ is a non-replicating circular phage DNA, which is integrating into the bacterial chromosome. After integration, the mini-λ replicates as part of the chromosome and can be excised and purified from the bacteria later on (chapter 4.1.6).

The temperature-sensitive repression and derepression of the mini-λ recombination system allows insertion of a desired construct flanked by homology arms into a defined gene locus in BAC clones. The result is a DNA construct that mimics a gene knock-in. The steps of homologous recombination are described in the following chapters.

4.1.6 Purification of mini-λ DNA

The mini-λ DNA was amplified by growing the bacterial strain DY380 on LB agar plates supplied with 12.5µg/ml tetracycline at 32°C (Table 4.1). A single colony was picked and grown in 2ml LB medium in the presence of 12.5µg/ml tetracycline for 7h at 32°C with shaking. Then, 100µl from the culture were added to 500ml LB medium with 12.5µg/ml tetracycline and grown overnight at 32°C. The next day, the culture was incubated for 20min at 42°C in a water bath in order to induce excision of the mini-λ DNA circles. The culture was then chilled on ice for 20min. The QIAGEN Plasmid Maxi Kit was used to purify the mini-λ DNA. After photometric determination of the mini-λ DNA concentration, the aliquots were stored at -80°C.

4.1.7 Induction of mini-λ recombination function

To introduce the mini-λ recombination system into the bacteria, 500ng of the purified mini-λ DNA was electroporated into the electro-competent DH10B bacterial strain harboring BAC (chapter 4.1.4). The transformed bacteria were plated on LB agar plates supplied with 12.5µg/ml tetracycline and 12.5µg/ml chloramphenicol. After overnight incubation at 32°C, a single colony was picked and grown overnight at 32°C with shaking in 2ml LB medium supplied with the same antibiotics as the LB agar plate. The next day, 0.1ml from the overnight culture was transferred into 50ml LB medium with tetracycline and chloramphenicol (each 12.5µg/ml) and grown until an OD_{600} of ~0.45. Then, one half of the culture (25ml) was placed for 15min into a gently shaking water bath tempered to 42°C to induce the mini-λ recombination function. The other half of the culture was left at 32°C as an uninduced control. After the 15min induction step, the cultures (induced and uninduced) were rapidly chilled on ice for 10min. The induced bacteria were made electro-competent (chapter 4.1.4) and stored at -80°C.

Whenever electroporation of linear plasmid DNA was followed by a mini-λ-mediated recombination reaction (see Table 4.1), the bacteria were treated as described above.

4.1.8 *E. coli* strains EL250 and EL350: confirmation of functional Flp and Cre target sites

The glycerol stocks of the bacteria were treated as described in chapter 4.1.1 and grown at 32°C without antibiotic selection. From the overnight culture 2.5ml was transferred into 50ml LB medium and grown at 32°C with orbital shaking to an OD_{600} of ~0.4. To induce the Flp or Cre recombinase, 10% (w/v) arabinose was added to a final concentration of 0.1% and the suspension was incubated for 1h at 32°C. The bacteria were then made electro-competent and electroporated with 250ng of the targeting construct (see chapter 4.1.4). The further procedure of plating and growing was done as described before (32°C, 100µg/ml ampicillin).

To control the removal of the FRT- or loxP-flanked sequences by the respective Flp or Cre recombinase, the DNA was isolated using a QIAGEN Plasmid Mini Kit and the specific cleavage patterns induced by restriction enzyme digestion were analyzed. Additionally, the DNA fragments of interest were cloned into the plasmid pBluescript II SK+ and sequenced.

4.1.9 Isolation of Plasmid DNA

Plasmid DNA was isolated using Plasmid Mini Kit, Plasmid Midi Kit and Plasmid Maxi Kit from QIAGEN according to manufacturer's protocols.

4.1.10 Isolation of Bacterial Artificial Chromosome (BAC) DNA

BAC clones harbored in the *E. coli* strain DH10B were received as glycerol stocks from LifeSciences. BACs contained the backbone vector pBACe3.6 with a chloramphenicol resistance gene. The bacteria were streaked on LB agar plates supplemented with chloramphenicol (20µg/ml) and were grown overnight at 37°C. Then, single colonies were incubated overnight in 5ml LB medium using the same conditions as for LB agar. 3ml of suspension were pelleted by centrifugation at 10.000g (1min). Bacteria were then resuspended in 300µl resuspension buffer containing 100µg/ml RNase A (buffer P1, Qiagen). Subsequently, 300µl lysis buffer (buffer P2, Qiagen) were added and mixed by gentle inversion. Thereafter, 300µl neutralization buffer (buffer P3, Qiagen) were added, mixed gently by inverting and centrifuged immediately for 10min at 12.000g, 4°C. The 750µl supernatant was transferred to a new tube, an equal volume (750µl) of 25:24:1 phenol-chloroform-isoamyl alcohol was added, vortexed for 15sec and centrifuged for 2min at 12.000g and RT. The upper phase was transferred to a new tube and 900µl of 100% ethanol was added. The mixture was inverted 10 times and centrifuged for 30min at 12.000g and 4°C. Thereafter, a pellet was visible. The supernatant was carefully removed and the pellet was washed with 75% ethanol by centrifugation for 10min at 12.000g and 4°C. After removal of the supernatant, the pellet was dried for 10min at RT and was resuspended in 80µl ddH$_2$0. The concentration of the isolated BAC DNA was determined using spectrophotometer as described in chapter 4.1.11.

4.1.11 Determination of DNA concentration

The concentration of the purified plasmid DNA was determined using a spectrophotometer. The absorbance was measured at a wavelength of 260nm. An absorbance of 1unit at 260nm corresponds to approximately 50µg/ml of double-stranded DNA. Thus, the plasmid DNA concentration was determined by the following formula $DNA\ (\mu g/\mu l) = \frac{OD_{260} \times dilution\ factor \times 50 \mu g/ml}{1000}$. The ratio $^{260nm}/_{280nm}$ estimates the DNA purity. A ratio of 1.8-2 is considered to be indicative for DNA samples free of contaminating proteins.

Besides the spectrophotometric determination of the DNA concentration, the so called quantitative agarose gel analysis was used to assess the DNA concentration. This analysis was used in case of DNA fragment eluates with a small volume (up to 12µl) and/or low estimated concentrations (up to 200ng/µl). In the quantitative agarose gel analysis the fluorescence emitted by an ethidium bromide-stained DNA sample was compared to the DNA standard marker of a known concentration. 6µl of Lambda DNA/HindIII marker and a DNA dilution of [2µl DNA eluate +8µl ddH$_2$O +1µl 10xloading dye] were used in a 1% agarose gel electrophoresis to estimate the DNA fragment concentration.

4.1.12 Restriction enzyme digestion of plasmid DNA

The desired amount of DNA was digested for 2h or overnight at 37°C in a 20µl digestion reaction with restriction enzymes and appropriate buffers supplied by the manufacturer.

DNA digestion reaction	
2µl	10xbuffer
1-6µg	DNA
0.5µl	restriction enzyme, 0.5µl each in case of a double digestion
to 20µl	ddH$_2$O

Following the digestion, 2µl of a 10xDNA loading dye was added to DNA digestion samples. The DNA fragments were separated via agarose gel electrophoreses.

4.1.13 Agarose gel electrophoresis

Dependent on the DNA fragments being separated, agarose gels (recipe in Table 3.1) with different pore sizes were prepared (0.7-1% agarose for large fragments or plasmids and 1.5-2.5% agarose for small fragments in 200bp-1kbp range). Samples were run at 100V for a minimum of 1h, 10µl of a 1kb DNA ladder were added as a control. After the run, the gel tray was put into the Gel Documentation system, visualized under the UV light and a picture was taken using software ChemiDoc.

4.1.14 Isolation of DNA from agarose gels (gel extraction)

Desired DNA fragments were cut out from the agarose gel with a sharp scalpel and DNA-containing gel blocks were transferred into a 1.5ml microcentrifuge tube. Tubes were weighed and three volumes of Qiagen buffer QG were added to one volume of gel (e.g. 0.3ml of QG to 0.1g of agarose). The gel slices were then dissolved by incubation at 50°C. One gel volume of isopropanol was added to the sample and this mixture was then

applied to the spin filter column (Invisorb® DNA CleanUp kit). The following cleaning procedure is described below, proceeding from step 2.

1. *Addition of 130µl buffer P to the reaction, mixing and applying to the spin filter column.*
2. *Centrifugation for 30sec at 5500g and discarding the filtrate.*
3. *Addition of 700µl wash buffer to the spin column.*
4. *Centrifugation for 30sec at 5500g and discarding the filtrate.*
5. *Transfer of the spin filter to a new 1.5ml receiver tube.*
6. *Addition of 12µl ddH$_2$O onto the spin filter and incubation for 5min at 50°C by gently shaking.*
7. *Centrifugation for 1min at 5500g.*
8. *Storage of the DNA eluate at 4°C.*

4.1.15 Polymerase-chain-reaction (PCR)

PCR was carried out to amplify DNA fragments for the following purposes:

- To gain specific DNA fragments for molecular cloning.

  PCR reactions used for molecular cloning are described in chapter 4.1.16

- To analyze a specific mutation in the DNA sequence (genotyping).

  Genotyping analyses of each mutant mouse model used in this study are described in chapter 4.3.

4.1.16 PCR for molecular cloning

Recombinant Pfu and LA Taq DNA polymerases were used to amplify specific DNA fragments for downstream ligation reactions. The polymerases were either supplemented with their buffers by the company or specific TaKaRa GC Buffer was used for the amplification of GC-rich regions. The typical Pfu and LA Taq PCR reactions were the following:

PFU PCR REACTION	
5µl	10xbuffer (cloned)
4µl	dNTPs Mix (2.5mM each)
0.8µl	forward primer (50µM)
0.8µl	reverse primer (50µM)
3µl	DNA template (150 to 450ng)
0.5µl	Pfu polymerase
to 50µl	ddH$_2$O

LA TAQ PCR REACTION	
5µl	10xbuffer (Mg^{2+} free)
5µl	MgCl$_2$ (25mM)
4µl	dNTPs Mix (2.5mM each)
0.8µl	forward primer (50µM)
0.8µl	reverse primer (50µM)
3µl	DNA template (150 to 450ng)
0.5µl	LA Taq polymerase
to 50µl	ddH$_2$O

LA TAQ PCR REACTION for GC-rich regions	
25µl	2x GC buffer
8µl	dNTPs Mix (2.5mM each)
0.8µl	forward primer (50µM)
0.8µl	reverse primer (50µM)
3µl	DNA template (150 to 450ng)
0.5µl	LA Taq polymerase
to 50µl	ddH$_2$O

For PCR reactions with Pfu polymerase the hot start method was used (addition of the enzyme after denaturation), while the cold start method (addition of the enzyme on ice) was used for PCR reactions with LA Taq polymerase. Following PCR programs were used:

PFU PCR PROGRAM	
94°C	3min
80°C	hold, add Pfu polymerase
start cycle 30x	
94°C *58°C 72°C	25sec 25sec **1min 15sec
end cycle	
72°C	10min
4°C	infinite

LA TAQ PCR PROGRAM	
94°C	3min
start cycle 30x	
94°C *56°C 72°C	30sec 30sec **1min 15sec
end cycle	
72°C	10min
4°C	infinite

*depends on the melting temperature of the primer
 **depends on the length of the amplifying fragment

4.1.17 Blunting of DNA fragments

Whereas Pfu DNA polymerase generates blunt-ended PCR fragments, LA Taq DNA polymerase or restriction digestion produces sticky-ended DNA fragments. DNA polymerases such as Klenow (fragment of *E. coli* DNA polymerase I) or T4 DNA polymerase were used to create blunt ends from cohesive ends. The exo$^-$ (exonuclease-free) Klenow fragment, which exhibits 5'→3' polymerase activity, but lacks both the 3'→5' and the 5'→3' exonuclease activities, was used for filling in the 5'-protruding (3' recessed) ends. The T4 DNA polymerase was used for its 5'→3' polymerase activity to fill 5'-protruding ends and for its 3'→5' exonuclease activity to remove 3' overhangs. For exo$^-$ Klenow and T4 DNA polymerases following reactions were prepared:

EXO$^-$ KLENOW FRAGMENT REACTION	
2µl	10xKlenow reaction buffer
1µl	dNTPs Mix (2.5mM each)
12µl	DNA eluate
1µl	exo$^-$ Klenow
to 20µl	ddH$_2$O
incubate the reaction for 10min at 30°C	

T4 DNA POLYMERASE REACTION	
10µl	5x reaction buffer
2µl	dNTPs Mix (2.5mM each)
20µl	DNA eluate
0.5µl	T4 DNA polymerase
to 50µl	ddH$_2$O
incubate the reaction for 20min at 11°C	

For further downstream applications the blunt-ended DNA fragments were purified using the Invisorb® DNA CleanUp kit. The procedure is described in chapter 4.1.14.

4.1.18 Dephosphorylation and Phosphorylation

In order to prevent self-ligation of cut DNA fragments, 5' phosphates were removed with the help of calf intestinal alkaline phosphatase (CIP) (Roche Diagnostics). After gel extraction, DNA fragments obtained from either a restriction enzyme digestion or PCR amplification were dephosphorylated in two different ways, depending on their nature (blunt ends or sticky ends). The dephosphorylation reaction for sticky-ended DNA fragments was as follows:

DEPHOSPHORYLATION REACTION for sticky end DNA fragment	
3µl	10xCIP buffer
26µl	DNA eluate
1µl	CIP
1h at 37°C	

After the dephosphorylation reaction, the DNA fragment was purified using the kit Invisorb® DNA CleanUp. The purification steps are described in detail in chapter 4.1.14. To dephosphorylate blunt-ended DNA fragments, a stepwise dephosphorylation was performed followed by purification as for the sticky end DNA fragment.

DEPHOSPHORYLATION REACTION FOR BLUNT ENDED DNA FRAGMENT
adding of 3µl 10xCIP buffer and 1µl CIP to the DNA eluate and incubation for 15min at 37°C
incubation for 15min at 56°C by adding 0.5µl CIP after 1min
incubation for 15min at 37°C by adding 0.5µl CIP after 1min
incubation for 15min at 56°C by adding 0.5µl CIP after 1min

PHOSPHORYLATION REACTION for sticky end DNA	
3µl	10xT4 ligase buffer
26µL	DNA eluate
1µl	T4 PNK
1h at 37°C	
20min at 65°C	

On the other hand a phosphorylation of one of the DNA fragments (insert or vector) is required in order to enable ligation of the two DNA fragments. The T4 Polynucleotide Kinase (PNK) catalyzes the phosphorylation reaction by transferring the γ-phosphate of ATP to the 5'-end of the DNA fragment.

The phosphorylation reaction was performed and followed by quantitative gel analysis.

4.1.19 Ligation

The procedure creating covalent phosphodiester bonds between the 3' hydroxyl of one and the 5' phosphate of another linear DNA fragment is called ligation. Both sticky and blunt end ligations were used during the cloning steps. After estimating the concentrations of the DNA fragments (ng/µl) using quantitative agarose gel analysis, the following formula was used to define the amount of the DNA fragments for a ligation:

$$Insert\ amount\ (\mu l)\ per\ 1\mu l\ vector = \frac{3 \times vector\ amount\ (ng) \times insert\ length\ (base\ pair)}{vector\ length\ (base\ pair) \times insert\ concentration\ (ng/\mu l)}$$

Sticky and blunt end ligation reactions differed slightly as shown in the following:

BLUNT END LIGATION APPROACH		
	negative control	ligation
vector	100 - 250ng	
insert	-	according to formula
10xT4 ligase buffer	1µl	
T4 ligase	1µl	
ddH$_2$O	to 10µl	
overnight at 16°C		

STICKY END LIGATION APPROACH		
	negative control	ligation
vector	100 - 250ng	
insert	-	according to formula
ddH$_2$O	to 10µl	
5min at 45°C→1min on ice		
10xT4 ligase buffer	1µl	
T4 ligase	1µl	
overnight at 16°C		

After overnight ligation, the ligation product was transformed into the chemo-competent DH5α bacteria, described in chapter 4.1.3.

4.1.20 Control of the directional cloning

Every amplified target DNA fragment or ligation product was subcloned into the plasmid pBluescript II SK+. After DNA amplification and isolation using the QIAGEN Plasmid Mini Kit, a restriction enzyme digestion was performed with restriction enzymes specific for a desired direction. Thereafter, the appropriate DNA was amplified, isolated with the QIAGEN Plasmid Midi Kit and sent for sequencing by Eurofins MWG Operon. Analysis of sequencing results was performed with the DNASTAR software.

4.2 Mouse embryonic stem cell culture and establishing the mouse models Npr2LacZ and Npr2CreERT2

Homologous recombination in embryonic stem (ES) cells was used to introduce targeted mutations and to generate the Npr2LacZ and Npr2CreERT2 mouse models. Handling of ES cell culture was based on the following literature: *Manipulating the Mouse Embryo: a Laboratory Manual* (Nagy et al. 2002) and *Laboratory protocols for conditional gene targeting* (Torres and Kuhn 1997). The experimental procedures for working with ES cells are described in the following chapters and Figure 4.1 gives an overview of individual steps to generate mutant mouse strains.
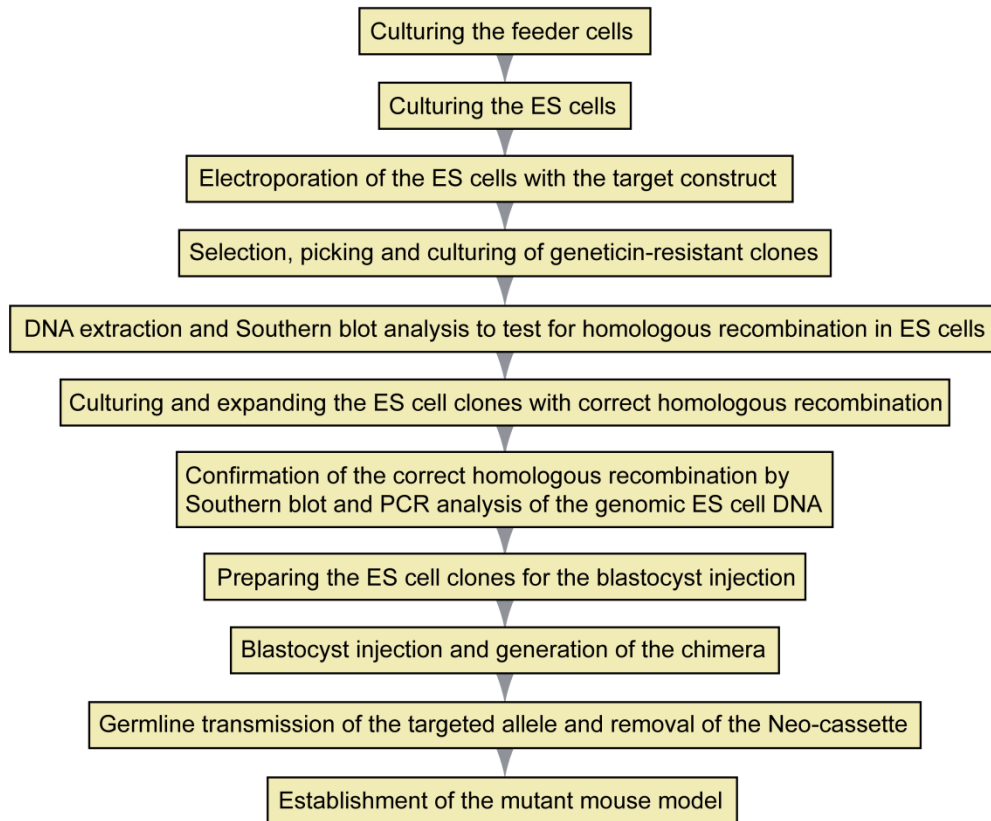
Figure 4.1: Outline of the experimental procedure to generate the mutant mouse strains.

4.2.1 Culturing of feeder cells

The mouse embryonic fibroblast (MEF) cells derived from mouse strains containing a *Neo* expression cassette were used as feeder cells and obtained from the group of Prof. Carmen Birchmeier-Kohler. Frozen feeder cells were thawed rapidly by adding pre-warmed feeder medium and transferring the cell suspension into a 10ml Falcon tube filled with pre-warmed feeder medium. Subsequently, the cells were centrifuged at 150g for 4min. The cell pellet was then resuspended in 10ml feeder medium and seeded on a 15cm cell culture dish as passage '-2P'. The cells were grown for 4 days changing the medium every second day. To split the feeder cells, they were washed twice with 1xPBS, then trypsinized in 3ml trypsin-EDTA and incubated for 4min at 37°C. After adding the feeder medium and transferring the cells into a Falcon tube, they were centrifuged at 150g for 4min. After supernatant removal, the pellet was resuspended in feeder medium and seeded onto four 15cm cell culture dishes as passage '-1P'. The cells were split at a ratio of 1:4 up to passage '2P', while cells in passage '0P' and '1P' were frozen in between.

To freeze the feeder cells, they were treated as described above for the splitting, but after the centrifugation the pellet was resuspended in 5ml freezing medium. Then 1ml aliquots were dispensed into pre-chilled cryovials and frozen at -80°C. To inactivate the mitosis of the feeder cells, the 15cm cell culture dish with confluent passage '2P' cells was treated

with mitomycine C at a final concentration of 10µg/ml in feeder medium for 2h at 37°C. Thereafter, the cells were either frozen as described above or washed with feeder medium to seed on three 10cm cell culture dishes. At this state the inactivated cells were used as feeders for ES cell culture. The cells were seeded on a corresponding number of plates: 1x15cm dish equates to 3x10cm dishes, 3x6 / 4x12 / 4x24 / 4x48 or 3x96-well plates. The dishes or plates with a feeder layer from now on will be designated feeder dishes or feeder plates.

4.2.2 Culturing of ES cells

The three different ES cell lines used in this study (see Table 3.4) were all grown under the same conditions (same ES cell medium and at 37°C). Working with ES cells requires daily change of the ES cell medium and the presence of Leukemia Inhibitory Factor (LIF) to prevent the differentiation of the cells.

The frozen cells were thawed as described for the feeder cells but using ES cell medium. After centrifugation and removal of the supernatant the ES cell pellet was resuspended in 5ml ES cell medium. Afterwards, the cells were seeded either onto a 6-well feeder plate or a 10cm feeder dish (depending on the dish size, from which the cells were frozen). The ES cells were grown for 1-2 days and then split at a ratio of 1:2 or 1:3 plating them onto 10cm feeder dishes (see the splitting procedure of the feeder cells). The ES cells were grown to get dense (not confluent) cultures with nicely rounded and sharp bordered ES cell clones, which were used for electroporation. The freezing procedure of the ES cells was similar to that of the feeder cells (see chapter 4.2.1).

4.2.3 Electroporation of ES cells

For the electroporation of the targeting construct into the ES cells, the DNA was linearized by a restriction enzyme digestion reaction. Linearization of both targeting constructs used in this study was carried out using the restriction enzyme PacI. The digestion reaction was as follows:

TARGETING CONSTRUCT DIGESTION REACTION FOR THE ELECTROPORATION	
20µl	10xbuffer 1
2µl	BSA (10mg/ml)
50-100µg	DNA
3µl	PacI
to 200µl	ddH$_2$O

After overnight digestion at 37°C, the completed digestion was verified by 1% agarose gel electrophoresis, applying an aliquot of 5µl digestion reaction mixed with 0.5µl 10xDNA loading buffer on the agarose gel.

The DNA was then purified by a phenol-chloroform-isoamyl alcohol extraction, which is similar to the BAC DNA purification described in chapter 4.1.10. In brief, an equal volume of phenol-chloroform-isoamyl

alcohol was added to the digestion reaction, vortexed and centrifuged. After carefully transferring the upper phase into a new tube, 1/10 volume of 3M sodium acetate was added to the solution and vortexed. Then 2.5 volumes of ice-cold 100% ethanol were added, mixed by vortexing and placed at -80°C for 15min. The solution was then centrifuged for 5min at 12.000g and the supernatant was removed. The pellet was washed twice by adding 1ml 70% ethanol, inverting several times and centrifuging as before. The DNA pellet was air dried and diluted in 1xPBS. The DNA concentration was determined using a spectrophotometer and adjusted to 1µg/µl. 25-35µg of DNA were used per electroporation.

The ES cells were prepared for the electroporation as follows: the grown ES cells described in chapter 4.2.2 were washed with 1xPBS, trypsinized with 300µl trypsin-EDTA and centrifuged as in the splitting procedure (chapter 4.2.1). The cell pellet was resuspended thoroughly in 10ml ES cell medium and 10µl of the resuspension was applied to a Neubauer cell counting chamber. The 10ml cell solution was centrifuged again at 150g for 4min and the pellet was resuspended in 1xPBS to a final concentration of 10^7 ES cells/800µl PBS.

For the electroporation 780µl ES cells and 25-35µg DNA were gently mixed in a 1.5ml tube. The mixture was transferred to an electroporation cuvette with a 0.2cm gap width, avoiding air bubbles. The electroporation was carried out at 280V and 500µF. Thereafter, the cuvette was cooled on ice for 10min. The mixture was transferred to a Falcon tube filled with ES cell medium. Cells were centrifuged at 150g for 4min, resuspended in 6ml ES cell medium and plated onto three 10cm feeder dishes filled with 6ml fresh ES cell medium.

4.2.4 Selection, picking and culturing of geneticin resistant clones

After the electroporation and plating, ES cells were grown for 2 days in ES cell medium without G418. From the third day onwards the ES cells were selected in the presence of 400µg/ml geneticin (G418). G418-resistant ES cell clones were round and displayed sharp borders. Eight days after the electroporation, single G418-resistant clones were picked under the microscope using a 200µl pipette adjusted to 25µl. Each ES cell clone was placed into one well of a 96-well plate. Then, 30µl trypsin-EDTA were added to the clones using the 8-multichannel pipette and incubated for 4min at 37°C. Thereafter, 100µl ES cell medium supplemented with G418 were added to the wells and the ES cell clones were singularized by pipetting up and down twenty times. The clones were then transferred to a 96-well feeder plate filled with 100µl ES cell medium and grown at 37°C

for 2-3 days (dependent on the cell density). The ES cell clones were then splitted into a 96-well feeder plate as described above by washing the wells twice with 100µl 1xPBS prior to trypsinization. After 2-3 days, the ES cell clones in 96-well feeder plate were splitted into one 96-well feeder plate and one 96-well gelatin plate (a 96-well plate covered with 0.1% (v/v) gelatin solution). Those cells in the 96-well gelatin plate were duplicated by splitting into two 96-well gelatin plates. These ES cell clones were overgrown to extract as much DNA as possible. ES cells clones from the 96-well feeder plate were trypsinized. After addition of 100µl ES freezing medium cells were singularized by pipetting up and down ten times. The plate was wrapped in papers, placed in a Styrofoam box and frozen at -80°C for 2-3 months.

4.2.5 Extraction of genomic ES cell DNA

To extract DNA from the ES cell clones grown in 96-well gelatin plates, the cells were washed twice with 100µl PBS and 50µl ES lysis buffer containing proteinase K at a final concentration of 200µg/ml was added to each well. The top of the plate was sealed with parafilm. The plate was then placed into a plastic box, covered with wet papers and incubated overnight at 55°C. The next day, 140µl of pre-chilled 3M sodium acetate were added to each well and the plate was incubated overnight at 4°C. The 96-well plates were inverted carefully to discard the supernatant and separate the DNA precipitate. The DNA was washed three times by adding 100µl 70% ethanol, dried and stored at RT.

DNA was also extracted from expanded ES cell clones on a 6-well plate. The cells were trypsinized and centrifuged as described in chapter 4.2.1. The cell pellet was then resuspended in 300µl ES lysis buffer and proteinase K was added to a final concentration of 200µg/ml. Cell lysis was performed with gentle shaking overnight at 55°C. The next day, the DNA was purified using the phenol-chloroform-isoamyl purification method described in chapter 4.2.3 and the concentration was determined using a spectrophotometer.

4.2.6 Southern blot analysis of homologous recombination

In order to screen for homologous recombination between the target construct and the target locus in the ES cell genome, the following steps were performed:

1. **Digestion of the genomic DNA to generate two distinct DNA fragments of the target construct, which are recognized by radioactively labeled DNA probes.**

To digest genomic ES cell DNA in a 96-well plate, the following reaction mixture was prepared:

GENOMIC DNA DIGESTION IN A 96-WELL PLATE	
0.5ml	10xbuffer 4
25µl	RNaseA (10mg/ml)
0.15ml	PstI-HF
4.325ml	ddH$_2$O

From the reaction mixture 45µl were pipetted into each well and the plate was sealed with parafilm. The plate was then placed into a plastic box with wet papers and incubated overnight at 37°C with gentle shaking. The next day, 5µl 10xloading buffer were added to each well and digested DNA was separated by agarose gel electrophoresis.

A general restriction enzyme digestion reaction of genomic DNA was as follows:

GENOMIC DNA DIGESTION	
6µl	10xbuffer 4
0.15µl	RNaseA (20mg/ml)
2.75µl	PstI-HF
10-20µg	DNA
to 60µl	ddH$_2$O

This digestion reaction was used to confirm the desired homologous recombination both in the ES cell genome (after expanding the ES cell culture) and in the mouse genome (after generating the mouse models with the targeted mutations). The digestion was performed in a 1.5ml tube as described above.

2. Electrophoresis of the genomic DNA for Southern blot analysis

The agarose gel electrophoresis of the genomic DNA was performed in the horizontal Maxigel system. A 1% agarose gel was prepared as described in Table 3.1 (v=500ml, no ethidium bromide). Different combs were used to apply the DNA to the gel; three combs with 36 teeth and 1.5mm thickness were used to apply 25µl digestion reaction per well of the 96-well plate, one or two combs (dependent on the number of the reactions) with 16 teeth and 1.5mm thickness were used to apply 60µl digestion reaction of the rescreening. 15µl of a 1kb DNA ladder were loaded as a control and electrophoresis was performed overnight at 25V. The next day, agarose gel was prepared for the DNA transfer onto the nylon Hybond N+ membrane.

3. Blotting

After electrophoresis, the gel was carefully transferred to a melanin dish filled with 300ml ddH$_2$O and 15µl ethidium bromide and incubated with gentle shaking at RT. To visualize the DNA, the gel was photographed using the Gel Doc system. Thereafter, the gel was washed twice with ddH$_2$O (15min each on a rotary shaker). DNA depurination was carried out for exactly 8min in 250ml of depurination buffer. After depurination, the gel was washed twice with ddH$_2$O (5min each). DNA denaturation was carried out for 15min in 250ml of denaturation buffer. The buffer was renewed and the gel was incubated in denaturation buffer for another 15min. In the meantime, the fitted nylon Hybond N+ membrane was incubated in water and in 10xSSC buffer (5min each). The denaturation

buffer was decanted and the gel was incubated in 250ml 20xSSC buffer for 5min. After decanting the 20xSSC buffer, the gel was put on the gel tray and another gel tray was placed on top, so that an inversion of the gel was possible. After inverting the gel, the prepared nylon Hybond N+ membrane was slid onto the gel and air bubbles were removed using a 20ml serological pipette. Three layers of fitted whatman paper soaked in 10xSSC buffer were placed onto the membrane followed by a stack of dry paper towels. A glass plate was placed onto the paper towels and the whole construction was inverted, so that it had the following order (from bottom to top): gel tray→ gel→ membrane→ whatman paper→ paper towel→ glass plate. A weight was placed onto the gel tray to fix the blotting construction. The DNA transfer was carried out overnight at RT. The next day, the membrane was washed twice for 5min in 2xSSC buffer and dried on whatman paper. It was then incubated for 2min in the UV crosslinker to cross-link the DNA to the material. The membrane was stored at RT until radiolabeling.

4. DNA detection by ^{32}P- radiolabeled probes

One critical step of Southern blot analysis is the design of DNA sequence specific for the desired target region of the genomic DNA. The DNA fragments used in this study were amplified from BAC DNA, cloned into pBluescript II SK+ and sequenced. Two DNA fragmnts were designed: one fragment with a short nucleic acid sequence binding to the genomic DNA at the 5'end, outside of the 5'homology arm and one fragment with a long sequence binding at the 3'end of the genomic DNA, outside and inside of the 3'homology arm.

To prepare the DNA fragments for radiolabeling, 3-5µg DNA (pBluescript II SK+ carrying the respective target sequence) were digested with HindIII and EcoRI. The size of the 3'probe DNA fragment was 1009bp, the size of the 5'probe DNA fragment was 657bp. The DNA fragments were separated by agarose gel electrophoresis and purified by gel extraction. An aliquot of the purified DNA fragment was analyzed by quantitative agarose gel electrophoresis. For the ^{32}P-radiolabeling of the fragments, the Prime-It® Random primer labeling kit was used. The required radiolabeled ^{32}P-dCTP was bought as a fresh solution on the day of use. DNA radiolabeling was carried out as follows:

1. *Preparation of DNA (50ng/µl) in a 1.5ml screw-cap tube.*
2. *Addition of ddH$_2$O to the dehydrated reaction mixture supplied with the kit, as to get a final volume of 42µl after mixing with DNA.*
3. *Preparation of another 1.5ml screw-cap tube with 10µg/µl sheared genomic DNA (10µl sheared genomic DNA with a concentration of 1µg/µl).*

The next steps were performed in the isotope lab.

4. *Denaturation of DNA in the 42µl reaction mixture for 10min at 95°C.*

5.   Addition of 5µl ^{32}P-dCTP and 3µl Magenta polymerase (supplied with the kit) to the hot 42µl DNA reaction mixture.

6.   Incubation for 10min at 37°C in a water bath.

7.   Addition of 2µl Stop mix (supplied with the kit): total volume = 52µl.

8.   Centrifugation of the G-50 spin column at 200g for 2min to remove the solution in the column and placement of the column into the tube with genomic DNA (see step 3).

9.   Application of the mix from step 7 to the G-50 spin column and centrifugation at 200g for 2min: total volume = 62µl.

10. Addition of 1ml Church buffer pre-warmed at 65°C.

11. Denaturation of the mixture for 10min at 95°C.

12. Incubation of the mixture in the screw cap tube for 30-120min at 65°C in the hybridization oven.

13. Filling of a hybridization glass bottle with 7ml church buffer pre-warmed at 65°C.

14. Soaking of the membrane in water and rolling of the membrane onto a 20ml serological pipette (DNA side of the membrane is showing inwards).

15. Deposition of the membrane on the wall of the hybridization glass bottle avoiding air bubbles between the glass and membrane.

16. Pre-hybridization of the membrane for 1h at 65°C in the hybridization oven.

17. Addition of the tempered mixture (see step 12) to the membrane and hybridization overnight at 65°C in the hybridization oven.

18. Decanting of the solution from the hybridization glass bottle and washing of the membrane first for 10min in 10ml Southern washing buffer I, then for 20min in Southern washing buffer II at 68°C.

19. Transfer of the membrane from the hybridization glass bottle to a lockable plastic box and sequential washing of the membrane in 10ml Southern washing buffer II, III, IV and V (10min each, at 68°C in a water bath, with shaking) until radioactivity is reduced to room background radioactivity (1Bq/cm^2), as measured by the contamination monitor.

20. Placement of the membrane onto a large smooth cling film with the DNA side facing towards the cling film.

21. Coverage of the back side of the membrane with whatman paper and a layer of copier foil and folding of the cling film to a closed envelope.

22. Placement of the envelope in a film cassette in the dark room.

23. Incubation for 5-7 days at -80°C. Thawing of the cassette at RT and development of the film in a developing machine.

4.2.7 Culturing and expanding ES cell clones with the correct homologous recombination

After identification of the correct homologous recombination in certain ES cells by primary Southern blot analysis, the corresponding duplicated and frozen ES cells in a 96-well plate were thawed. After thawing, the cell pellets were resuspended in 200µl ES cell medium and pipetted into a new 96-well feeder plate. After 2 or 3 days, the ES cell clones were visible. The medium was again exchanged daily and G418 was added freshly to the medium. The ES cells were then plated into 48-well feeder plates by trypsinizing and resuspending in 1ml ES cell medium. Cells were cultured as described above and after 2 days they were plated into 24-well feeder plates. Later, the ES cells were expanded in a 6-well feeder plates. The ES cells were also splitted and frozen between expansion steps (see chapters 4.2.1), so that several aliquots of the ES cell clone with correct homologous recombination were obtained.

4.2.8 Confirmation of the correct homologous recombination

To confirm the correct homologous recombination in the expanded ES cells, a secondary Southern blot analysis of the genomic ES cell DNA was performed. DNA extraction and Southern blot analysis are described in chapters 4.2.5 and 4.2.6. Additionally, the targeted mutation was confirmed by PCR analysis using the genotyping protocols for Npr2LacZ and Npr2CreERT2 mouse models described in chapters 4.3.3 and 4.3.5, respectively.

4.2.9 Blastocyst injection and generation of the chimera

Prior to blastocyst injection, positive ES cells were thawed and cultured for five days. An ES cell aliquot frozen from a 6-well plate was thawed, plated into a new 6-well feeder plate and cultured in the absence of G418. After two days of growing, the cells were splitted in a ratio of 1:3 onto a 6-well gelatin plate and on the fifth day the well was half-full with sharp rounded ES cell clones.

Blastocyst injections into C57Bl/6 mice were carried out by the Transgenic Core Facility of the Max Delbrück Center for Molecular Medicine. The ES cells were delivered to the facility in 300µl ES cell medium. Prior to delivery, ES cells were washed, trypsinized, resuspended in 2ml ES cell medium and incubated in 12-well plate for 45min at 37°C in order to roughly separate the feeder from ES cells. After 45min, the ES cell medium containing floating feeder cells was aspirated and the adherent ES cells were

resuspended in 300µl ES cell medium. Thereafter, the ES cells were immediately brought to the Transgenic Core Facility.

4.2.10 Germline transmission, removal of the Neo-cassette and establishing the mouse strains Npr2LacZ and Npr2CreERT2

The successful germline transmission was validated by the appearance of brown offspring after mating the chimeras with wildtype C57Bl/6 mice followed by PCR analysis of the inserted mutation. Additionally, to remove the Neo-cassette the Npr2CreERT2 chimeras were crossed with an Flp-deleter mouse strain and the brown offspring were analyzed by PCR, both for insertion of the mutation and for excision of the Neo-cassette. In case of the Npr2LacZ mouse model, the Neo-cassette was removed by expressing the self-excising Cre recombinase under the control of a germline-specific promoter (Bunting et al. 1999).

To reduce the genetic variability, the Npr2LacZ and Npr2CreERT2 mouse models were established by 7 or more backcross matings of the heterozygous mice with the C57Bl/6 mice. The genotypes were confirmed by PCR and Southern blot analysis using genomic DNA isolated from mouse tail and liver tissue, respectively. The isolation of genomic DNA for PCR analysis is described in chapter 4.3. To confirm the genotypes of the mouse models by Southern blot analysis (chapter 4.2.6), the genomic liver DNA was isolated using Genomic-tip 500/G, Genomic DNA Buffer Set, Proteinase K and RNase A from QIAGEN according to the supplied protocol.

4.3 Mouse genotyping

Isolation of mouse genomic DNA from tails or embryonic tissue was carried out using the High Pure PCR Template Preparation Kit according to the manufacturer's instructions. The only difference was the elution volume: in case of tail biopsies the DNA was eluated in 50µl elution buffer and in case of embryonic tissue in 30µl elution buffer.

The genotyping protocols for the mouse strains used in this study are described in the following chapters. The primers were purchased from MWG Eurofins Operon. The lyophilized primers were diluted in ddH$_2$0 to a concentration of 50µM and stored at -20°C.

The hot-start PCR method was used as indicated; otherwise the polymerase was added to the reaction mixture on ice. The genotyping of the mouse strains was carried out using Taq DNA polymerase supplied with 10xbuffer and 50mM MgCl$_2$. In all PCR protocols a 2.5mM dNTPs Mix was used.

In the multiplex PCR reactions the forward primer is common for wildtype and mutant DNA sequences, while the reverse primers are binding specifically to either the wildtype or

the mutated DNA sequence. After the PCR reaction, 10xDNA loading buffer was added to the reaction mixture and samples were analyzed by agarose gel (2%) electrophoresis.

4.3.1 Genotyping of the Flp-deleter mouse strain

PRIMER NAME	PRIMER SEQUENCE
Forward primer Flp (P1)	CTAATGTTGTGGGAAATTGGAGC
Reverse primer Flp (P2)	CTCGAGGATAACTTGTTTATTGC

30µl REACTION MIXTURE	
3µl	10xbuffer
0.75µl	dNTPs Mix
0.9µl	MgCl$_2$
0.4µl	P1
0.4µl	P2
2µl	DNA
0.25µl	Taq
22.3µl	ddH$_2$O

PCR PROGRAM	
95°C	5min
58°C	3min
72°C	5min
	start cycle 35x
90°C	30sec
58°C	1min
72°C	1min
	end cycle
4°C	infinite

REACTION PRODUCT
600bp

4.3.2 Genotyping of the Z/AP mouse strain

PRIMER NAME	PRIMER SEQUENCE
Forward primer Z/AP (P1)	TCCGCGTTACATAACTTACGG
Reverse primer Z/AP (P2)	ATGGGGAGAGTGAAGCAGAAC

30µl REACTION MIXTURE	
3µl	10xbuffer
1.5µl	dNTPs Mix
1.8µl	MgCl$_2$
0.2µl	P1
0.2µl	P2
3µl	DNA
0.25µl	Taq
20.05µl	ddH$_2$O

PCR PROGRAM	
95°C	4min
	start cycle 35x
95°C	45sec
58°C	30sec
72°C	40sec
	end cycle
72°c	7min
4°C	infinite

REACTION PRODUCT
347bp

4.3.3 Genotyping of the Npr2LacZ mouse strain

PRIMER NAME	PRIMER SEQUENCE
Forward primer wt-LacZ (P1)	TGCCACCCTATCCTTAGTCC
Reverse primer wt (P2)	GTGTTCTGGCAGCACCAC
Reverse primer LacZ (P3)	TCGCTATTACGCCAGCTG

25µl REACTION MIXTURE	
2.5µl	10xbuffer
2µl	dNTPs Mix
0.75µl	MgCl$_2$
0.4µl	P1
0.4µl	P2
0.4µl	P3
2.5µl	DNA
0.25µl	Taq
15.8µl	ddH$_2$O

PCR PROGRAM	
94°C	3min
80°C	hold, add Taq polymerase
start cycle 30x	
94°C	30sec
57°C	30sec
72°C	30sec
end cycle	
72°C	10min
4°C	infinite

REACTION PRODUCT	
wildtype	348bp
heterozygous	398bp 348bp
knockout	398bp

4.3.4 Genotyping of the Npr2(cn) mouse strain

PRIMER NAME	PRIMER SEQUENCE
Forward primer Npr2cn (P1)	TTCACAGCGCTGTCAGCTGAG
Reverse primer Npr2cn (P2)	ACTTAGGGAGCGCTGACTGTGG

25µl REACTION MIXTURE	
2.5µl	10xbuffer
2µl	dNTPs Mix
0.75µl	MgCl$_2$
2µl	P1
2µl	P2
5µl	DNA
0.25µl	Taq
10.5µl	ddH$_2$O

PCR PROGRAM	
95°C	3min
80°C	hold, add Taq polymerase
start cycle 35x	
94.5°C	35sec
62°C	25sec
72°C	35sec
end cycle	
72°C	10min
4°C	infinite

The PCR product was digested in a subsequent digestion reaction for 2h at 37°C.

DIGESTION REACTION	
22µl	PCR product
2.5µl	10xbuffer
0.25µl	100xBSA
0.25µl	restriction enzyme Afl III

REACTION PRODUCT	
wildtype	348bp
heterozygous	348bp, 188bp, 160bp
knockout	188bp and 160bp

4.3.5 Genotyping of the Npr2CreERT2 mouse strain

PRIMER NAME	PRIMER SEQUENCE
Forward primer wildtype-CreERT2 (P1)	CTCAGATTCCTCCCTTCTCG
Reverse primer wildtype (P2)	GGCATAGCTCAGGTTGTGTT
Reverse primer CreERT2 (P3)	TTGGACATGGTGGAATTCAT

25µl REACTION MIXTURE	
2.5µl	10xbuffer
2µl	dNTPs Mix
0.75µl	MgCl$_2$
0.4µl	P1
0.4µl	P2
0.4µl	P3
2.5µl	DNA
0.25µl	Taq
15.8µl	ddH$_2$O

PCR PROGRAM	
94°C	3min
80°C	hold, add Taq polymerase
start cycle 30x	
94°C	30sec
57°C	30sec
72°C	30sec
end cycle	
72°C	10min
4°C	infinite

REACTION PRODUCT	
wildtype	456bp
heterozygous	456bp 356bp
knockout	356bp

In order to examine whether the Flp recombinase deleted the Neo-cassette flanked by FRT-sites, the following protocol was used:

PRIMER NAME	PRIMER SEQUENCE
Forward primer FRT site (P4)	CGGAAAGAACCCTGCAGATA
Reverse primer FRT site (P5)	GCTTTCCCAATCAAACCTGA

25µl REACTION MIXTURE	
2.5µl	10xbuffer
2µl	dNTPs
0.75µl	MgCl$_2$
0.4µl	P1
0.4µl	P2
2µl	DNA
0.25µl	Taq
16.7µl	ddH$_2$O

PCR PROGRAM	
94°C	3min
80°C	hold, add Taq polymerase
start cycle 35x	
94°C	30sec
57°C	30sec
72°C	2min 30sec
end cycle	
72°C	10min
4°C	infinite

REACTION PRODUCT	
deleted	469bp
not deleted	2288bp

4.3.6 Genotyping of the mGFP mouse strain

PRIMER NAME	PRIMER SEQUENCE
Forward primer mGFP (P1)	CAGGACAGTCGTTTGCCGTCTGA
Reverse primer mGFP (P2)	CAGAGGATGATGCTCGTGACGG

25µl REACTION MIXTURE	
2,5µl	10xbuffer
2µl	dNTPs
0.75µl	MgCl$_2$
0.4µl	P1
0.4µl	P2
2µl	DNA
0.25µl	Taq
16.7µl	ddH$_2$O

PCR PROGRAM	
95°C	3min
start cycle 34x	
94.5°C	45sec
58°C	30sec
72°C	40sec
end cycle	
72°c	5min
4°C	infinite

REACTION PRODUCT
600bp

4.4 Histology

Histological analyses were performed by means of whole mount tissue preparation and cryosectioning of the tissue at different embryonic, postnatal and adult stages of mouse development. For the analysis at embryonic stages of development, the females were checked for a vaginal plug to determine if mating had occurred. The procedure is termed from now on as timed pregnant mice. If a plug was visible, the embryonic day (E) was determined as E0.5 and the embryonic days were counted and determined as E9.5, E10.5, E11.5, E12.5, E13.5 and E14.5 until E17.5. The day of birth was defined as P0 and the successive postnatal days (P) of development as P5, P10, P15, P20 and P25. Mice at these postnatal stages of development and also adult mice were perfused with Zamboni's fixative (recipe in Table 3.1) to dissect the brain and the spinal cord. The different staining methods and corresponding tissue preparation are described in the following chapters.

4.4.1 Detection of the β-galactosidase activity: X-Gal staining on the whole mounts

At the appropriate day of embryonic development, the timed pregnant mouse was euthanized by cervical dislocation. The abdominal coat was soaked with 70% ethanol and cut to open the abdominal cavity. The entire uterus containing all embryos was dissected out and transferred to a Petri dish with ice-cold 1xPBS. Under the Stemi DRC stereomicroscope single embryos were dissected out from the uterus by occasionally changing the Petri dish with fresh ice-cold 1xPBS. The dissected embryos were transferred into a 12-well plate with ice-cold 1xPBS, while the corresponding amnion of each embryo was transferred to a 1.5ml tube for genotyping (chapter 4.3). After transferring all embryos to a 12-well plate, another 12-well plate was filled with the X-Gal fixative (recipe in Table 3.1). Since the activity of the β-galactosidase is sensitive to fixation, distinct fixation times were used to fix whole embryos of different age and size (Table 4.2).

Table 4.2

AGE	FIXATION TIME
E9.5	30min
E10.5	45min
E11.5	1h
E12.5	1h 30min
E13.5	2h

After fixation with gentle shaking at RT, the embryos were transferred to a 12-well plate containing X-Gal washing buffer (recipe in Table 3.1). The embryos were washed for 90min, renewing the buffer three times. Thereafter, the embryos were incubated overnight in the X-Gal staining solution (recipe in Table 3.1) at RT with gentle shaking and protected from light. The next day, the embryos were washed in 20mM $MgCl_2$ for 90min, renewing the solution three times. The embryos were postfixed in 4% PFA (recipe in Table 3.1) for 60min at 4°C and then washed in

1xPBS for 60min, renewing the PBS three times. The embryos were stored at 4°C with gentle shaking until the imaging or clearing.

4.4.2 Clearing and imaging of the whole mounts

The X-Gal stained mouse embryos at embryonic stages E11.5, E12.5 and E13.5 were cleared in a solution containing 4M urea, 10% (v/v) glycerol and 0.1% (v/v) Triton X-100. Embryos were incubated in this solution for 4 days at 4°C. Thereafter, embryos were incubated in a solution containing 8M urea and 0.1% (v/v) glycerol for 4 days at 4°C. If a clearance was observable, embryos were imaged, if not, embryos were incubated again in the first solution with 4M urea, 10%(v/v) glycerol and 0.1% (v/v) Triton X-100 for a week or longer until the desired clearance was achieved. In case of a longer incubation, the solution was renewed several times.

The imaging of the whole mount mouse embryos was carried out using a 6cm dish with a 0.5% agarose layer, a stereomicroscope Stemi SV11 with AxioCam camera, a light panel and gooseneck lights. The embryos were placed onto the dish and covered with 1xPBS. After adjusting the light and embryo position, the embryos were imaged using the AxioVision3.1 software.

4.4.3 Detection of the β-galactosidase activity: X-Gal staining on cryosections

β-galactosidase activity was detected on cryosections of embryonic, postnatal and adult tissues. The fixation of the mouse embryonic tissue was carried out by separating the head and torso of the embryo, whereas the postnatal and adult tissues were dissected and fixed after the perfusion of the mouse. The mouse embryos were dissected as described in chapter 4.4.1 and the head and torso were separated after dissecting the embryo from the uterus. The tissues were transferred to a 5ml screw cap glass vial with Zamboni's fixative (recipe in Table 3.1) and fixed for a defined time scale dependent on the tissue's age and size as indicated in Table 4.3. Likewise, the postnatal and adult tissues were fixed after mouse perfusion and dissection.

The fixation was performed under rotating conditions at RT. Thereafter, the tissues were transferred to a 5ml screw cap glass vial with 1xPBS and washed renewing the PBS several times. To clear the tissue from the yellow color of Zamboni's fixative, an overnight washing step was performed at 4°C with gentle rotation. The larger tissues were washed for two days. After washing, the tissues were transferred into a 30% (w/v) / 1xPBS sucrose solution and incubated overnight at 4°C with gentle shaking. For embedding, the tissues were immersed shortly in ddH$_2$O, then transferred into a Petri dish and the solution

was carefully removed with a paper towel. Different silicon rubber embedding molds matching the tissue size were used to embed the tissues. Half of the embedding mold was filled with Tissue-Tek® O.C.T. compound and the tissue was placed there, taking notice of the precise orientation of the tissue. The tissue was then covered with Tissue-Tek® O.C.T. compound avoiding air bubbles. The embedding mold was then placed on dry ice until the embedding medium solidified. The frozen tissue blocks were stored at -80°C until cryosectioning.

Table 4.3

AGE	TISSUE	FIXATION TIME
E11.5	head and torso	1h 30min
E12.5	head and torso	1h 30min
E13.5	head and torso	1h 45min
E14.5	head and torso	2h
E17.5	head and torso	2h 30min
P0	brain, spine and eyes	2h
P5	brain, spine and eyes	2h 30min
P10	brain, spine and eyes	3h
P15	brain, spine and eyes	4h
P20	brain, spine and eyes	5h
P25	brain, spine and eyes	6h
adult	brain, spine and eyes	6h 30 min

β-galactosidase activity was detected on cryosections with a thickness of 25µm immobilized on SuperFrost Ultra Plus® slides (Thermo Scientific). After sectioning, the cryosections were dried for 4-5h at RT. Thereafter, they were either frozen at -20°C for later use (frozen sections should be dried for 30min at RT before usage) or directly prepared for X-Gal staining. For X-Gal staining the slides were placed in a glass cuvette with X-Gal washing buffer and washed for 30min, renewing the buffer three times and shaking slowly. Staining was carried out overnight at RT in the X-Gal staining solution. The next day, the slides were washed for 30min with 20mM $MgCl_2$, renewing the solution three times, then treated similarly with 1xPBS. Slides were immerged in ddH_2O and excess fluid was removed with tissue paper. Sections were mounted using a few drops of Immu-mount™ and 50mm cover slips. After hardening of the Immu-mount™ for several hours, the edges of the cover slip were encircled with nail polish to prevent the admission of air bubbles. Slides were stored at 4°C and imaged using a Keyence fluorescence microscope.

4.4.4 Immunohistochemistry on cryosections

For immunohistochemical analyses the tissues were fixed, embedded and stored as described in chapter 4.4.3. Immunohistochemistry studies were performed with cryosections of 15µm thickness placed onto SuperFrost Ultra Plus® slides. The used antibodies and applied concentrations are listed in Table 3.8. The procedure for the immunostaining of cryosections was as follows:

1.   *Encircling of sections using a PAP-pen liquid blocker (Science Services).*
2.   *Addition of 300µl Immuno-blocking buffer (Table 3.1), blocking for 1h at RT.*

3.   *Removal of the blocking buffer and addition of the primary antibody diluted in 300µl blocking buffer.*

4.   *Incubation overnight at 4°C.*

5.   *Washing of slides with Immuno-washing buffer (recipe in Table 3.1) for 30min, renewing the buffer three times.*

6.   *Addition of the appropriate fluorophore-conjugated secondary antibody, diluted in 300µl blocking buffer, incubation for 2h at RT protected from light.*

7.   *Washing of slides with Immuno-washing buffer for 30min, renewing the buffer three times.*

8.   *Washing of slides with 1xPBS for 10min, renewing the buffer two times.*

9.   *Mounting of slides using Immu-mount™.*

A double or triple immunostaining was performed by serial addition of the primary antibodies and their appropriate secondary antibodies. Slides were stored at 4°C protected from light and imaged using a Zeiss LSM710 confocal microscope.

4.4.5 Detection of alkaline phosphatase (AP) activity on whole mounts and vibratome sections

The AP activity was detected on whole mount preparations of the spinal cord with attached DRG. After dissection of E12.5 or E13.5 embryos as described in chapter 4.4.1, the head and the torso were separated. The torso was used for whole mount preparations of the spinal cord with DRG as visualized in *DiI-Labeling of DRG Neurons to Study Axonal Branching in a Whole Mount Preparation of Mouse Embryonic Spinal Cord* (Schmidt and Rathjen 2011). In the meantime, the head was transferred to a 12-well plate with AP fixative and fixed for 1h in case of E12.5 or for 1.5h in case of E13.5 at RT with gentle shaking. The dissected spinal cords with DRG were fixed for 30min at RT. Thereafter, both tissues were transferred to a new 12-well plate with 1xPBS and heated at 65°C for 1h in the water bath to inactivate endogenous AP. The tissues were then rinsed in 1xPBS / 100mM $MgCl_2$ and incubated overnight at 4°C. The next day, the spinal cords with DRG were rinsed first in AP washing buffer for 30min at RT, then in AP staining solution. The staining was performed overnight at RT with shaking and protected from light. Thereafter, the spinal cords with DRG were washed in 1xPBS, postfixed overnight in 4% (v/v) PFA, cleared in 80% (v/v) glycerol / 1xPBS and embedded as described previously (Schmidt and Rathjen 2011). For imaging the Axiovert135 microscope was used.

The heads were transferred to 1xPBS and stored at 4°C until embedding in SeaKem® LE Agarose. Agarose was melted in 1xPBS (3.5% (w/v)) and the hot solution was filled into Peel-A-Way® disposable embedding molds (Polysciences, #18986) pre-chilled on ice.

After cooling of the agarose in the mold for 3min, the heads were bisected through the midline and were placed in separate molds. The embedded heads were cooled on ice for 30min. Thereafter, 250µm floating sections were made using the Vibratome VT1000S. Each section was placed into a well of a 24-well plate filled with 1xPBS. The sections were then washed in AP washing buffer for 30min at RT, transferred to AP staining solution and stained for several days at RT with gentle shaking and protected from light until the axons were visibly labeled. After staining, the sections were washed in 1xPBS and dehydrated using ethanol series (25%, 50%, 75%, 100% (v/v); each step was carried out for 20min at RT, only the last step was carried out overnight at -20°C). After dehydration, the sections were cleared in 1:2 benzyl alcohol/benzyl benzoate (BABB). The floating sections were imaged in BABB using glass dishes and a Zeiss microscope and AxioVision3.1 software. Sections were stored at 4°C in 100% ethanol.

4.5 Administration of 4-hydroxytamoxifen (OHT) and tamoxifen

Cre recombinase activity was induced by oral application of the tamoxifen or OHT. Both tamoxifen and OHT were diluted in corn oil to the concentration of 20mg/ml and 10mg/ml, respectively. Tamoxifen was dissolved by incubation at 37°C for several hours with rigorous shaking / occasional vortexing and protected from light. Aliquots of 400µl were stored at -20°C for four weeks. OHT was first mixed with pure ethanol (1/8 of the end volume), and then corn oil was added. The dissolution of OHT was performed by heating to 50°C and sonicating for 30min. Aliquots of 150µl were stored at -20°C protected from light and thawed freshly before use by sonicating at 37°C for 7min.

Both tamoxifen and OHT were orally administered using reusable feeding needles (Fine Science Tools, #18060-20) attached to a 1ml syringe. Tamoxifen was applied at a concentration of 0.1mg per gram body weight, whereas OHT was applied at the range of 0.002mg to 0.04mg per gram body weight. Tamoxifen and OHT were applied to timed pregnant mice at E9.5 or 10.5. The mice were weighed both on the application day and on the plug day. In case of a weight difference of 2-2.5 grams, a pregnancy was likely. A standard volume of 250µl was applied to the timed pregnant mice by mixing tamoxifen or OHT of a desired concentration with the corn oil prior to administration.

4.6 Mouse perfusion

Mice at developmental stages P0, P5, P10, P15, P20, P25 and adults were perfused before dissecting the brain, eyes and spine. The mice were anesthetized by

intraperitoneal injection of the anesthetic mixture (recipe in Table 3.1, 8µl anesthetic mixture per gram body weight). After ensuring deep anesthetization, the mice were spread-eagled on a styrofoam block and the limbs were secured using tapes. The thoracic cavity was opened up so that the heart was exposed and a cannula was inserted into the left ventricle. The procedure was carried out under the stereomicroscope Stemi DRC. Over a pump with variable speed the cannula was connected to the tubing, which was immersed in the flushing solution (recipe in Table 3.1). The flow of the flushing solution was turned on and the mouse was flushed until the exit fluid was clear and no more bleeding was visible. Then the tubing was switched to Zamboni's fixative and the fixative was administered for 5-10min. Thereafter, the pump was switched off and the cannula was removed from the heart. The brain, eyes and spine were dissected under the stereomicroscope and further processed as described in chapter 4.4.2.

4.7 Stimulation of DRG by the cGMP analogue 8-pCPT-cGMP and CNP-22

Activation of cGMP-dependent kinase I (cGKI) was performed on living DRG after dissecting the mouse embryonic spinal cord with DRG at E12.5 without fixation. The DRG were dissected from the spinal cord using a microscopic scissor and kept on ice in 1xPBS. DRG were counted and collected by aspirating them in a 1ml pipette and transferring them to a 1.5ml tube filled with 1xPBS. The collected DRG were centrifuged for 5min at 100g and 4°C. The PBS was removed and either 1mM cGMP analogue 8-pCPT-cGMP or 1µM CNP-22 diluted in 1xPBS was added to the DRG pellet in the presence of phosphatase inhibitors (1µM calyculin A and 1µM okadaic acid). Treated DRG were termed "stimulated" material. In case of the "non-stimulated" control only 1xPBS with phosphatase inhibitors was added to the DRG pellet. Stimulation of DRG by the cGMP analogue 8-pCPT-cGMP was carried out for 5min at 37°C and stimulation by CNP-22 was carried out for 15min at 37°C. The "non-stimulated" control material was treated in the same way. After stimulation, the DRG were centrifuged for 5min at 100g. After removal of the supernatant, the DRG were quick-frozen on dry ice and stored at -80°C until further use.

4.8 Western blot analysis of DRG

The frozen "stimulated" and "non-stimulated" DRG were thawed on ice for 5min and resuspended in 0.2% (v/v) CHAPS solution with protease inhibitors (recipe in Table 3.1). The DRG were homogenized, incubated for 30min at 4°C under rotating conditions and

centrifuged for 10min at 150g and 4°C to remove nuclei. The supernatant was transferred to a new tube and centrifuged for 15min at 47000g to remove the insoluble fraction. For the fractionation of DRG into membrane- and cytoplasm-containing fractions, the DRG were resuspended in 1xPBS with protease inhibitors, homogenized and centrifuged as described above. The respective fractions were resuspended in 1xPBS in the presence of protease blockers.

Protein concentration was determined measuring the absorbance of the solution with a spectrophotometer (λ = 280nm). The measured value was divided by 1.25 (an extinction coefficient for a protein mixture). With the approach described above and in chapter 4.7, the protein amount was estimated to range between 1-2µg protein per DRG.

Aliquots of the supernatant were stored at -80°C or mixed with 5x Laemmli buffer for Western blot analysis. After boiling for 5min at 95°C, the samples were applied to an SDS-PAGE. Proteins separated on a polyacrylamide gel were transferred to a nitrocellulose membrane. Following transfer of the proteins, the nitrocellulose membrane was blocked using Western blocking buffer (recipe in Table 3.1) and probed with a primary antibody diluted in the blocking buffer. After overnight incubation at 4°C, the membrane was then washed in the Western washing buffer (recipe in Table 3.1) for 25min, renewing the buffer 5 times. The bound primary antibody was detected with an HRP-conjugated secondary antibody diluted in 1xABS (recipe in Table 3.1, incubation for 2h at RT). The detection was carried out using a chemiluminescent reagent, the ChemiDoc system and the software Quantity One.

4.9 DiI-labeling of the DRG sensory axons

The method used in this study to label the sensory axons of the DRG is visualized in *DiI-Labeling of DRG Neurons to Study Axonal Branching in a Whole Mount Preparation of Mouse Embryonic Spinal Cord* (Schmidt and Rathjen 2011).

4.10 Maintenance and breeding of mice

The mice were kept under required conditions at the Animal Facility of the Max Delbrück Center for Molecular Medicine. For breeding, two females of the appropriate age (starting from 8 weeks) were mated with a male (preferably older than the females). The offspring were weaned at the age of three weeks and genotyped by tail biopsies using PCR analysis.

5. Results

5.1 Generation of the Npr2LacZ mouse line for monitoring Npr2 expression

To ask whether there are other neuronal subpopulations than DRG, in which axon bifurcation is regulated by Npr2, the localization of Npr2-positive neurons was studied in the developing mouse nervous system. For this purpose, the Npr2LacZ reporter line was generated as described in chapters 5.1.1-5.1.3.

5.1.1 Cloning strategy

The targeting construct for the Npr2LacZ mouse model was generated using a BAC clone and mini-λ-mediated homologous recombination (Copeland et al. 2001; Court DL et al. 2003). To identify BAC clones that contain the mouse gene locus for Npr2, a sequence alignment of the corresponding mouse genomic DNA with an appropriate BAC library was carried out using the Ensembl browser. According to the results of this alignment the BAC clone bMQ331a20 carrying the Npr2 gene locus on the backbone vector pBACe3.6 was chosen to design the targeting construct (Figure 5.1).
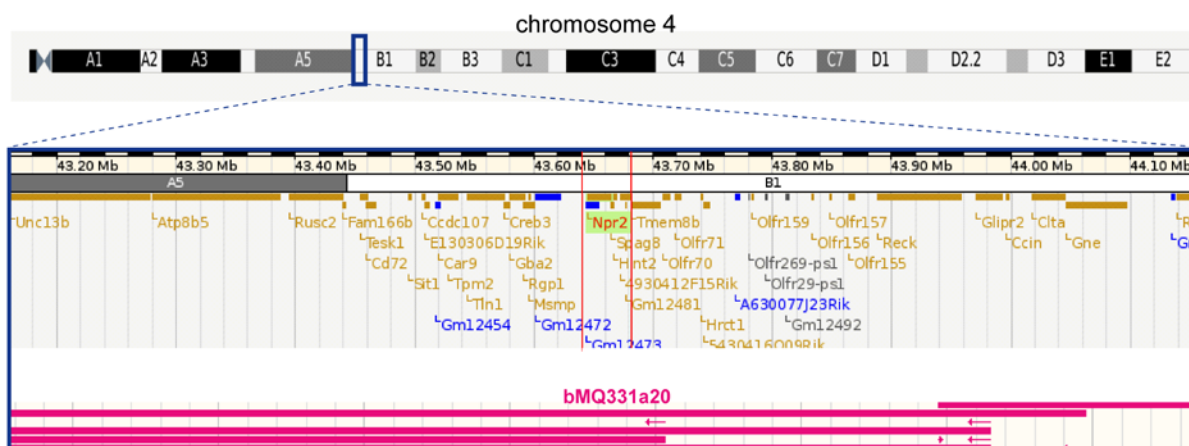
Figure 5.1: Screenshot of the Ensembl browser (Mus musculus version 56.37i (NCBIM37) Chromosome 4: 43.154.451-44.154.450Mb) representing the Npr2 gene locus on chromosome 4 and aligned BAC clones (pink lines). The selected BAC clone is marked bMQ331a20.

5.1.1.1 Construction of the mini-targeting vector

The generation of the mini-targeting vector is illustrated in Figure 5.2. In brief, the mini-targeting vector contains two homology arms (5' and 3' homology arm), a LacZ-cassette with a nuclear localization sequence (NLSLacZ) followed by a polyA-stretch and a Cre recombinase cassette (Cre-Neo/Kan), which is flanked by loxP-sites and contains a testis-

specific promoter as well as a neomycin resistance gene. Upon passage through the germline the neomycin selection marker self-excises.

The BAC amplification products were cloned into the plasmid pBluescript II SK+ either by blunt end or sticky ligation. The ligation was followed by a control digestion and sequencing analysis. The description of each plasmid as well as the primer sequences used for amplification and sequencing analysis can be found in the appendix (sequence data are available on the appended CD-ROM). The details concerning the cloning procedure are described in the Methods section.
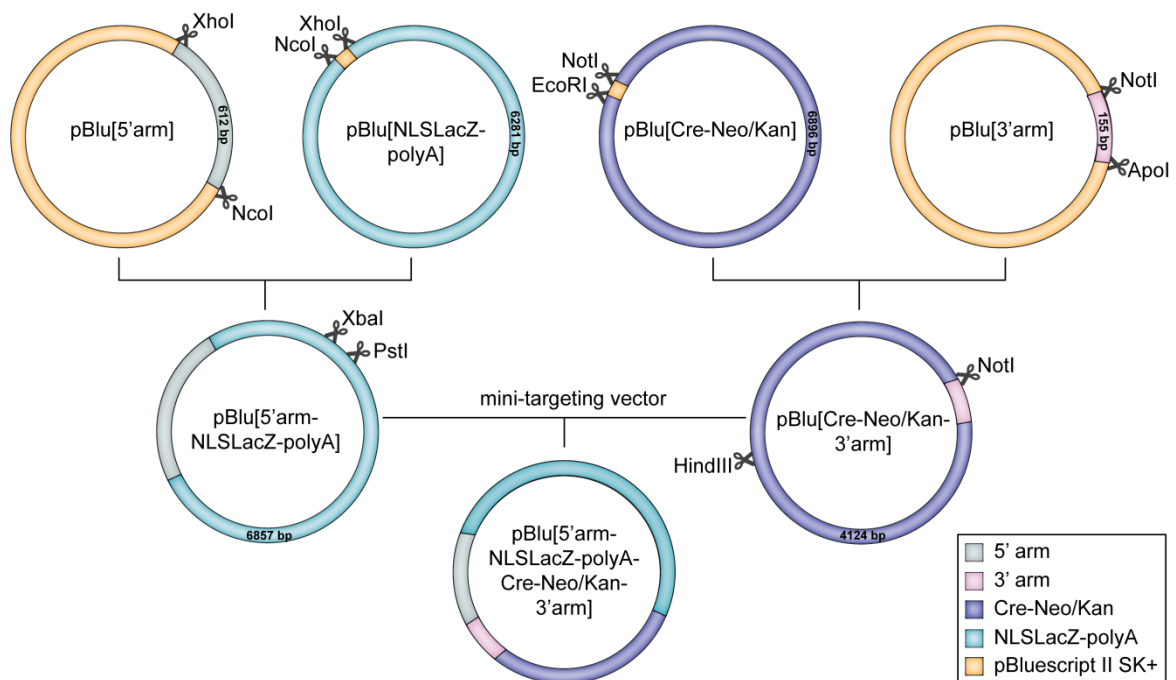

Figure 5.2: Cloning strategy for the mini-targeting vector. Left, cloning of the 5'arm (612bp) into the plasmid pBlu[NLSLacZ-polyA] (6281bp) by sticky end ligation using the cleavage sites of the restriction enzymes NcoI and XhoI. Right, cloning of the 3'arm (155bp) into the plasmid pBlu[Cre-Neo/Kan] (6896bp) by sticky end ligation using the cleavage sites of the restriction enzymes ApoI, EcoRI and NotI. Center, the final mini-targeting vector pBlu[5'arm-NLSLacZ-polyA-Cre-Neo/Kan-3'arm] (10.986bp) after blunt end ligation of desired fragments obtained from the plasmids pBlu[5'arm-NLSLacZ-polyA] (6857bp) and pBlu[Cre-Neo/Kan-3'arm] (4124bp) using the restriction enzymes HindIII, NotI, PstI and XbaI.

5.1.1.2 Subcloning of the Npr2 gene locus

Subcloning of the Npr2 gene locus was carried out using the mobile recombination system mini-λ. The mini-λ DNA was introduced into the DH10B strain carrying the BAC clone bMQ331a20 by electroporation. To subclone the desired Npr2 gene locus fragment, a pDTA vector was provided with homology arms consisting of genomic DNA sequences flanking exons 1 to 3 of the Npr2 gene (Figure 5.3). The pDTA vector containing these homology arms was linearized and introduced into the DH10B strain carrying the BAC clone and mini-λ DNA. After positive selection with ampicillin, the correct homologous

recombination was verified by restriction enzyme digestion. After electroporation of the pDTA vector with the subcloned Npr2 gene fragment into the DY380 strain, the correct recombination was confirmed by sequence analysis.
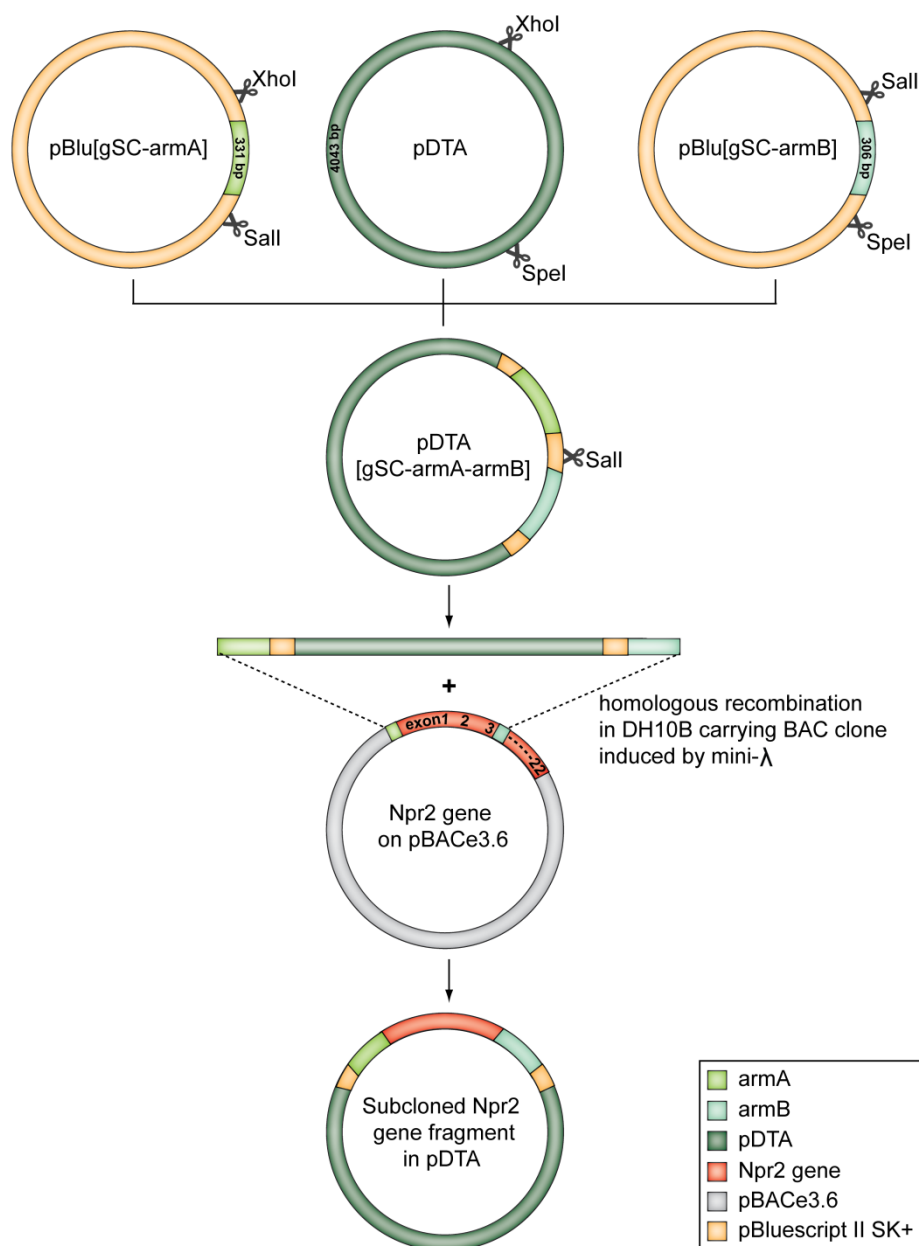
Figure 5.3: The strategy of subcloning the Npr2 gene fragment into pDTA. First, the pDTA vector was provided with homology arms by a triple sticky end ligation of homology arm fragments (armA and armB with respective lengths of 331bp and 306bp) using the cleavage sites of restriction enzymes XhoI, SalI, SpeI. The resulting plasmid pDTA[gSC-armA-armB] (4724bp) was then linearized by SalI to retrieve the Npr2 genomic fragment (exon1 to 3 on pBACe3.6) by homologous recombination at the homology regions surrounding the fragment. The resulting pDTA plasmid containing the subcloned Npr2 gene fragment had a length of 14.524bp.

5.1.1.3 Generation of the Npr2NLSLacZ targeting vector

In the bacterial strain DY380, which contains a temperature inducible lambda recombination system, the mini-targeting vector was introduced in frame with exon 1 of the Npr2 gene by homologous recombination. Consequently, the open reading frame of exon 1 was disrupted with 5' and 3' homologous arms of the mini-targeting vector and the [NLSLacZ-polyA-Cre-Neo/Kan] mutation was brought under the control of the Npr2 promoter (Figure 5.4). The final targeting vector provided with 5' and 3' homology regions (2200bp and 7600bp, respectively) was thus prepared for a homologous recombination event in embryonic stem cells.
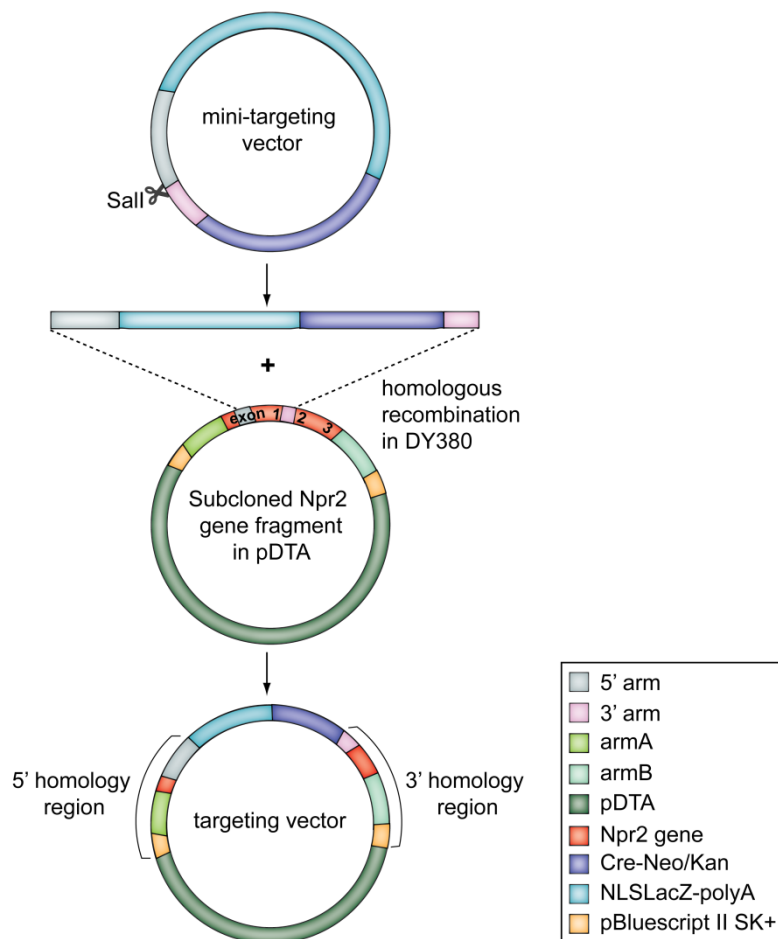
Figure 5.4: Designing the Npr2NLSLacZ targeting construct. The 10.986bp long mini-targeting vector containing the homology arms was linearized by SalI and inserted into exon 1 of the Npr2 gene locus subcloned in pDTA (14.524bp) by homologous recombination in DY380. The resulting targeting vector Npr2NLSLacZ with a length of 21.199bp contained the desired mutation construct [NLSLacZ-polyA-Cre-Neo/Kan] under the control of Npr2 promoter and 5' and 3' homology regions for homologous recombination in embryonic stem cells.

5.1.2 Homologous recombination in embryonic stem (ES) cells

The Npr2NLSLacZ targeting vector was introduced into ES cells (the ES cell lines are summarized in Table 5.1) by electroporation. Before electroporation the targeting vector was linearized with PacI producing an 18.270bp fragment (Figure 5.5A). ES cells that incorporated the targeting vector were positively selected with G418. ES cell clones with a correct insertion of the targeting vector were identified by Southern blot analysis. A primary screen with the 3'probe identified four primary positive clones from 355 clones tested, which gives a recombination efficiency of 1%. A rescreen with 5', Neo and 3'probes confirmed the accurate insertion of the targeting vector into the genome of three ES cell clones tested (primary screen and rescreen of two clones in Figure 5.5B).
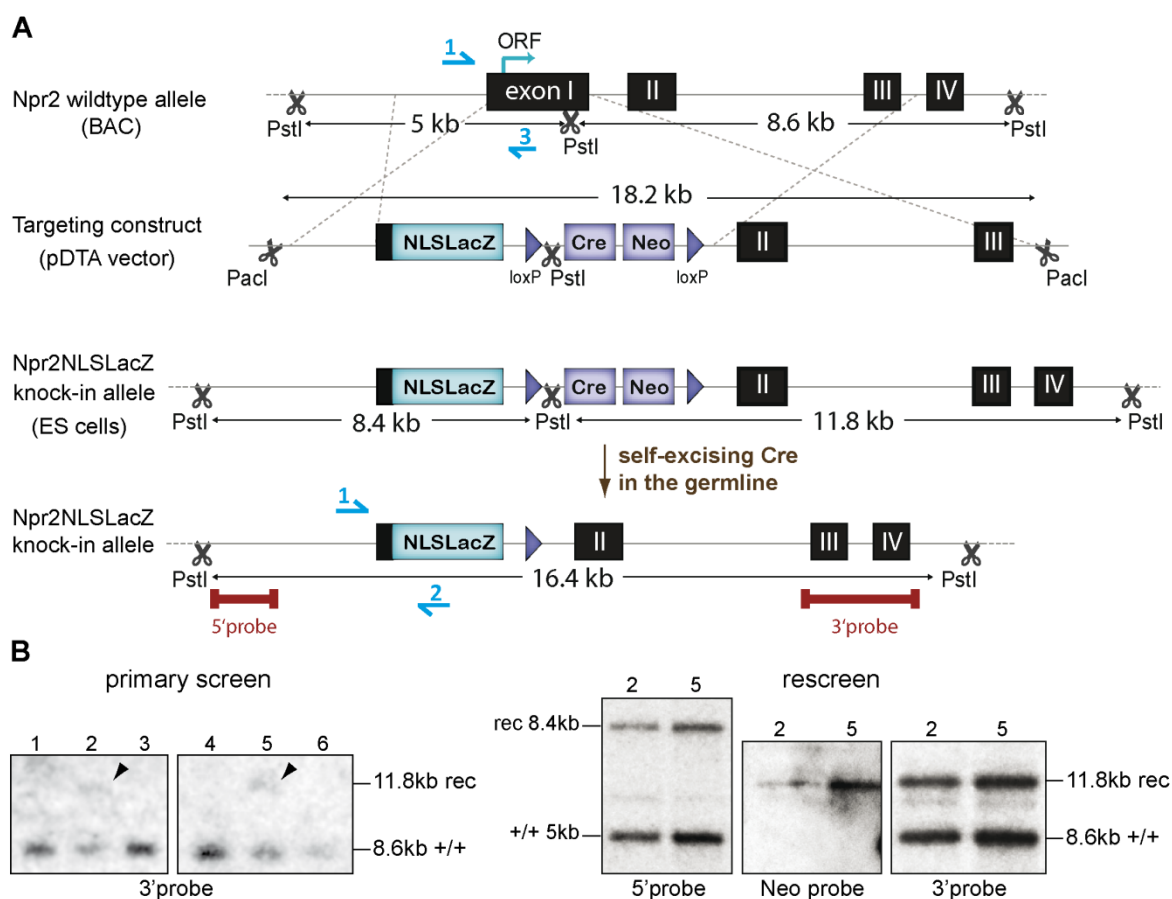
Figure 5.5: Generation of the Npr2LacZ mouse model. **(A)** Scheme of the targeting strategy for the generation of the Npr2LacZ mouse: the targeted region of the wildtype Npr2 gene locus is illustrated (dashed lines) and PstI cleavage sites producing 5kb and 8.6kb fragments by digestion are indicated. The targeting construct shows PacI cleavage sites producing the linearized 18.2kb DNA fragment that was introduced into ES cells by electroporation. After homologous recombination, the targeting construct was inserted into the ES cell genome. While the PstI cleavage sites outside of the targeted region persisted, a new PstI cleavage site was introduced by the targeting construct producing 8.4kb and 11.8kb fragments after digestion with the PstI restriction enzyme. Germline transmission of the targeted ES cells led to the Cre recombinase expression and self-excision of the loxP-flanked Cre/Neo-cassette.

(B) Southern blot analysis using PstI-digested ES cell DNA and DNA probes (binding regions are shown as red bars in A) with unique sequences within the genome: a 5'probe with a length of 657bp detected a 5' region outside of the homology region of the targeting construct and a longer 3'probe with a length of 1009bp detected a region both in- and outside of the 3'homology region of the targeting construct. The third Neo probe with a length of 700bp gained from pHW025 after NcoI cleavage recognized the Neo-cassette to confirm the single insertion. The primary screen employing the 3'probe identified recombinant clones (indicated by black arrowheads). The rescreen using all probes confirmed the correct homologous recombination of the primary positive clones.

5.1.3 Blastocyst injection, chimera production and germline transmission

In order to produce chimeric mice, three confirmed positive ES cell clones were injected into C57Bl/6 blastocysts by the Transgenic Core Facility of the Max Delbrück Center for Molecular Medicine (summarized in Table 5.1).

Table 5.1

ES cell line	# of electro-poration	# of tested ES cell clones	# of positive clones	blastocyst injection	# of chimera	germline transmission
E14.1	2	250	2	✓ , ✓	1 , 3	1x
AB2.1	1	80	1	✓	5	1x
R1	1	25	1	-	-	-

Table 5.1: Summary of the ES cell lines used in this study; given are the number of performed electroporations and the number of ES cell clones tested by primary Southern blot analysis, the number of positive clones with a correct homologous recombination in individual ES cell lines, the number of performed blastocyst injections of positive ES clones and the corresponding number of male chimeric offspring given rise to germline transmission.

The generated male chimeras exhibited patches of bright colored coat and were analyzed by PCR for the presence of the transgene (Figure 5.6). The male chimeras were mated to C57Bl/6 females and the resulting offspring with brown coat color, indicative for germline transmission with concomitant removal of the Neo-cassette, were analyzed by PCR genotyping using appropriate primers (see chapter 4.3.3). The binding sites of the primers are indicated in Figure 5.5A with numbers 1, 2, 3 and half arrows in blue. Primers 1 and 3 were binding in the wildtype sequence and amplifying a 348bp DNA fragment, primer 2 was binding in the NLSLacZ knock-in sequence and together with primer 1 was amplifying a 398bp DNA fragment.

Figure 5.6: Left, a 3.5-week-old male chimera generated from the E14.1 ES cell injection into C57Bl/6-derived blastocysts. The white patch on the chimera coat was derived from E14.1 ES cells. PCR analysis confirmed the presence of the transgene by amplification of a 398bp fragment. In contrast, the PCR yielded a single band at 348bp in wildtype *(+/+)*. Right, a 3-week-old brown offspring of the F1 generation was heterozygous (*LacZ/+*) for the Npr2LacZ transgene as verified by PCR genotyping.

5.2 Verification of the Npr2LacZ mouse line

Before the Npr2LacZ mouse was used for the analysis of the Npr2-positive neuronal subpopulations, the mouse line was verified by Southern blot analysis, PCR genotyping, Western blot and immunohistochemical analysis. Phenotypic characteristics of the Npr2LacZ mouse line were verified by analysis of the axonal branching phenotype and growth reduction in the Npr2-deficient mice.

5.2.1 Molecular genetic analysis of the Npr2LacZ mouse

Heterozygous offspring obtained from mating the male chimeras to C57Bl/6 females were backcrossed to wildtype C57Bl/6 mice for several generations to get a C57Bl/6 genetic background. Breedings of heterozygous Npr2LacZ mice were setup to produce homozygous Npr2-deficient mice. Southern blot analysis of genomic DNA from wildtype (+/+), heterozygous Npr2 (*LacZ/+*) and Npr2 knockout (*LacZ/LacZ*) mice digested with PstI confirmed the correct integration of the targeting construct in the Npr2LacZ mouse line (Figure 5.7A). The PCR analysis is shown in Figure 5.7B (see chapter 4.3.3 for PCR genotyping of the Npr2LacZ mouse strain).
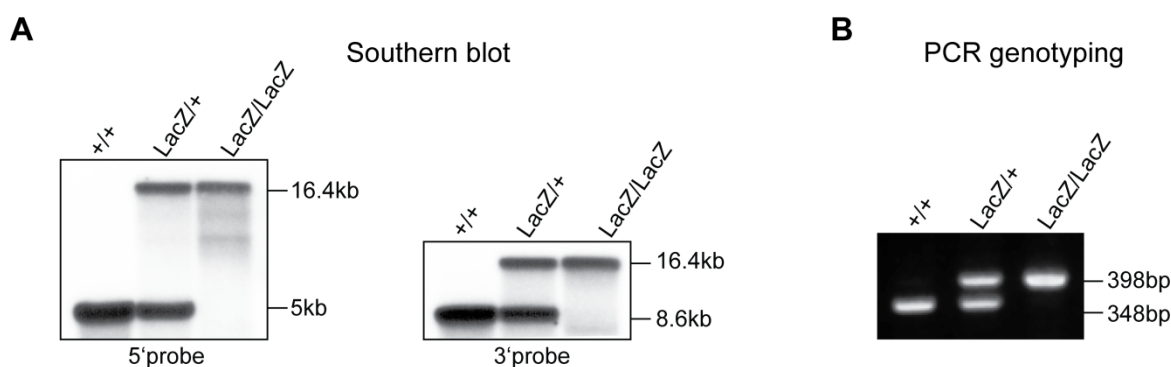
Figure 5.7: Verification of the Npr2LacZ mouse line by Southern blot analysis and PCR genotyping. **(A)** Southern blot analysis using DNA extracted from the liver of 3-week-old wildtype (+/+), heterozygous Npr2 (*LacZ/+*) and Npr2 knockout (*LacZ/LacZ*) mice. The digestion of purified genomic DNA by PstI produced DNA fragments of 5kb and 8.6kb for the wildtype, 5kb, 8.6kb and 16.4kb for the heterozygous Npr2 and of 16.4kb for the Npr2 knockout/LacZ knock-in mice. The 5' and 3'probes were the same as those used for Southern blot analysis of ES cells (Figure 5.5). The 5'probe recognized the 5kb fragment of the wildtype allele and the 16.4kb fragment of the NLSLacZ knock-in allele. The 3'probe recognized the 8.6kb of the wildtype allele and the 16.4kb fragment of the LacZ knock-in allele. **(B)** Genotyping-PCR using genomic DNA from wildtype (+/+), heterozygous Npr2 (*LacZ/+*) and Npr2 knockout (*LacZ/LacZ*) mice. Amplification products of 348bp for wildtype, 348bp and 398bp for heterozygous Npr2 and 398bp for Npr2 knockout were analyzed by agarose gel electrophoresis.

5.2.2 Biochemical analysis of the Npr2LacZ mouse

Expression of Npr2 in the Npr2LacZ mouse line was analyzed using Western blot and immunohistochemical analysis (Figures 5.8 and 5.9). Embryos from either wildtype (+/+) or heterozygous Npr2 (*LacZ/+*) or Npr2 knockout (*LacZ/LacZ*) mice were taken for the analyses.

DRG protein lysates obtained from the three different genotypes were analyzed by Western blot using antibodies against γ-tubulin, which served as a loading control, β-galactosidase (β-gal) and Npr2. The anti-β-gal antibody recognized the 117kDa band of β-gal in heterozygous Npr2 as well as Npr2 knockout mice (Figure 5.8A). The anti-Npr2 antibody recognized a double band of Npr2 at 120-122kDa in wildtype and heterozygous Npr2 mice (Figure 5.8B). As expected, no expression of β-gal was detected in wildtype littermates, while the heterozygous littermates expressed less β-gal compared to the homozygous Npr2 littermates. Analogously there was no expression of Npr2 in the Npr2 knockout littermates, while the wildtype and heterozygous littermates expressed Npr2 at variable levels, depending on the number of alleles carrying the LacZ-mutation.
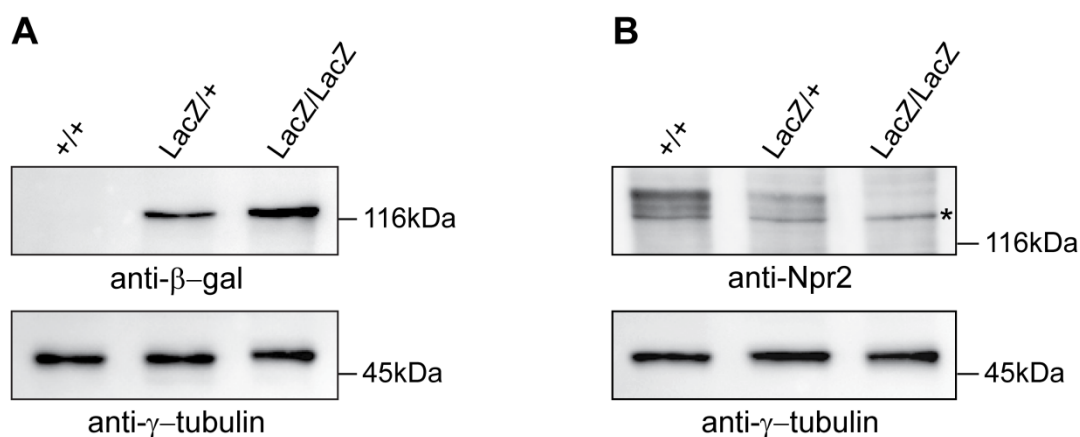
Figure 5.8: Verification of the Npr2LacZ mouse line by Western blot analysis. For Western blotting the DRG were dissected at E13.5 and collected for each embryo of an offspring separately. After genotyping the frozen samples were thawed and combined according to their genotypes. 10µg of protein were separated on a denaturing polyacrylamide gel (7.5%). Mouse monoclonal anti-γ-tubulin antibody recognized a band at 48kDa (loading control). **(A)** Chicken anti-β-gal antibody recognized the 117kDa band of β-gal in heterozygous Npr2LacZ (*LacZ/+*) and Npr2 knockout (*LacZ/LacZ*) mice. **(B)** Guinea pig anti-Npr2 antibody recognized Npr2 in the molecular mass range of 120-122kDa in wildtype (+/+) and heterozygous Npr2 (*LacZ/+*) mice. The star (*) indicates a band of unknown identity recognized by anti-Npr2 antibody.

A triple-immunohistochemical analysis using antibodies against Npr2, β-gal and neurofilament-M (NF-M) detected (i) the presence or absence of Npr2 in the respective heterozygous and knockout mice, (ii) expression of β-gal in both heterozygous and knockout mice and (iii) neuronal cells (Figure 5.9A, B). The merged image of the Npr2- and β-gal expression in the presence of DAPI-staining showed an expression of Npr2 in

sensory neurons and nuclear localization of β-gal (Figure 5.9A, B third column). Additionally, the immunostaining using anti-NF-M antibody revealed a reduced size of the dorsal funiculus in the Npr2 knockout mice (Figure 5.9A, fourth column) as reported previously (Schmidt et al. 2007). Consistent with previously published *in situ* hybridization studies (Schmidt et al. 2007), all neurons appeared to be positive for β-gal (Npr2) as shown in Figure 5.9B at higher magnification.
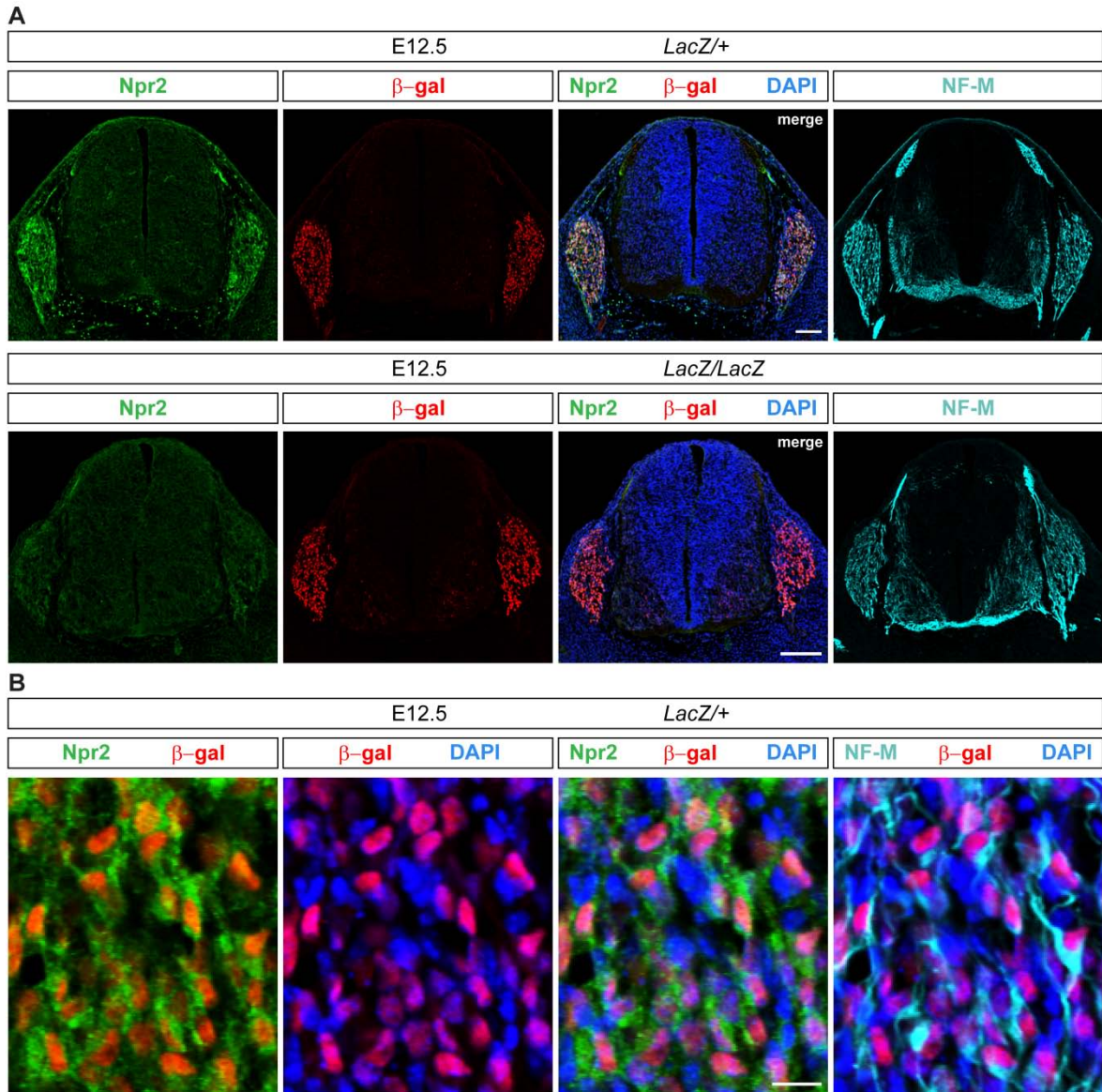
Figure 5.9: Verification of the Npr2LacZ mouse line by immunohistochemical analysis. For both Npr2 heterozygous and knockout mice 15μm transversal cryosections of E12.5 embryos were stained using guinea pig anti-Npr2, chicken anti-β-gal, rabbit anti-NF-M antibodies and DAPI. **(A)** Npr2 and NF-M were expressed in sensory neurons of the heterozygous Npr2 mice, whereas β-gal was restricted to the nuclei of Npr2-expressing cells (upper row). As expected, Npr2 expression was absent in the Npr2 knockout mice, while the expression of β-gal did not change (lower row). The NF-M staining depicted the neuronal cells and reduced size of the dorsal funiculus. DAPI served as a general nuclear marker. Scale bar 100μm. **(B)** Higher magnification images of DRG cells showing nuclear localized β-gal together with either Npr2 and/or DAPI or NF-M. The neuronal cell-specific expression of Npr2 was detected using anti-NF-M and anti-β-gal antibodies and DAPI-staining. Scale bar 10μm.

5.2.3 Phenotypic verification of the Npr2LacZ mouse

Previous investigations on mouse models with an inactivated Npr2 receptor uncovered several phenotypic characteristics of Npr2 deficiency: achondroplastic dwarfism due to impaired endochondral ossification (Sogawa et al. 2007; Tamura et al. 2004; Tsuji and Kunieda 2005), defects in oocyte maturation (Zhang et al. 2011; Zhang et al. 2010), gastrointestinal function (Sogawa et al. 2010), cardiac growth (Langenickel et al. 2006; Pagel-Langenickel et al. 2007) and impaired axonal bifurcation at the DREZ (Schmidt et al. 2007).

Homozygous Npr2LacZ mice were examined for their size and axonal branching pattern (Figure 5.10). Homozygous Npr2LacZ mice revealed a severely decreased body size in comparison to their wildtype littermates (Figure 5.10A). The axonal branching pattern of Npr2 homozygous mice *(LacZ/LacZ)* was disturbed: when the primary sensory axons grew toward the spinal cord, they made a turn at the DREZ instead of bifurcating in rostral and caudal directions as is the case in the wildtype (Schmidt et al. 2007) (Figure 5.10B).
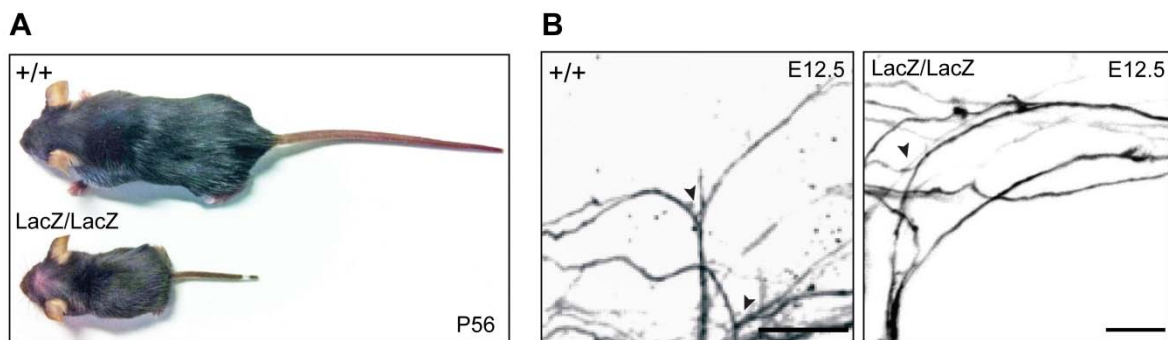
Figure 5.10: Phenotype of the homozygous Npr2LacZ mice. **(A)** Size comparison of an 8-week-old Npr2 knockout *(LacZ/LacZ)* mouse and its wildtype littermate showed the respective dwarf and normal phenotype. **(B)** DiI-labeling of DRG in wildtype and Npr2 knockout *(LacZ/LacZ)* mice at E12.5 demonstrated that the central projections of DRG neurons in Npr2 knockout embryos lacked the bifurcation at the DREZ seen in wildtype. Scale bar 10µm.

Thus, the Npr2LacZ mouse line turned out to be a reliable mouse model to study the localization of Npr2 in the heterozygous state (*LacZ/+*). In addition, the Npr2LacZ mouse line gave rise to Npr2 knockout mice (*LacZ/LacZ*), which proved useful in studies comparing wildtype and Npr2 knockout tissues.

5.3 Embryonic expression pattern of Npr2

Npr2 expression at embryonic stages of development was analyzed using heterozygous Npr2LacZ mice. For this purpose heterozygous Npr2LacZ mice were crossed with C57Bl/6 wildtype mice. The time point of plug detection was defined as E0.5. The timed pregnant mice were dissected at the appropriate day of embryonic development. A

subsequent clearing procedure (see chapter 4.4.2) enabled the visualization of Npr2 expression in whole mount embryos from embryonic day 9.5 to 13.5. Due to the NLS of the LacZ expression cassette, X-Gal staining revealed a nuclear Npr2 expression pattern in Npr2-positive cells. Expression of β-gal (indicative for Npr2) was detected from E10.5 onwards (Figure 5.11). At this stage of development Npr2 was expressed in DRG and in cranial sensory ganglia. While there was a strong expression in the trigeminal ganglion, the expression in other cranial sensory ganglia just began and the different ganglia such as the facio-vestibulocochlear ganglion complex were not entirely differentiable. A further expression of Npr2 was also detectable in the mesencephalon and hindbrain region (detailed view in Figure 5.12). From E11.5 onwards Npr2 was strongly expressed in all DRG as well as cranial sensory ganglia and there was a visible expression in the mesencephalon, midbrain-hindbrain boundary, hindbrain and nasal cavity. From E12.5 onwards Npr2 was also expressed in bones. Additionally, from E13.5 onwards Npr2 expression was detectable in the eye (Figures 5.11, 5.12 and Tables 5.2, 5.3).
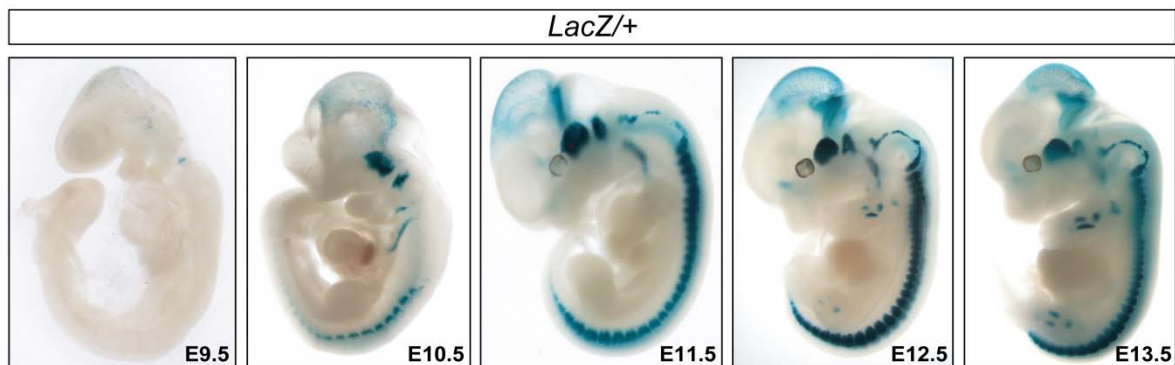
**Figure 5.11**: Npr2 expression in whole mount embryos of heterozygous Npr2LacZ mice. Visualization of β-gal expression (blue) during mouse development from E9.5-E13.5 using X-Gal staining of whole mount embryos: the expression of β-gal (Npr2) started at E10.5 with strong X-Gal staining in DRG, the trigeminal ganglion and facio-vestibulocochlear ganglion complex. From E11.5 onwards Npr2 was found in DRG and cranial sensory ganglia.
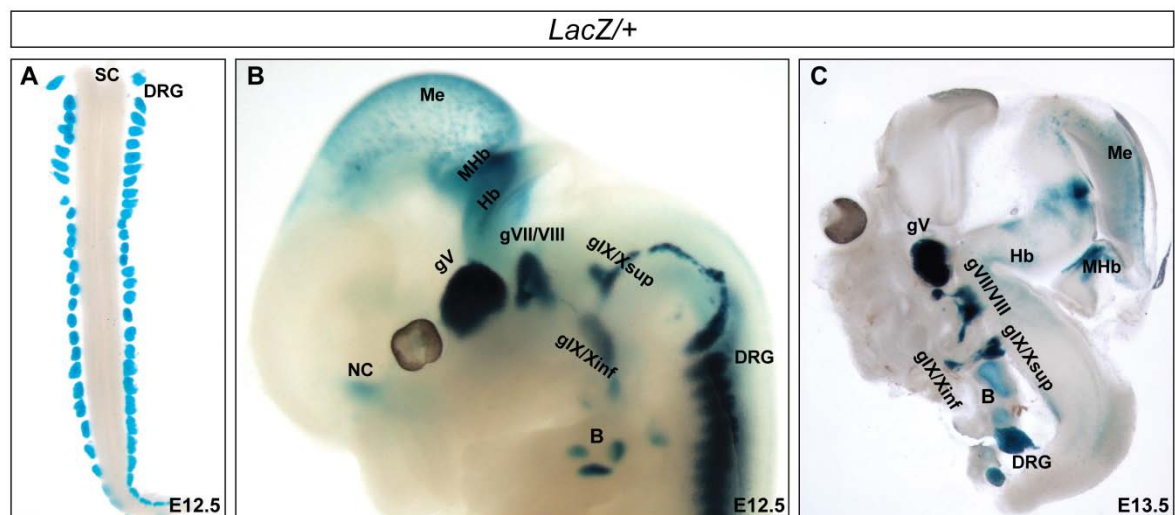
Figure 5.12: Prominent expression of Npr2 in DRG and cranial sensory ganglia. **(A)** A dorsal view onto the X-Gal-labeled whole mount spinal cord with attached DRG at E12.5 revealed Npr2 expression in DRG. **(B)** The magnification of the X-Gal-labeled E12.5 whole mount embryo from Figure 5.11 emphasized the strong expression of Npr2 in cranial sensory ganglia: trigeminal (gV), geniculate (gVII), vestibulocochlear (gVIII) as well as superior (gIX/Xsup) and inferior (gIX/Xinf) components of the IX/X ganglia. Npr2 expression was apparent in the mesencephalon, midbrain-hindbrain boundary, hindbrain, nasal cavity and bones. **(C)** A 200µm sagittal vibratome section of an E13.5 heterozygous Npr2LacZ mouse head labeled by X-Gal displayed the assembly of Npr2-positive cranial sensory ganglia in the hindbrain region. B, bones; g, ganglion; Hb, hindbrain, MHb midbrain-hindbrain boundary, NC, nasal cavity.

These data revealed that in addition to the expected distribution in embryonic DRG, Npr2 was also prominently expressed in cranial sensory ganglia (summarized in Table 5.2). The striking expression of Npr2 in all cranial sensory ganglia during the time when their central projections grew into the hindbrain prompted a detailed analysis of their branching behavior to answer the question whether CNP-induced cGMP signaling in neurons of the cranial sensory ganglia serves a similar function in the control of bifurcation as in DRG neurons (see chapter 5.7.1).

Table 5.2

Ganglion number	Ganglion name	Corresponding cranial nerve
gV	Trigeminal	Trigeminal
gVII	Geniculate	Facial
gVIII	Cochlear	Cochlear
gVIII	Vestibular	Vestibular
gIX$_{sup}$	Superior	Glossopharyngeal
gIX$_{inf}$	Petrosal	Glossopharyngeal
gX$_{sup}$	Jugular	Vagus
gX$_{inf}$	Nodose	Vagus

Table 5.2: Summary of the cranial sensory ganglia expressing Npr2 from E11.5 with the appropriate ganglion number, ganglion name and the corresponding cranial nerve.

To obtain an overview of spatial and temporal Npr2 expression in the head region during embryonic development of mice, β-gal expression was examined systematically in serial sections as well as whole mounts from E10.5 to E14.5. Specific regions and cell populations with visible Npr2 expression (based on X-Gal staining) were identified using the *Atlas of the prenatal mouse brain* (Schambra et al. 1992) and the respective database of the *Allen brain atlas* (www.brain-map.org). The regions with an apparent Npr2 expression from E10.5 to 14.5 are summarized in Table 5.3. Furthermore, coronal and transversal head sections of heterozygous Npr2LacZ mice at E14.5 are shown in Figures 5.13 and 5.14, representative for the detailed mapping of areas with β-gal activity.

Table 5.3

Structure	E10.5	E11.5	E12.5	E13.5	E14.5
Dorsal root ganglia	✓	✓	✓	✓	✓
Cranial sensory ganglia	✓	✓	✓	✓	✓
Mesencephalic tegmentum	✓	✓	✓	✓	✓
Midbrain-hindbrain boundary	✓	✓	✓	✓	✓
Hindbrain	✓	✓	✓	✓	✓
Olfactory epithelium		✓	✓	✓	✓
Bones			✓	✓	✓
Nasal septum				✓	✓
Basicranium				✓	✓
Eye					✓
Dental papilla					✓

Table 5.3: Temporal dynamics of Npr2 expression during embryonic development from E10.5-E14.5 as detected by X-Gal staining of heterozygous Npr2LacZ mice.
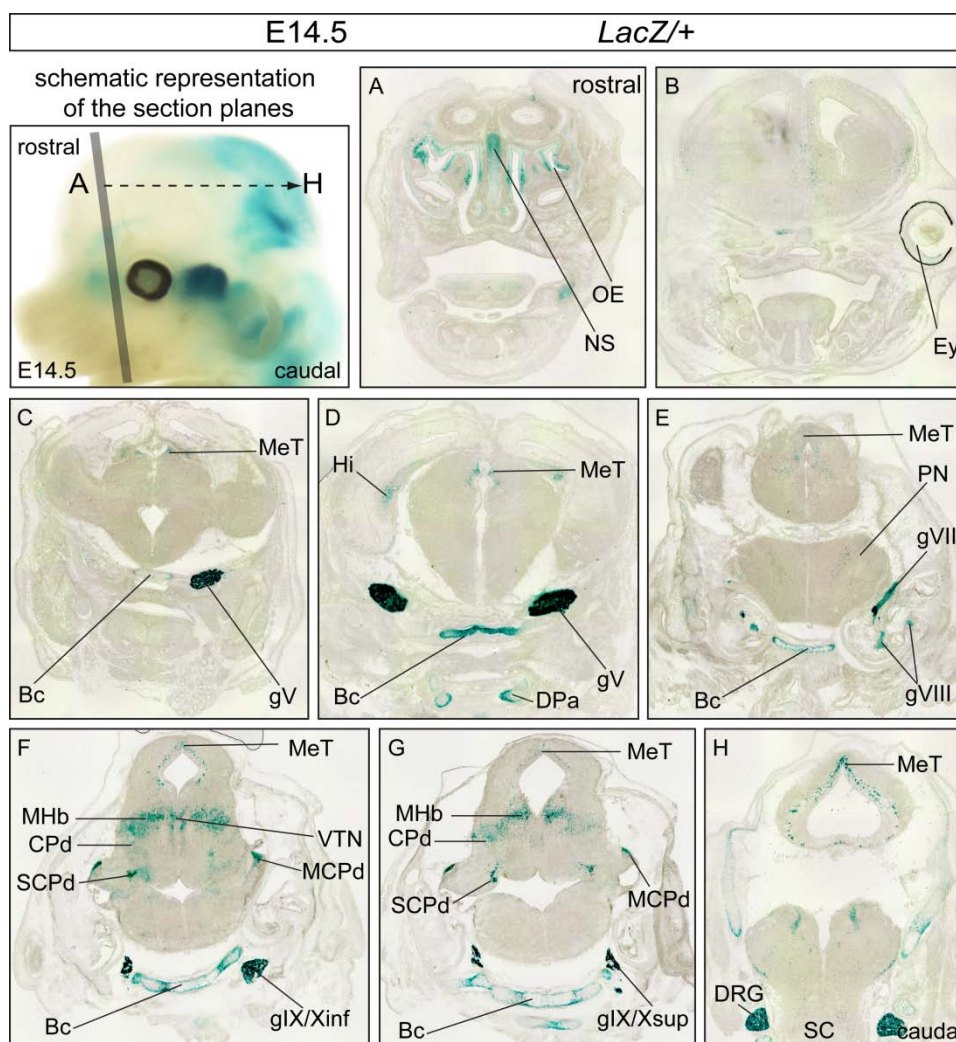
Figure 5.13: Expression of Npr2 in coronal head sections of heterozygous Npr2LacZ mouse at E14.5. Cell populations in the following structures were found to be Npr2-positive as detected by X-Gal staining: basicranium (Bc), cerebral peduncle (CPd), dental papilla (DPa), dorsal root ganglia (DRG), eye (E), cranial sensory ganglia (gV, gVII/VIII, gIX/Xsup, gIX/Xinf), hippocampus (Hi), middle cerebellar peduncle (MCPd), mesencephalic tegmentum (MeT), midbrain-hindbrain boundary (MHb), nasal septum (NS), olfactory epithelium (OE), pontine nuclei (PN), spinal cord (SC), superior cerebellar peduncle (SCPd) and ventral tegmental nucleus (VTN).
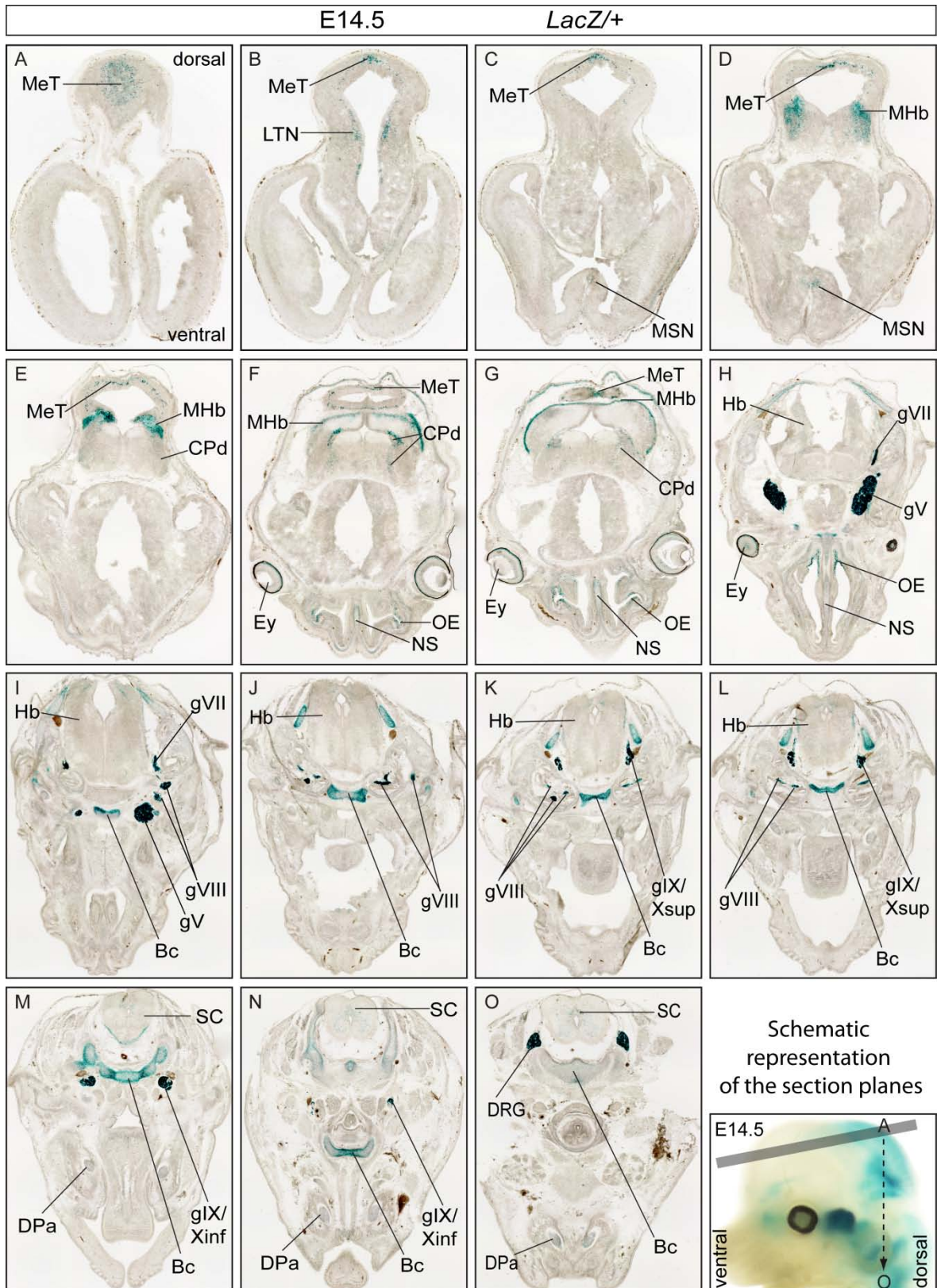
Figure 5.14: Expression of Npr2 in transversal head sections of heterozygous Npr2LacZ mouse at E14.5. Cell populations in the following structures were found to be Npr2-positive as detected by X-Gal staining: basicranium (Bc), cerebral peduncle (CPd), dental papilla (DPa), dorsal root ganglia (DRG), eye (Ey), cranial sensory ganglia (gV, gVII/gVIII, gIX/Xsup, gIX/Xinf), hindbrain (Hb), lateral tegmental nucleus (LTN), mesencephalic tegmentum (MeT), midbrain-hindbrain boundary (MHb), medial septal nucleus (MSN), nasal septum (NS), olfactory epithelium (OE) and spinal cord (SC).

5.4 Co-localization of Npr2 and cGKIα in neuronal cells of early mouse embryos

Besides the CNP and Npr2, cGKIα is the third component of the cGMP-dependent signaling pathway that regulates bifurcation of sensory axons at the dorsal root entry zone (Schmidt et al. 2009; Schmidt et al. 2007; Schmidt et al. 2002; Zhao and Ma 2009; Zhao et al. 2009). cGKIα and Npr2 are expressed in an overlapping pattern by sensory neurons of DRG (Schmidt et al. 2007; Schmidt et al. 2002). Studies on genetic mouse models for cGKI and Npr2 demonstrated the implication of both proteins in the bifurcation process of sensory neurons.

Using the Npr2LacZ mouse strain, Npr2 and cGKIα localization was analyzed by immunohistochemistry. Immunohistochemical analyses were performed on Npr2-expressing cell populations, which were identified by X-Gal staining. As shown in Figure 5.15, the DRG, which harbor the cell bodies of DRG sensory neurons, showed a strong X-Gal-staining. Immunohistochemical analyses using anti-β-gal for Npr2 and anti-cGKIα demonstrated a complementary localization of β-gal in the nuclei and of cGKIα in the cytoplasm of DRG sensory neurons.
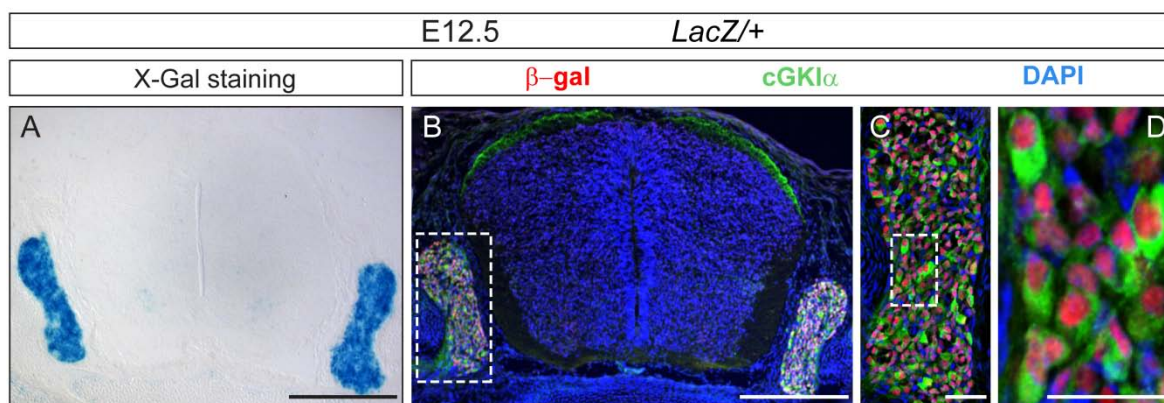
Figure 5.15: Co-localization of Npr2 and cGKIα in DRG neurons of heterozygous Npr2LacZ mice at E12.5. **(A)** An X-Gal-stained transversal cryosection of the spinal cord showed a strong expression of β-gal (Npr2) in the DRG. **(B-D)** Immunohistochemical analysis of a transversal cryosection using anti-β-gal, anti-cGKIα antibodies and DAPI-staining demonstrated the co-localization of β-gal (Npr2) and cGKIα in DRG. **(D)** At a higher magnification the immunohistochemical analysis clearly showed β-gal expression in the nuclei and cGKIα expression in the cytoplasm of DRG neurons. Scale bar 100µm for A, B and 10µm for C, D.

Similarly, the identified cell populations expressing Npr2 (Figures 5.11, 5.12 and Tables 5.2, 5.3) were analyzed for a co-localization of Npr2 and cGKIα. Co-immunostaining for neurofilament-M using the anti-NF-M antibody helped to confirm the expression of both Npr2 and cGKIα in neuronal cells (Figures 5.16-5.19).

The images in Figure 5.16 give an overview of the cranial sensory ganglia stained with X-Gal and with antibodies against β-gal, cGKIα and NF-M.
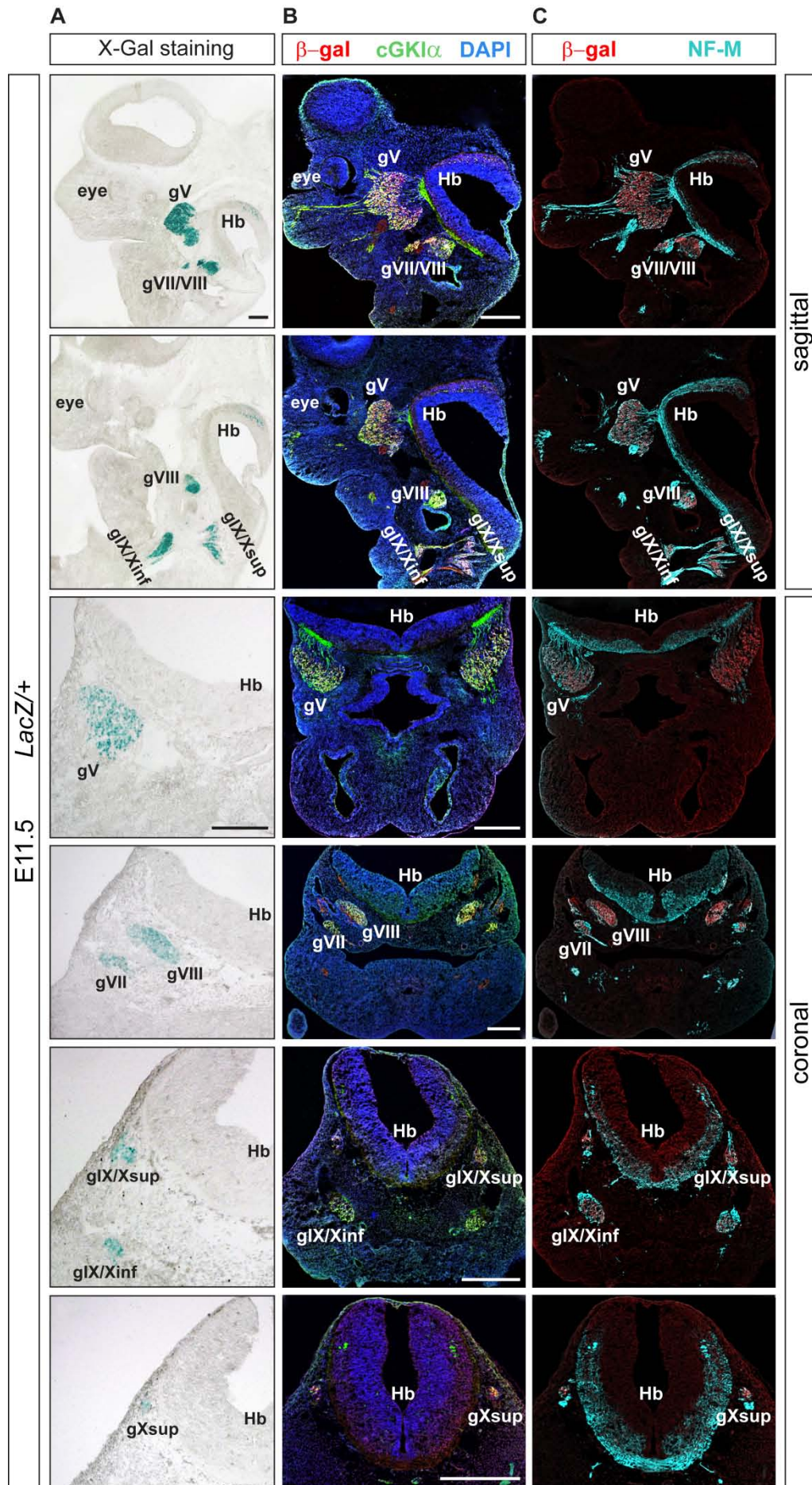
Figure 5.16: Overview of Npr2-positive cranial sensory ganglia by X-Gal staining and immunohistochemical analysis on cryosections of heterozygous Npr2LacZ mice at E11.5. **(A)** X-Gal staining of sagittal and coronal sections revealed the distinct expression of Npr2 in cranial sensory ganglia. **(B)** Immunohistochemical analysis of sagittal and coronal sections gave a general view of co-localized Npr2 by β-gal staining and cGKIα in the cranial sensory ganglia (gV, gVII/VIII, gIX/Xsup and gIX/Xinf) and hindbrain (Hb). **(C)** Co-immunostaining using the anti-NF-M antibody revealed the specific expression of Npr2 in neuronal cells of cranial sensory ganglia. DAPI-staining showed the whole sectioned tissue. g, ganglion; Hb, hindbrain. Scale bar 100µm.

Figure 5.17 shows a higher magnification of the cranial sensory ganglia. The magnified boxed regions illustrate the nuclear expression of β-gal, the cytoplasmic expression of cGKIα and NF-M encircling the β-gal-labeled/Npr2-positive cells.
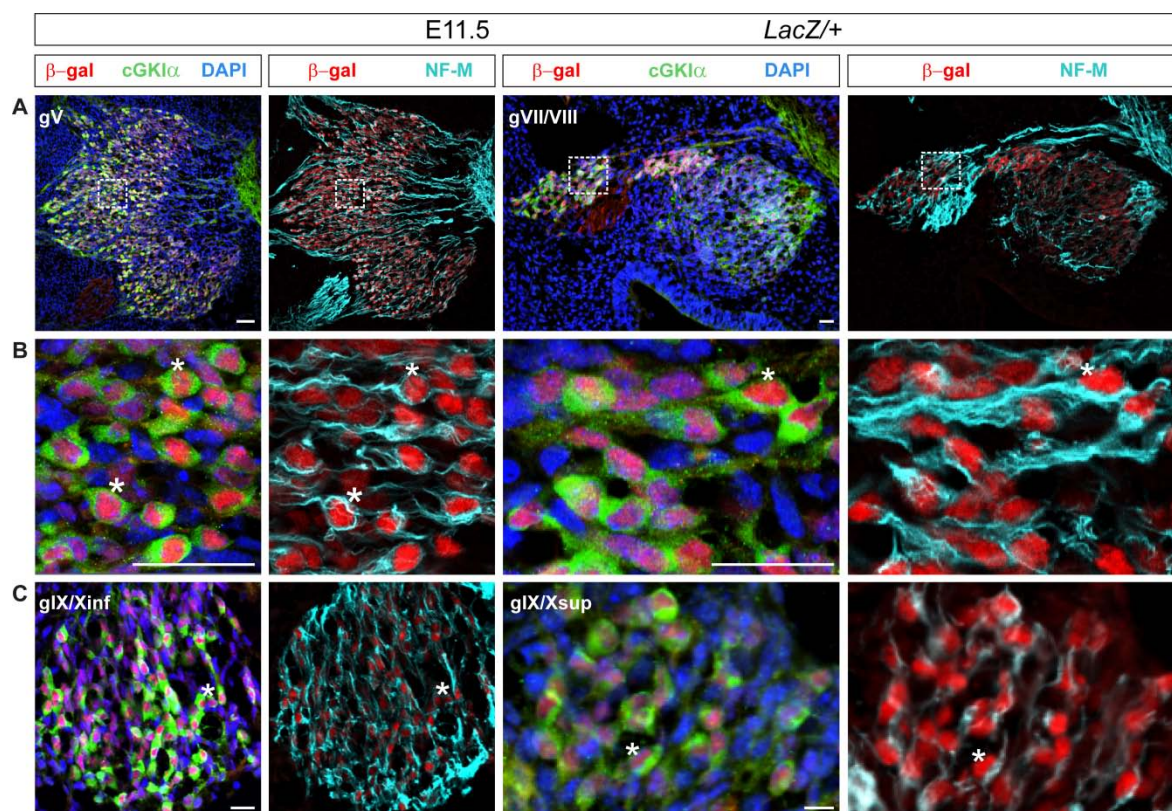
Figure 5.17: Co-localization of Npr2, cGKIα and NF-M in all cranial sensory ganglia neurons performing immunohistochemistry on cryosections of heterozygous Npr2LacZ mice at E11.5. **(A, C)** Magnifications of ganglia gV, gVII/VIII, gIX/Xinf and gIX/Xsup of the sagittal section shown in Figure 5.16 display the whole ganglia including the merged fluorescence of β-gal either with cGKIα and DAPI or with NF-M. **(B)** Higher magnifications of the indicated regions (A, dashed box) immunostained against β-gal, cGKIα and NF-M revealed the nuclear expression of Npr2 and the cytosolic expression of both cGKIα and NF-M throughout the sensory neurons. Representative cells with an apparent co-localization of Npr2, cGKIα and NF-M are marked with an asterisk. Scale bar 10µm.

X-Gal staining of heterozygous Npr2LacZ embryos at E11.5 revealed that besides the cell populations described above, there are further neuronal cell populations in the mouse mesencephalon and hindbrain that express Npr2 (Figures 5.11-12 and Figure 5.18A). The timing and localization of β-gal expression in these neuronal cells in mesencephalon together with cGKI expression in whole mount embryos (Schäffer 2006) suggest that

Npr2-positive cells are the mesencephalic trigeminal nuclei (MTN) neurons. The MTN neurons as well as the small neuronal cell population in rhombomere 1 showed a co-localized expression of β-gal (Npr2) and cGKIα, as illustrated in Figure 5.18.
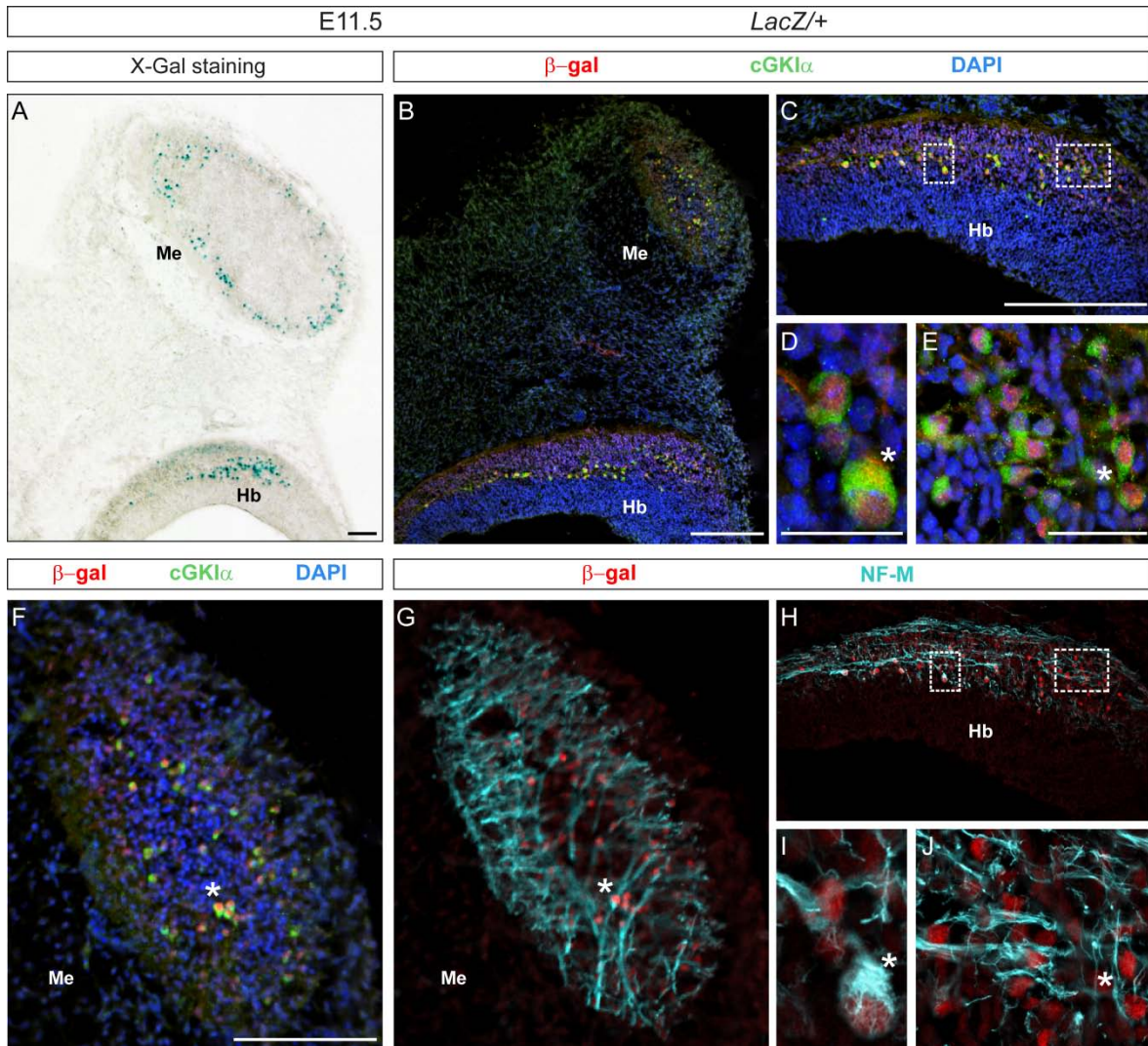
Figure 5.18: Co-localization of Npr2 and cGKIα in the mesencephalon and hindbrain of heterozygous Npr2LacZ mice at E11.5. **(A)** X-Gal staining of a sagittal section showed the Npr2-positive cell populations in Me and Hb. **(B-J)** Immunohistochemical analysis on sagittal sections confirmed the localization of Npr2 in the Hb and Me. **(B-F)** Co-localization of Npr2 (anti-β-gal-staining) and cGKIα (anti-cGKIα-staining) with a DAPI-staining. **(D-F)** Higher magnification images revealed the nuclear β-gal (Npr2) and cytoplasmic cGKIα expression. Representative cells are marked with an asterisk. **(G-J)** Npr2 expression specifically in neuronal cells was demonstrated by an immunostaining using anti-β-gal and anti-NF-M antibodies. The corresponding higher magnification images shown in C, D, E, F revealed the Npr2-positive cells to be neuronal cells with co-localized expression of β-gal and NF-M in the mesencephalon (G) and the hindbrain region (H-J). Hb, hindbrain; Me, mesencephalon. Scale bar 100µm for A, B, C, F and 10µm for D, E.

In addition to the NF-M co-immunostaining studies expression of Npr2 and cGKIα in neuronal cells was detected using the NeuN nuclear marker for post-mitotic neurons. Figure 5.19 shows the co-immunostaining analysis using antibodies against NeuN and cGKIα as well as DAPI-staining. The localization of NeuN in the neuronal nuclei and the

co-localization of cGKIα in the cytoplasm are illustrated at higher magnifications (dashed boxes). All cells expressing cGKIα were also positive for NeuN, indicating that the expression of cGKIα in the cranial sensory ganglia and in the cells in hindbrain is restricted to the neuronal cells.
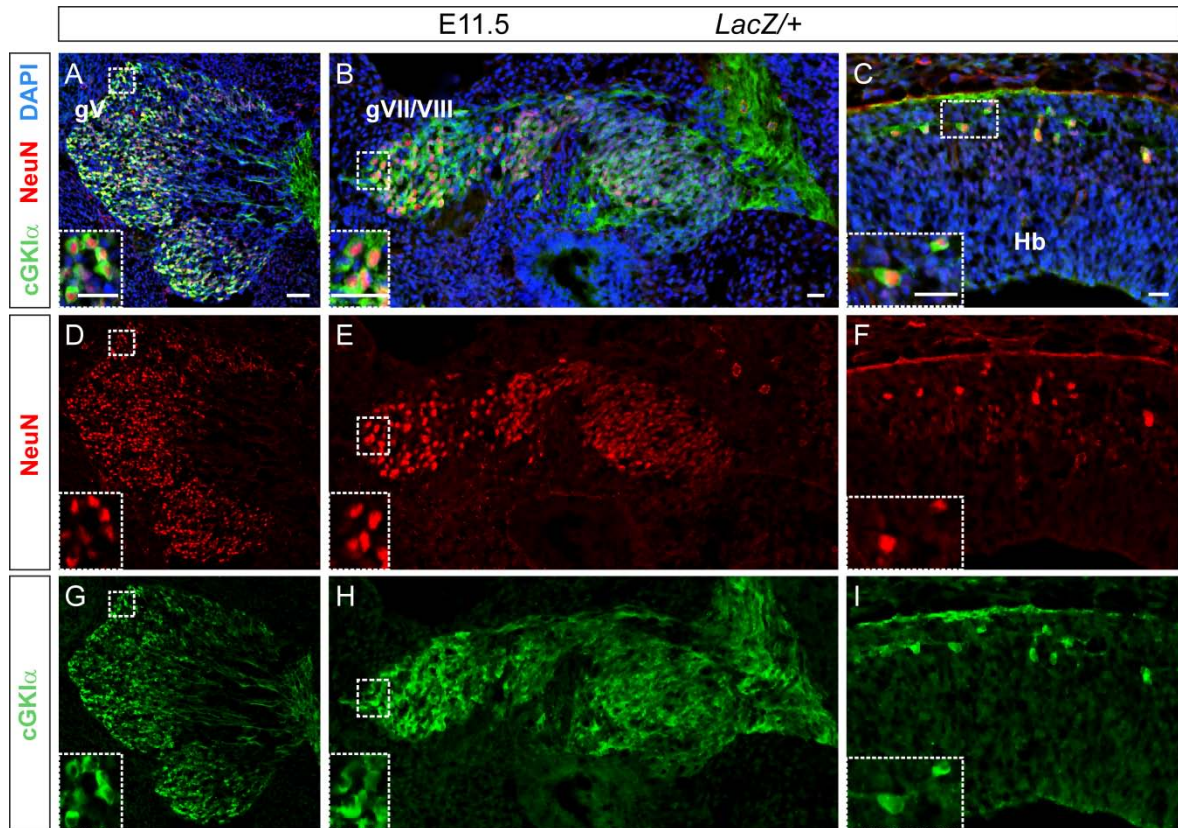
Figure 5.19: Expression of cGKIα in NeuN-positive cells. **(A-C)** Merged illustrations of the immunohistochemical analysis using antibodies against NeuN and cGKIα in the presence of DAPI-staining showed the nuclear expression of NeuN in all cells expressing cGKIα. **(D-E)** NeuN-positive cell nuclei in gV, gVII/VIII ganglia and in the hindbrain. **(G-I)** The cytoplasmic cGKIα expression in the cells of the gV, gVII/VIII ganglia and the hindbrain. Higher magnifications (dashed boxes) detailed the nuclear and cytoplasmic co-localization of NeuN and cGKIα, respectively. g, ganglion, Hb, hindbrain. Scale bar 10μm.

5.5 Expression of Npr2 in postnatal and adult mouse brain

Embryonic expression of Npr2 was of particular interest in this study, as the bifurcational mode of axonal branching takes place from about embryonic day 10.5. However, expression of Npr2 was also investigated in postnatal and adult brains in order to identify Npr2-expressing regions in the brain. X-Gal staining of sagittal and coronal cryosections from heterozygous Npr2LacZ mouse brains revealed brain regions with β-gal expression. Here, expression of β-gal was observed at different postnatal (P0, P5, P10, P25) and adult stages of development (Figure 5.20). Npr2-positive brain regions identified by β-gal expression at different developmental stages are also summarized in Table 5.4. Overall,

Npr2 expression was low to moderate in postnatal and adult brain and β-gal-expression was restricted to specific brain regions in a developmental stage-dependent manner. Analysis of brain cryosections by X-Gal indicated that Npr2 has the highest expression level at P0 and the lowest expression level at P5. In the anterior olfactory nucleus (AON), dentate gyrus (DG), habenula (Hbl), nucleus of facial nerve (NFN) and thalamic nuclei (TN) Npr2 is expressed throughout the postnatal and adult stages of development (Table 5.4).
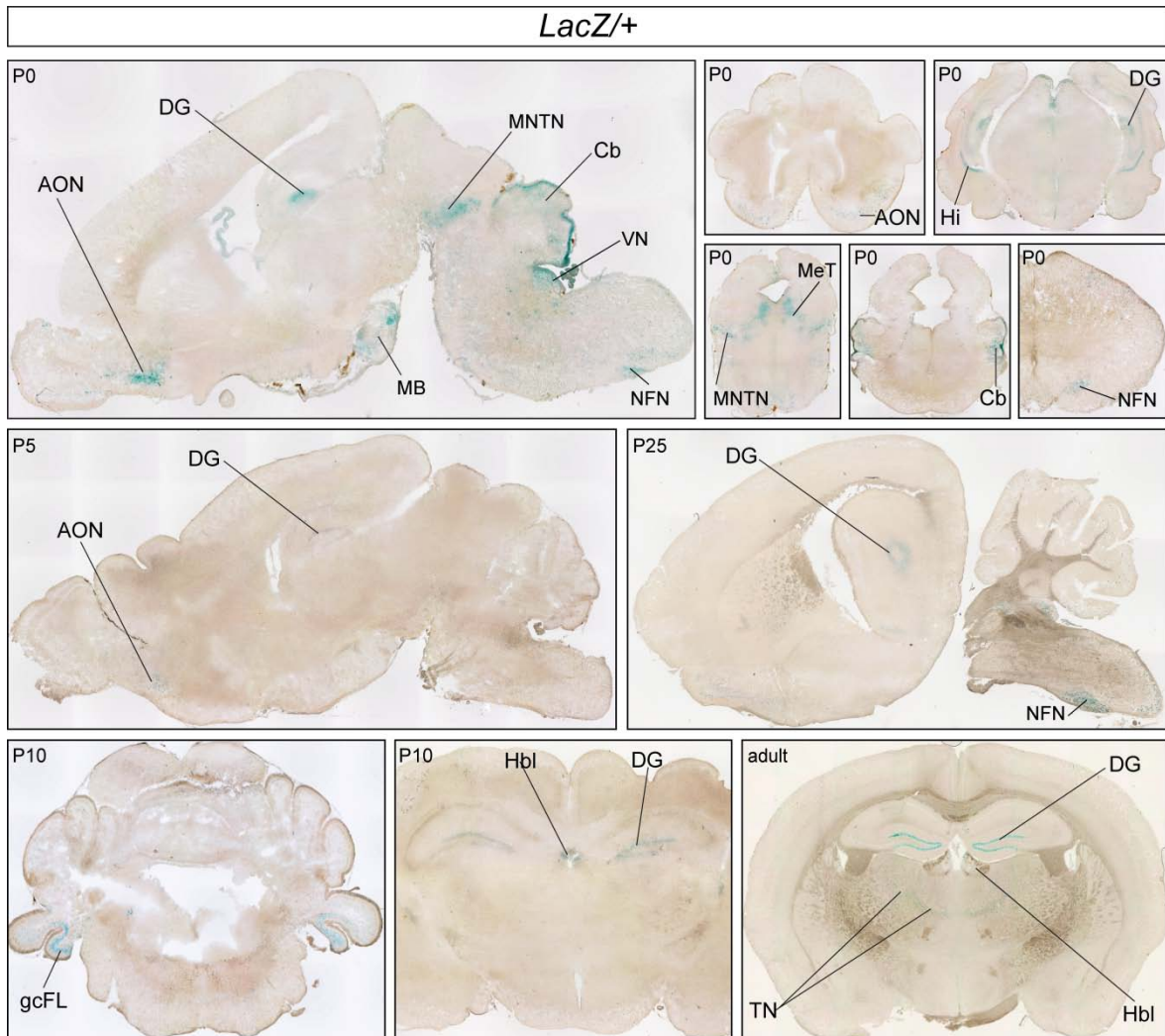
Figure 5.20: Expression of Npr2 in postnatal and adult stages of brain development. Representative images of sagittal and coronal cryosections from heterozygous Npr2LacZ mouse brains stained with X-Gal revealed β-gal expression in the following brain regions: anterior olfactory nucleus (AON), cerebellum (Cb), dentate gyrus (DG), granule cell layer of flocculus (gcFL), habenula (Hbl), hippocampus (Hi), mammillary body (MB), mesencephalic tegmentum (MeT), mesencephalic nucleus of trigeminal nerve (MNTN), nucleus of facial nerve (NFN), thalamic nuclei (TN), vestibular nuclei (VN).

Table 5.4

Structure	P0	P5	P10	P25	adult
Anterior olfactory nucleus (AON)	✓	✓	✓	✓	✓
Cerebellum (Cb)	✓	✓	✓		
Dentate gyrus (DG)	✓	✓	✓	✓	✓
Granule cell layer of flocculus (gcFL)	✓	✓	✓		
Habenula (Hbl)	✓	✓	✓	✓	✓
Hippocampus (Hi)	✓				
Mammillary body (MB)	✓				
Mesencephalic tegmentum (MeT)	✓				
Mesencephalic nucleus of trigeminal nerve (MNTN)	✓				
Nucleus of facial nerve (NFN)	✓	✓	✓	✓	✓
Thalamic nuclei (TN)	✓	✓	✓	✓	✓
Vestibular nuclei (VN)	✓				

Table 5.4: Summary of detected β-gal expression in heterozygous Npr2LacZ mice at different postnatal (P0, P5, P10, P25) and adult stages of brain development.

5.6 Generation of the Npr2CreERT2 mouse line for sparse labeling of Npr2 expressing neurons

After having identified Npr2-positive neurons that also express cGKIα, the intention was to characterize the axonal branching of these neurons. For sparse labeling of Npr2-expressing neurons a genetic strategy was chosen combining an Npr2 promoter-driven tamoxifen-inducible CreERT2 mouse (Npr2CreERT2) and reporter lines. Crossing of the newly generated Npr2CreERT2 line with a reporter line such as Z/AP and mGFP would allow following the trajectories of single Npr2-positive neurons in Npr2 heterozygous mice. In addition, complete inactivation (knockout) of Npr2 would allow studying the branching behavior of Npr2-positive neurons.

5.6.1 Cloning strategy

The cloning strategy of the Npr2CreERT2 mouse model is identical to that of the Npr2LacZ mouse model based on the usage of the same BAC clone bMQ331a20 (see chapter 5.1.1) and the same homology arm-flanked pDTA vector with a subcloned Npr2 gene fragment (see chapter 5.1.1.2).

5.6.1.1 Construction of the mini-targeting vector

The construction of the mini-targeting vector is illustrated in Figure 5.21. The mini-targeting vector contains two homology arms (5' and 3' homology arm), a CreERT2-cassette followed by a polyA-stretch and the pHW025 vector containing the neomycin resistance marker gene flanked by FRT-sites (FRT-Neo-FRT).

The BAC amplification products were cloned into the plasmid pBluescript II SK+ either by blunt end or sticky end ligation. The ligation was followed by a control digestion and sequencing analysis. The description of each plasmid as well as the primer sequences used for amplification and sequencing analysis can be found in the appendix. Details concerning the cloning procedure are described in the Methods chapter.
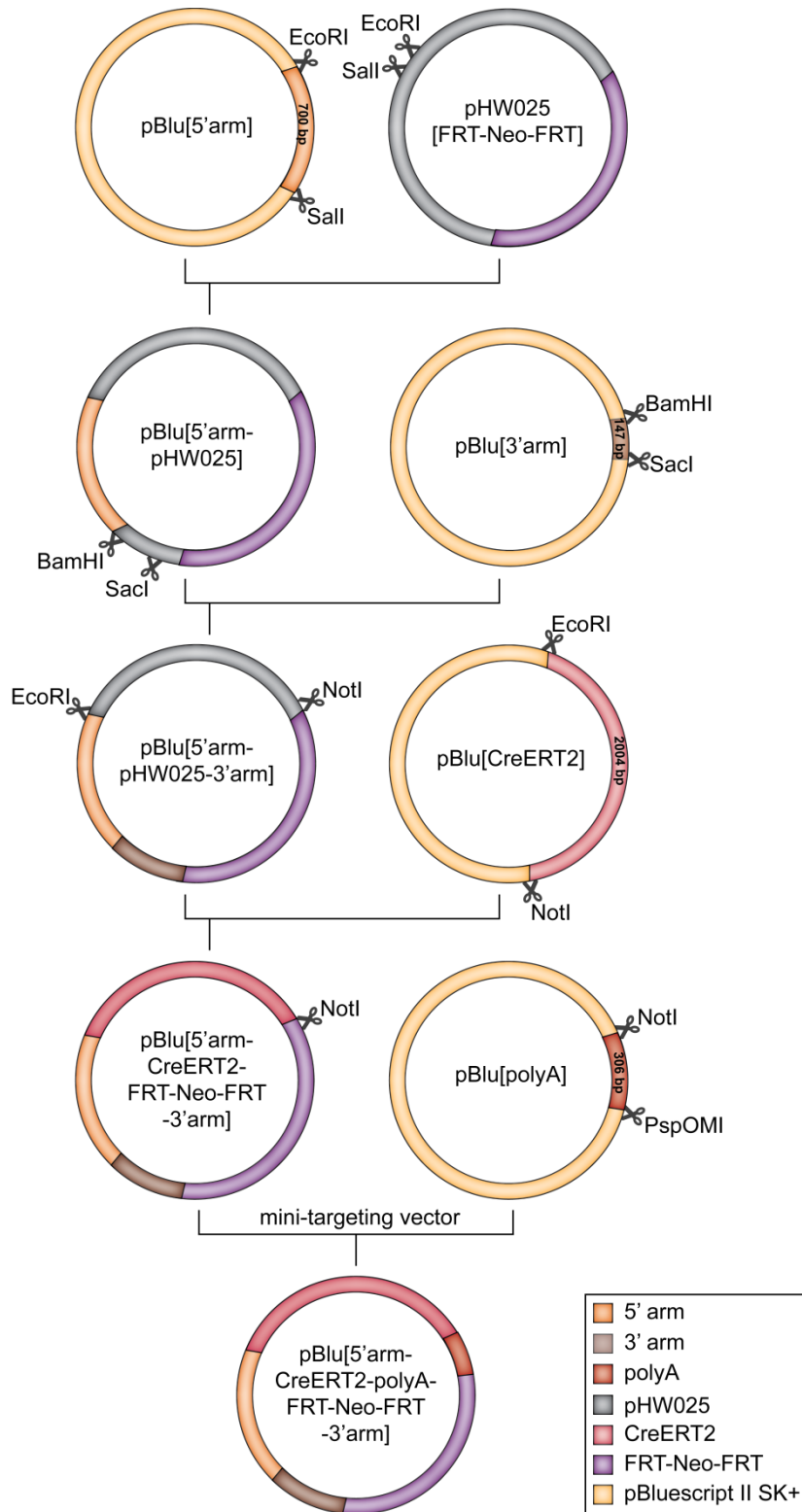
Figure 5.21: Cloning strategy of the mini-targeting vector for the Npr2CreERT2 targeting construct. A flow diagram of cloning steps starting with the cloning of the 5'arm (700bp) into the pHW025 plasmid by a sticky end ligation using the cleavage sites of the restriction enzymes EcoRI and SalI, followed by the cloning of the 3'arm (147bp) into the plasmid pBlu[5'arm-pHW025] (5515bp) by sticky end ligation using the cleavage sites of the restriction enzymes BamHI and SacI. The CreERT2-cassette (2004bp) was cloned into pBlu[5'arm-pHW025-3'arm] (5650bp) by sticky end ligation using the cleavage sites of the restriction enzymes EcoRI and NotI. Using a NotI cleavage site a polyA-sequence (306bp) was cloned into pBlu[5'arm-CreERT2-FRT-Neo-FRT-3'arm] (7654bp) resulting in the mini-targeting vector pBlu[5'arm-CreERT2-polyA-FRT-Neo-FRT-3'arm] (7956bp).

5.6.1.2 Construction of the Npr2CreERT2 targeting vector

To generate the Npr2CreERT2 targeting construct, the mini-targeting vector was introduced in frame with exon 1 of the Npr2 gene. Analogous to the mini-targeting vector for the Npr2NLSLacZ targeting construct, exon 1 was disrupted with 5' and 3' homologous arms of the mini-targeting vector and the [CreERT2-polyA-FRT-Neo-FRT] mutation was brought under the control of the Npr2 promoter (Figure 5.22). The final targeting vector contained 5' and 3' homology regions of 2200bp and 7600bp, respectively and was then prepared for a homologous recombination event in ES cells.
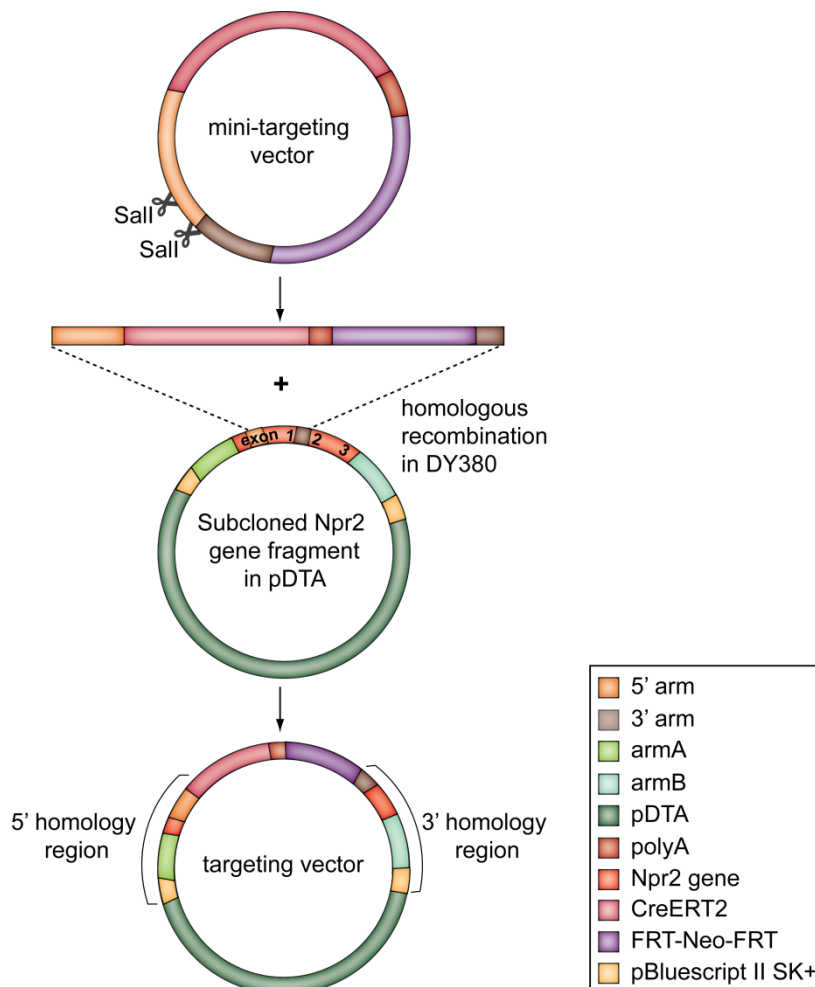
Figure 5.22: Design of the Npr2CreERT2 targeting construct. The mini-targeting vector with a length of 7956bp and homology arms was linearized by SalI and inserted into exon 1 of the Npr2 gene locus (subcloned in pDTA, 14524bp) by homologous recombination. The resulting targeting vector pDTA[gNpr2-CreERT2] with a length of 21.199bp contained the desired mutation construct [CreERT2-polyA-FRT-Neo-FRT] under the control of the Npr2 promoter and 5', 3' homology regions for homologous recombination in ES cells.

5.6.2 Homologous recombination in ES cells

As for the generation of the Npr2LacZ mouse model, the targeting vector was introduced into ES cells by electroporation (the used ES cell lines are summarized in Table 5.5). The targeting vector was linearized with PacI producing a 15149bp fragment to be electroporated (Figure 5.23A). After positive selection of ES cell clones with G418, the correct insertion of the targeting vector by homologous recombination was verified by Southern blot analysis. A primary screen with the 3'probe testing 1060 clones identified two primary positive clones (recombination efficiency of 0.2%). A rescreen with 5', Neo and 3'probes confirmed the accurate insertion of the targeting vector into the genome of the two ES cell clones tested (primary screen and rescreen of one clone is illustrated in Figure 5.23B).
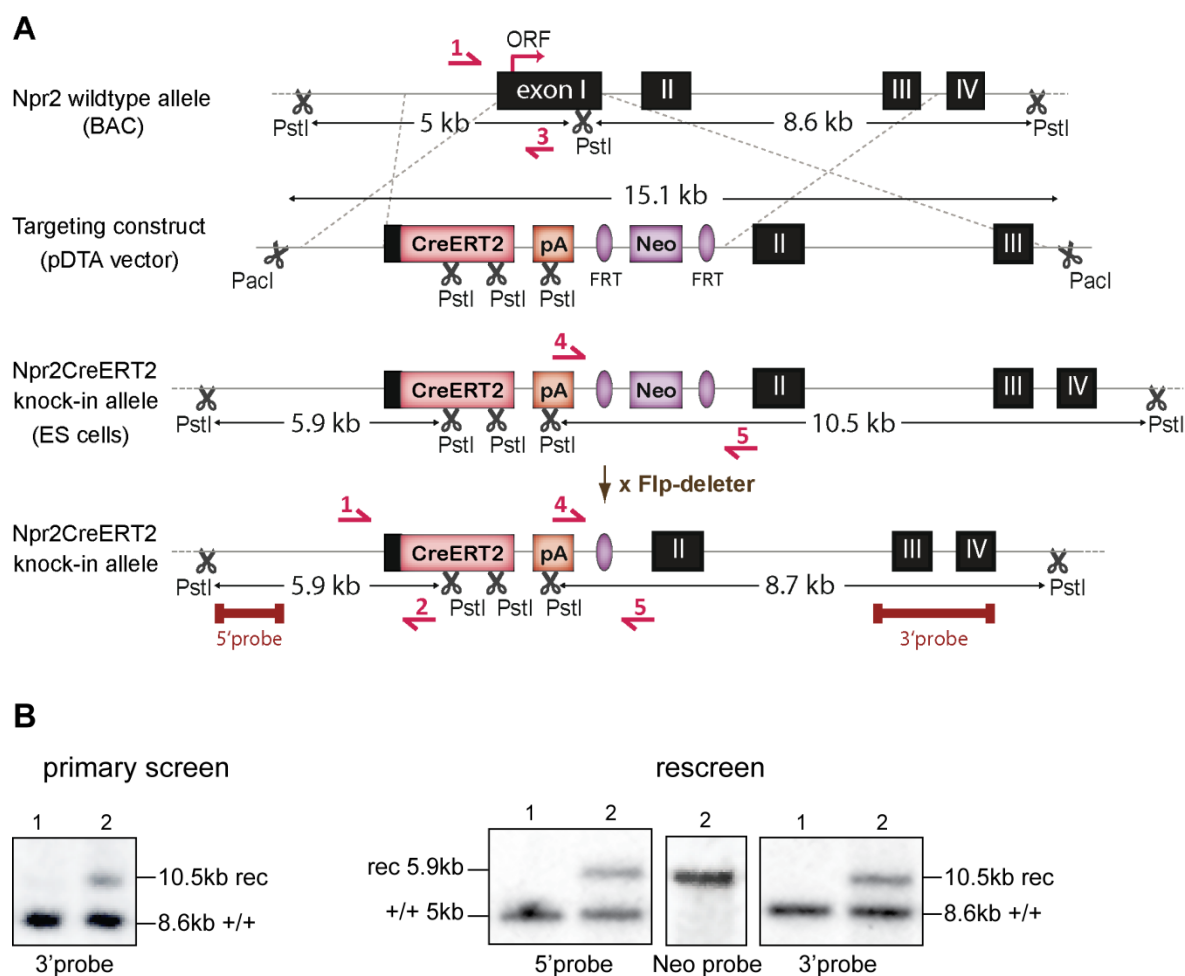
Figure 5.23: Generation of the Npr2CreERT2 mouse line. **(A)** Scheme of the targeting strategy in ES cells: the targeted region of the wildtype Npr2 gene locus (dashed lines) is illustrated by exons I, II, III, IV and PstI cleavage sites producing 5kb and 8.6kb fragments are indicated. The targeting construct was digested with PacI producing a 15.1kb DNA fragment to be electroporated into ES cells. After homologous recombination the targeting construct was inserted into the ES cell genome. Whereas PstI cleavage sites outside of the targeted region persisted, three new PstI cleavage sites were added by the targeting construct producing 5.9kb and 10.5kb fragments during PstI digestion. The germline transmission of the targeted ES cells and excision of the Neo-cassette was performed by crossing the chimera with the Flp-deleter strain. **(B)** Southern blot analysis using PstI-digested ES cell DNA and sequence-specific DNA probes (binding regions are shown as red bars in A). The probes were the same as for the Npr2LacZ mouse model. The recombinant clone was identified by a primary screen using the 3'probe. A rescreen using 5', Neo and 3'probes the respective bands at 5.9kb and 10.5kb confirmed the correct homologous recombination.

5.6.3 Blastocyst injection, chimera production and germline transmission

After a positive rescreen of ES cell clones by Southern blot, two confirmed positive ES cell clones were injected into C57Bl/6 blastocysts by the Transgenic Core Facility of the Max Delbrück Center for Molecular Medicine (summarized in Table 5.5).

Table 5.5

ES cell line	# of electro-poration	# of tested ES clones	# of positive clones	blastocyst injection	# of chimera	germline transmission
E14.1	2	700	1	✓	5	-
AB2.1	1	360	1	✓	5	1x

Table 5.5: Summary of the ES cell lines used in this study; given are the number of performed electroporations and the number of ES cell clones tested by primary Southern blot analysis, the number of positive clones with a correct homologous recombination in individual ES cell lines, the number of performed blastocyst injections of positive ES clones and the corresponding number of male chimeric offspring giving rise to germline transmission.

The generated male chimera exhibited patches of colored coat and were analyzed by PCR genotyping for the presence of the transgene (Figure 5.24). The male chimeras were mated to Flp-deleter females and the resulting offspring with brown coat color were indicative for germline transmission with concomitant removal of the Neo-cassette and generation of heterozygous animals. This was confirmed by PCR using appropriate primer (see chapter 4.3.5).
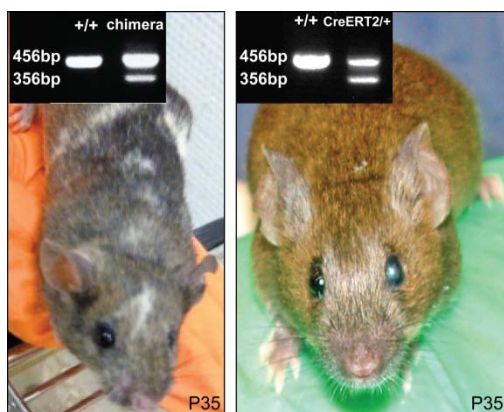
Figure 5.24: Left, a 5-week-old male chimera generated from AB2.1 ES cell injection into C57Bl/6-derived blastocysts. The white patches on the chimera coat were derived from the AB2.1 ES cells. PCR analysis confirmed the presence of the transgene in chimera (band at 356bp), whereas wildtype *(+/+)* showed a band at 456bp. Right, a 5-week-old brown offspring of the F1 generation was heterozygous for the transgene *(CreERT2/+)* as verified by PCR analysis.

5.6.4 Establishment of the Npr2CreERT2 mouse line

The heterozygous offspring obtained in chapter 5.6.3 were backcrossed to wildtype C57Bl/6 mice for several generations to get a C57Bl/6 genetic background. Southern blot analysis of wildtype *(+/+)* and heterozygous Npr2 *(CreERT2/+)* mice confirmed the generation of the Npr2CreERT2 mouse line (Figure 5.25A). PCR studies analyzing the removal of the Neo-cassette by crossing with Flp-deleter strain (see chapter 4.3.1) and genotyping the Npr2CreERT2 mouse line (see chapter 4.3.5) are shown in Figure 5.25B.
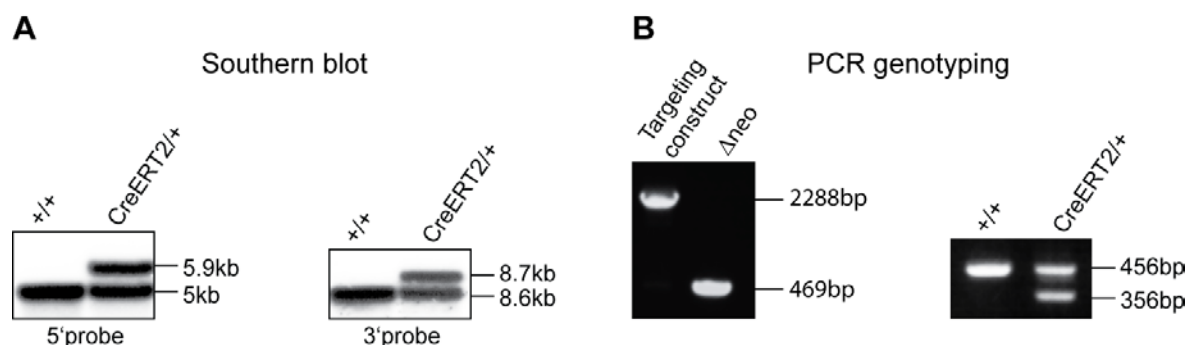
Figure 5.25: Establishing the Npr2CreERT2 mouse model. **(A)** Southern blot analysis using DNA extracted from the liver of wildtype *(+/+)* and heterozygous Npr2 *(CreERT2/+)* mice. DNA digestion by PstI produced DNA fragments of 5kb and 8.6kb for wildtype *(+/+)* and 5.9kb and 8.7kb for the mutant Npr2 allele *(CreERT2/+)*. The 5' and 3'probes were the same as those used in Southern blot analysis of ES cells (Figure 5.23). The 5'probe recognized the 5kb fragment of the wildtype and the 5.9kb fragment of the CreERT2 knock-in allele. The 3'probe recognized the 8.6kb fragment of the wildtype and the 8.7kb fragment of the CreERT2 knock-in allele. **(B)** PCR analysis confirmed the deletion of the Neo-cassette in the Npr2CreERT2 mouse (Δneo) by amplification of a 469bp fragment using primers 4 and 5 indicated in Figure 5.23A. The targeting construct with the Neo-cassette served as a control amplifying a 2288bp fragment. Right, the PCR analysis of wildtype *(+/+)* and heterozygous Npr2 *(CreERT2/+)* mouse DNA. Binding sites of the primers 1, 2, 3 are indicated in Figure 5.23A. Primers 1 and 3 bound in the wildtype sequence and amplified a 456bp DNA fragment, while the primer 2 bounds in the CreERT2 knock-in sequence and together with primer 1 amplified a 456bp DNA fragment. Amplification products were analyzed by agarose gel electrophoresis.

5.7 Phenotypic verification of the Npr2CreERT2 mouse

As described in chapter 5.2.3, mutations in the Npr2 gene leading to a nonfunctional protein cause achondroplastic dwarfism and a lack of bifurcation of DRG sensory axons at the DREZ (Schmidt et al. 2007; Sogawa et al. 2007; Tamura et al. 2004; Tsuji and Kunieda 2005). Figure 5.26A shows five-week-old homozygous Npr2CreERT2 (*CreERT2/CreERT2*) mouse displaying a dwarf phenotype and its wildtype littermate displaying normal growth. The phenotype of bifurcation failure at the DREZ is discussed in chapter 5.7.1. In order to test Npr2-specific expression of the Cre recombinase, immunohistochemical analyses were performed on DRG of heterozygous Npr2CreERT2

(*CreERT2/+*) and wildtype mice at E12.5 (Figure 5.26B). The analysis demonstrated the targeted Cre expression in DRG of heterozygous Npr2CreERT2 mouse embryos.
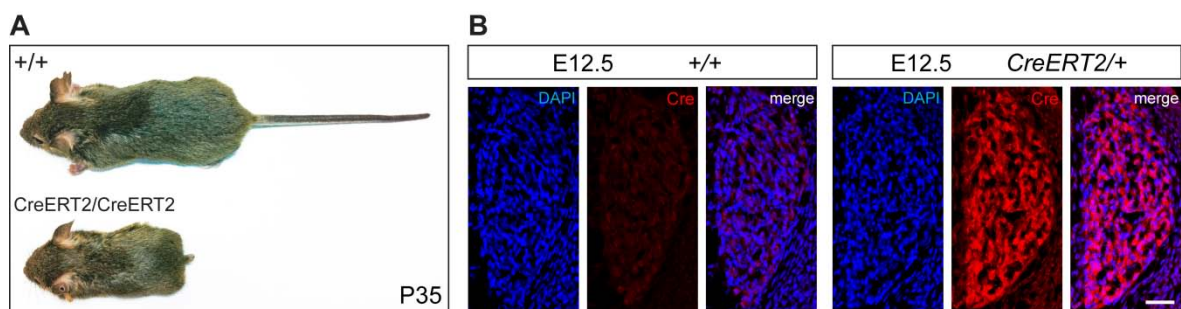
Figure 5.26: Phenotype and Npr2-specific Cre expression in the Npr2CreERT2 mouse. **(A)** A 5-week-old homozygous Npr2CreERT2 mouse (*CreERT2/CreERT2*) in comparison to its wildtype littermate. **(B)** Immunohistochemistry using a rabbit-α-Cre antibody and DAPI-staining to demonstrate the specific expression of Cre recombinase under the control of the Npr2 promoter in DRG of a heterozygous Npr2CreERT2 mouse (*CreERT2/+*) at E12.5. Scale bar 10µm.

5.8 Sparse neuron labeling using the Npr2CreERT2 mouse

The general strategy of spatially and temporally controlled single cell labeling is introduced in chapter 1.6 and its subchapters. The mouse breeding strategy and genetic manipulations used in this study to produce Npr2-knockout versus Npr2-expressing mice or embryos for visualization of single neurons is illustrated in Figure 5.27. In order to avoid higher expression levels of CreERT2 in homozygous Npr2CreERT2 mice in comparison to heterozygous Npr2CreERT2 mice, another Npr2 mutant mouse line was introduced in the breeding strategy: the Npr2(cn) line carrying a loss-of-function mutation of the Npr2 gene (Tsuji and Kunieda 2005).

In the first step of the breeding strategy (Figure 5.27, 1.) the heterozygous Npr2(cn) (*cn/+*) mice were crossed with a reporter line (either Z/AP or mGFP). The reporter gene was silent because of the loxP-flanked STOP-cassette upstream of the specific reporter gene cassette. 25% of the offspring from this crossing carried both to the *cn/+*-mutation and the silent reporter gene (either $Npr2^{cn/+}Z/AP$ or $Npr2^{cn/+}mGFP$). In the second step of the breeding strategy (Figure 5.27, 2.) these mice were then mated with the heterozygous Npr2CreERT2 mice (*CreERT2/+*). 12.5 % of the resulting embryos carried the heterozygous Npr2 genotype of interest (either $Npr2^{CreERT2/+}Z/AP$ or $Npr2^{CreERT2/+}mGFP$) and another 12.5 % carried the Npr2 knockout genotype of interest (either $Npr2^{CreERT2/cn}Z/AP$ or $Npr2^{CreERT2/cn}mGFP$). The Npr2 heterozygous mice were phenotypically indistinguishable from wildtype mice.

After administration of tamoxifen or 4-hydroxytamoxifen to the timed pregnant mice (E9.5 or E10.5), the Cre recombinase became activated in Npr2-expressing cells as it

translocated into the nucleus and performed the excision of the loxP-flanked STOP-cassette. Thus, the reporter genes AP or mGFP were only expressed in cells, which expressed Npr2.
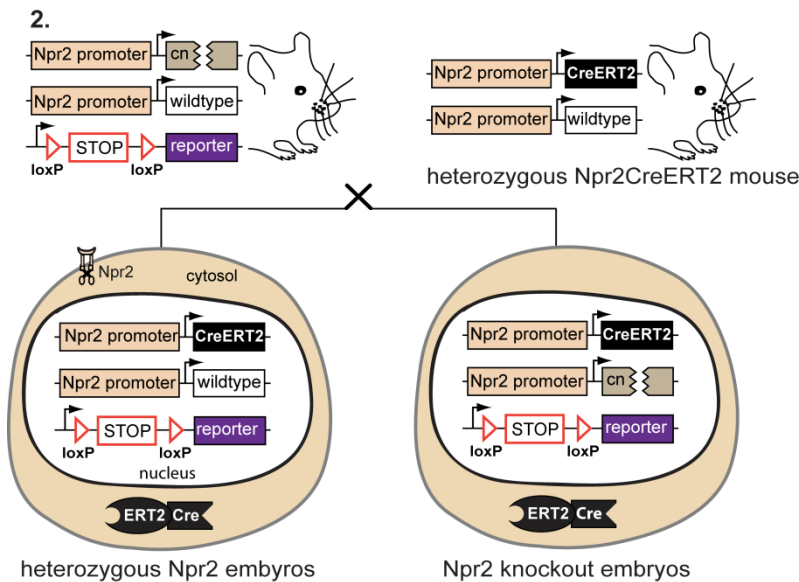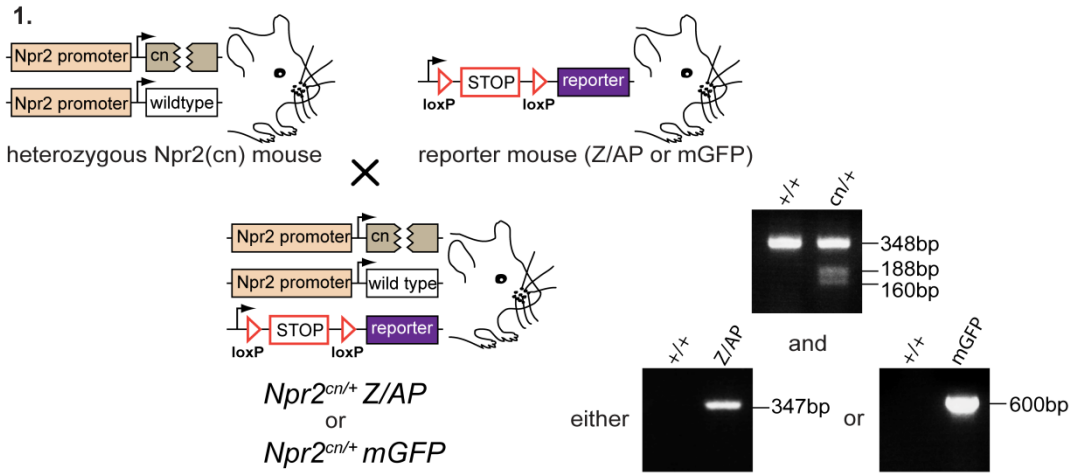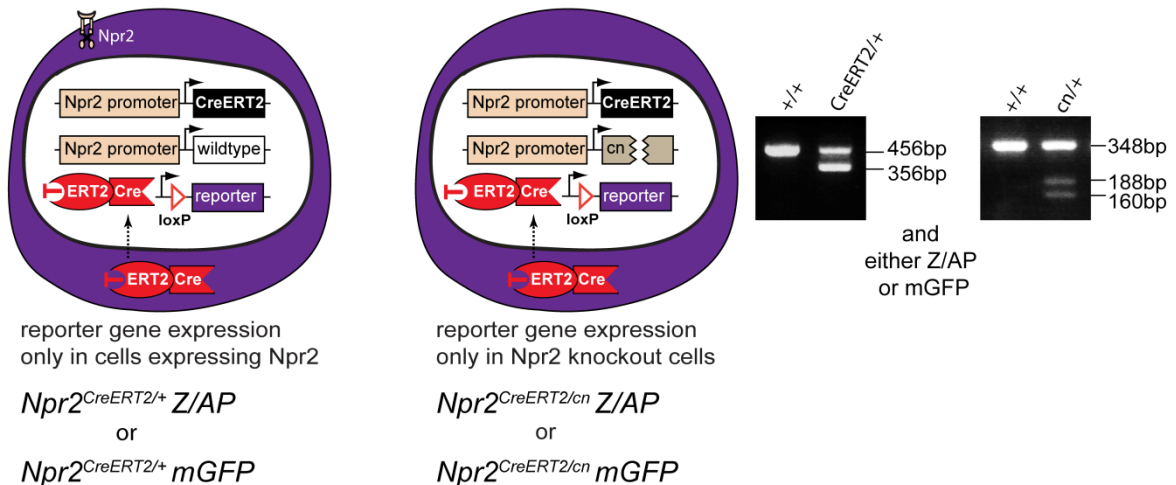
Figure 5.27: Mouse breeding strategy for sparse labeling of Npr2-expressing neurons. First, the heterozygous Npr2(cn) mice (*cn/+*) were crossed with one of the reporter lines (either Z/AP or mGFP) and the offspring were genotyped for the (*cn/+*)- and reporter gene-mutations (the genotype is denoted as *Npr2^{cn/+}Z/AP* or *Npr2^{cn/+}mGFP*). PCR genotyping of the (*cn/+*) and reporter gene mutation was analyzed by agarose gel electrophoresis. In the second crossing, *Npr2^{cn/+}Z/AP* or *Npr2^{cn/+}mGFP* mice were mated with the heterozygous Npr2CreERT2 mice (*CreERT2/+*). The administration of tamoxifen or 4-hydroxytamoxifen to the timed pregnant mice resulted in activation of Cre recombinase, excision of the STOP-cassette and thus expression of the reporter gene in embryonic cell populations that express Cre under the control of the Npr2 promoter. The genotypes of interest were either Npr2 heterozygous (*Npr2^{CreERT2/+}Z/AP* or *Npr2^{CreERT2/+}mGFP*) or Npr2 knockout (*Npr2^{CreERT2/cn}Z/AP or Npr2^{CreERT2/cn}mGFP*).

5.8.1 Proof-of-principle: using the Npr2CreERT2 mouse for single axon labeling and branching analysis

The genetic approach described in chapter 5.7 for visualization of single Npr2-expressing neurons was verified in embryonic DRG - an established system to control the role of Npr2 and its cGMP-dependent signaling pathway in the branching of sensory axons during development (Schmidt et al. 2009; Schmidt et al. 2007; Schmidt et al. 2002). For that purpose the Z/AP reporter line was used and a treatment described in chapters 4.4.5 and 4.5 yielded the following results: DRG sensory axons stained by the Z/AP reporter line demonstrated a bifurcation at the DREZ in heterozygous Npr2 mice (*Npr2^{CreERT2/+}Z/AP*) but a lack of bifurcation in Npr2-deficient mice (*Npr2^{CreERT2/cn}Z/AP*) (Figure 5.28A).

Previous studies have shown that the branching of sensory axons in heterozygous Npr2 or cGKIα mouse mutants is identical to the wildtype (Schmidt et al. 2007). The quantification of bifurcation (Figure 5.28B, C) was performed by analyzing 88 single AP-labeled DRG sensory axons in 586 DRG from 16 heterozygous Npr2 mouse embryos treated with 0.1mg tamoxifen per gram body weight. The bifurcation error was quantified by analyzing 63 single AP-labeled DRG sensory axons in 498 DRG from 14 Npr2 KO mouse embryos at E12.5 or E13.5. The branching of single axons was evaluated at cervical, thoracic, lumbar and sacral regions of the spinal cord (Figure 5.28B). These data show that in the heterozygous Npr2 mice all DRG sensory axons bifurcate (blue balks at 100% in Figure 5.28B), while in the Npr2 KO mice all sensory axons turn in either rostral or caudal direction with a slight preference for the rostral direction.

A

B

C

Number of	*Npr2^{CreERT2/+} Z/AP*	*Npr2^{CreERT2/cn} Z/AP*
Embryos	16	14
DRG	586	498
Labeled axons	88	63
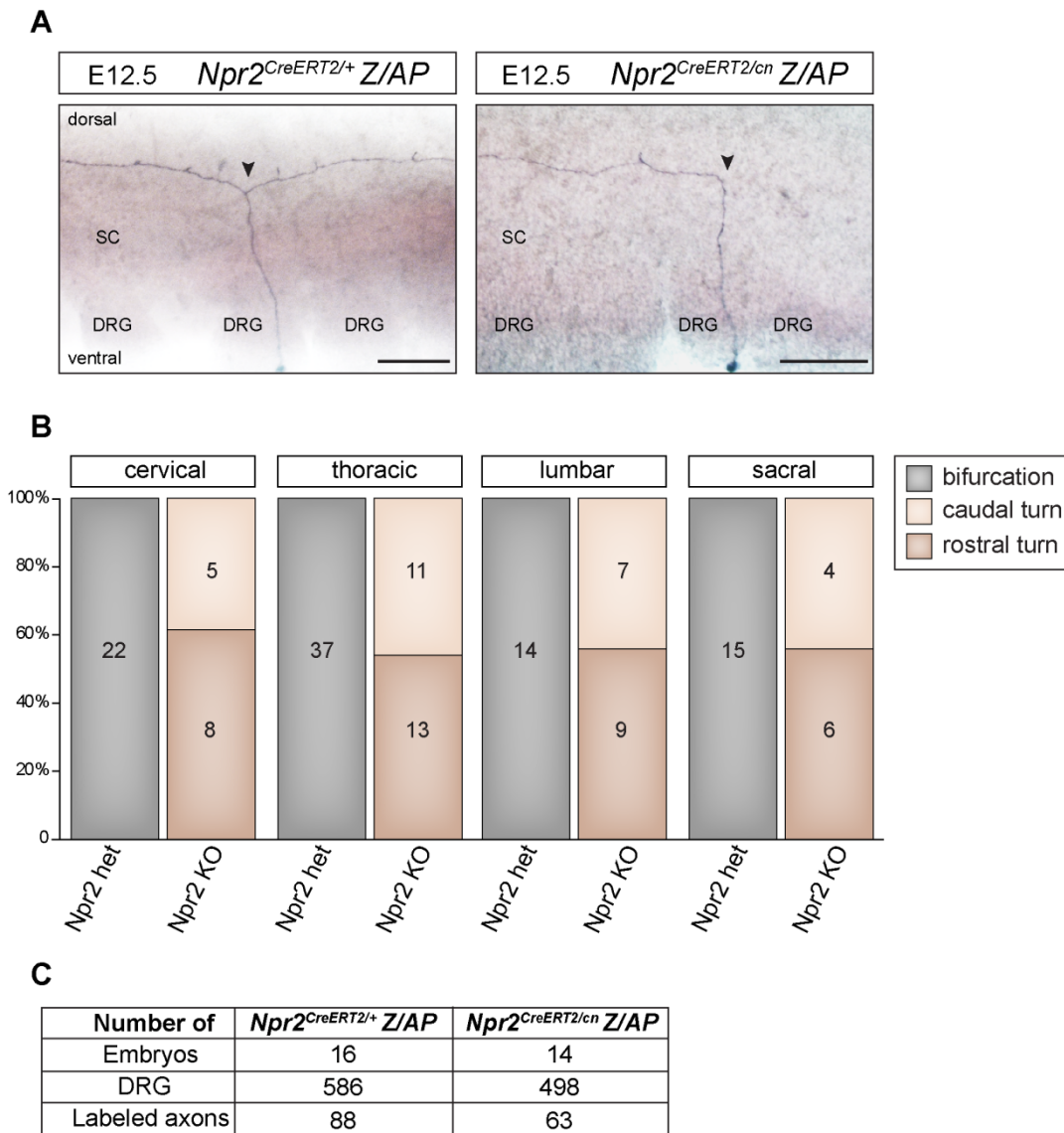
Figure 5.28: Proof-of-principle of tamoxifen-dependent AP-labeling of Npr2-positive cells using DRG sensory neurons. **(A)** Images of single DRG sensory axons in heterozygous Npr2 (*Npr2^{CreERT2/+}Z/AP*) and Npr2 knockout (KO) (*Npr2^{CreERT2/cn}Z/AP*) mouse embryos at E12.5. The staining for AP specifically expressed in Npr2-expressing neurons visualized the soma (dark dot on the DRG) and the axons extending into the spinal cord (SC). The arrowheads indicate the bifurcation at the DREZ in the heterozygous Npr2 and the lack of bifurcation in the Npr2 knockout mice. Scale bar 100μm. **(B)** Quantification of the bifurcation in heterozygous Npr2 (Npr2 het) and Npr2 knockout (Npr2 KO) mice. The numbers in the balks indicate the counted single axons at cervical, thoracic, lumbar and sacral regions of the spinal cord. The subdivision of the quantification balk in the Npr2KO indicates the turning directions of sensory axons, either caudal or rostral. **(C)** Summary of embryo, DRG and labeled sensory axon numbers used for the quantification of the bifurcation in heterozygous Npr2 and Npr2 KO mice.

Thus, the single labeled DRG sensory axons and the quantification data in Figure 5.28 provide an evidence for (i) the reliability of the Npr2CreERT2 mouse model and the genetic approach of sparse labeling of Npr2-expressing neurons to analyze their branching pattern, (ii) impaired bifurcation of DRG sensory axons at the DREZ in the absence of Npr2 as reported previously (Schmidt et al. 2007).

5.9 Analyzing the branching pattern of cranial sensory axons

After validation of the Npr2CreERT2 mouse model as a useful tool to study axonal branching of Npr2-expressing neurons (chapter 5.8.1.) and identification of cranial sensory ganglia as cell populations with a prominent Npr2 expression co-localized with cGKIα (chapters 5.3 and 5.4), next, the central projections of cranial sensory axons were explored using two different reporter lines. Branching pattern analyses utilizing the Z/AP and mGFP reporter mice are discussed in the following subchapters. Additionally, cell populations identified by X-Gal staining and immunohistochemical analysis were further characterized by sparse axon labeling (chapter 5.9.2).

5.9.1 Visualization of axon projections of single cranial sensory neurons by crossing of Npr2CreERT2 mouse with the Z/AP reporter line

As demonstrated for DRG neurons, crossing of Npr2CreERT2 with Z/AP reporter mice allows the visualization of axonal projections of individual neurons. Npr2-expressing neurons from cranial sensory ganglia were labeled by tamoxifen treatment on timed pregnant mice (E9.5 or E10.5) using a tamoxifen concentration of 0.1mg per gram body weight. Cre-mediated recombination and expression of AP in Npr2-expressing cells occurred during the next 72h. After preparation of the embryos at E12.5 or E13.5, appropriate AP-staining and clearing of 250μm vibratome sections in BABB (see chapter 4.4.5), single axonal projections of cranial sensory ganglion neurons were studied (Figures 5.29 and 5.30).
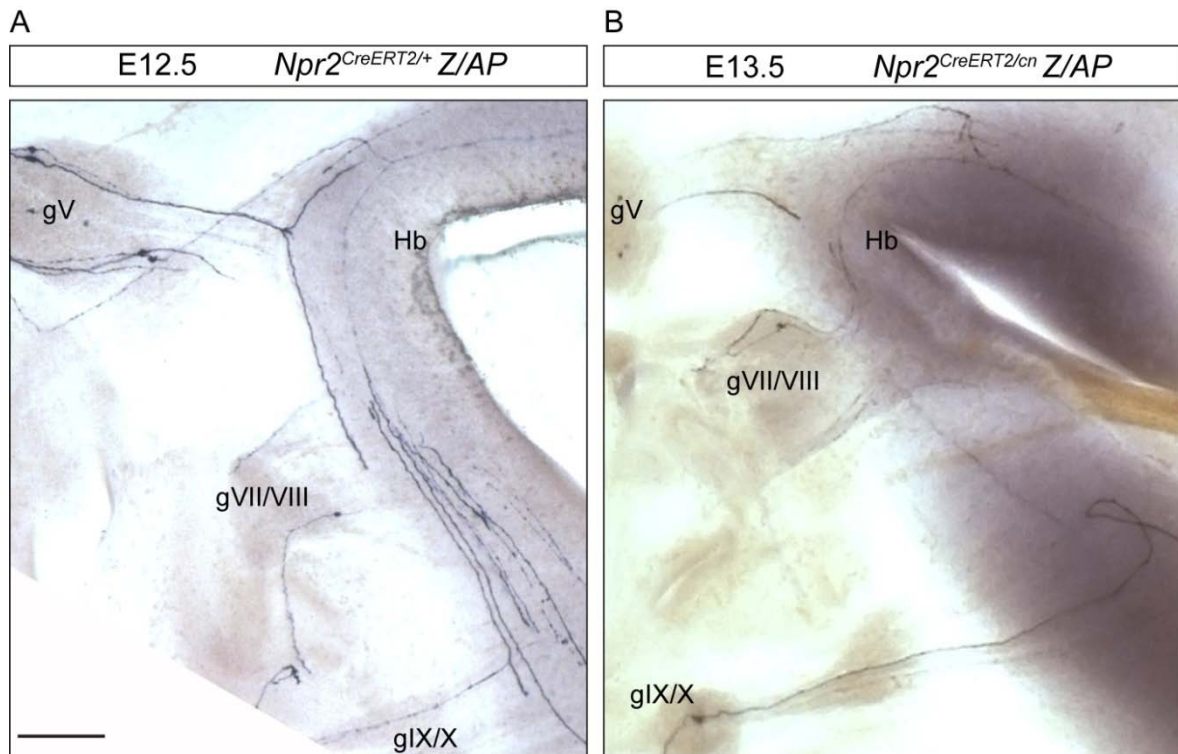
Figure 5.29: An overview of AP-labeled cranial sensory neurons in **(A)** heterozygous Npr2 (*Npr2^CreERT2/+^Z/AP*) mice at E12.5 and **(B)** Npr2 knockout (*Npr2^CreERT2/cn^Z/AP*) mice at E13.5. The overview images of 250µm sagittal vibratome sections show the expression of AP in all cranial sensory ganglia (gV, gVII/VIII and gIX/X) and single central projections of cranial sensory axons growing toward the hindbrain. g, ganglion; Hb, hindbrain. Scale bar 100µm.

Figure 5.29 gives a low magnification overview of the AP-staining performed on sagittal vibratome sections. The AP-staining visualized both the soma of sensory neurons in corresponding cranial sensory ganglia (gV, gVII/VIII and gIX/X) and their central projections growing toward the hindbrain. The staining showed how the axons enter the hindbrain, bifurcate at the entry zone in case of the heterozygous Npr2 (*Npr2^CreERT2/+^Z/AP*) mouse or make a turn in case of the Npr2 knockout (*Npr2^CreERT2/cn^Z/AP*) mouse. This is illustrated in more detail in Figure 5.30. Figures 5.29 and 5.30 demonstrate that this genetic approach can be used to track single Npr2-expressing axonal projections and evaluate the functional role of Npr2 and the cGMP–dependent signaling pathway in bifurcation of cranial sensory axons.
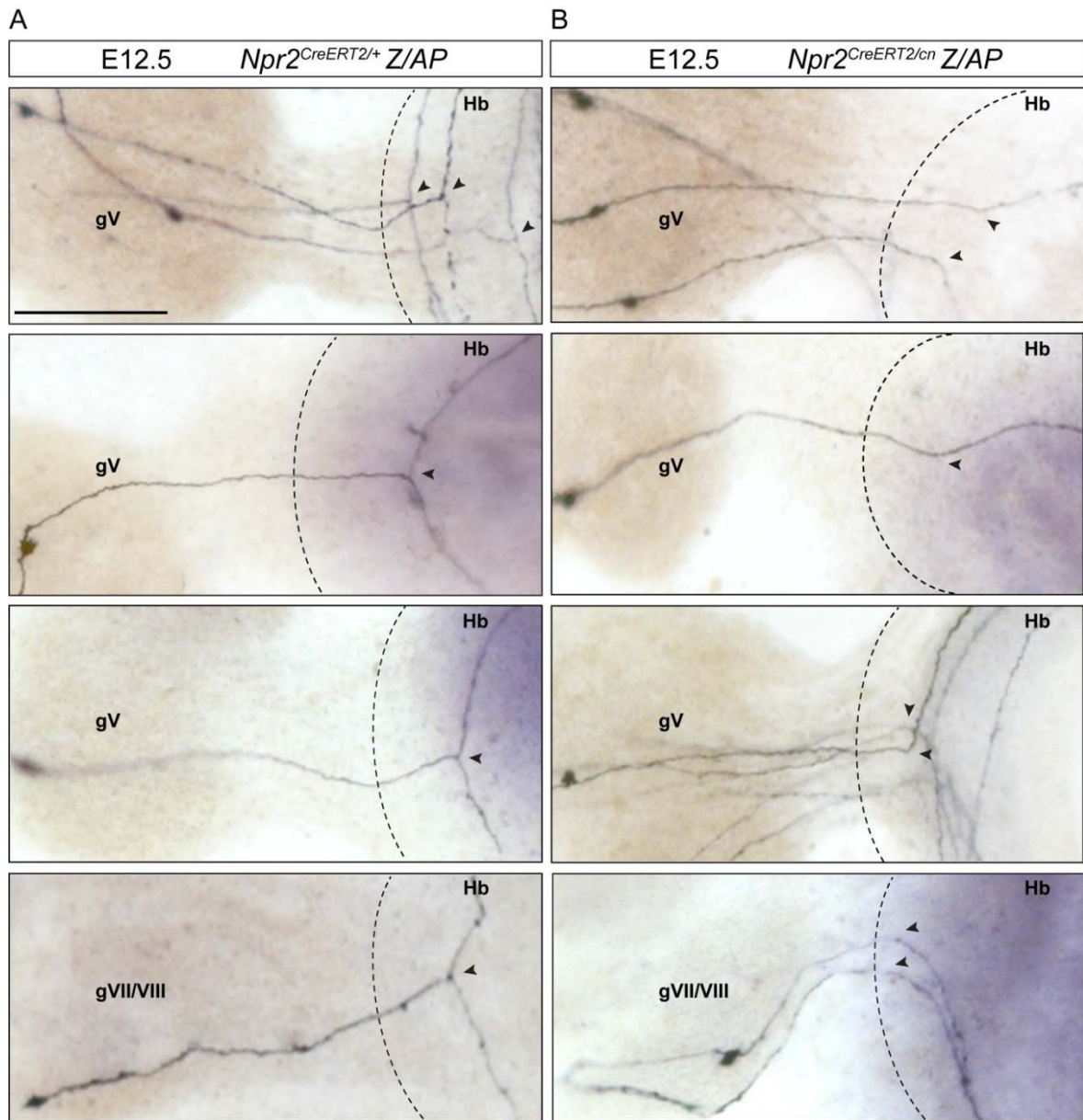
Figure 5.30: Visualization of single axonal projections of cranial sensory neurons by Cre-dependent AP expression at E12.5. **(A)** Whereas the central projections of sensory neurons from gV and gVII/VIII ganglia bifurcated upon entering the hindbrain in heterozygous Npr2 (*Npr2$^{CreERT2/+}$Z/AP*) mice, **(B)** no bifurcation could be detected in Npr2 knockout (*Npr2$^{CreERT2/cn}$Z/AP*) mice. The dashed lines demonstrate the hindbrain border. g, ganglion; Hb, hindbrain. Scale bar 100µm.

5.9.2 Visualization of axon projections of single cranial sensory neurons by crossing of Npr2CreERT2 mouse with the mGFP reporter line

The second reporter line used in this study to visualize single axonal projections of Npr2-positive neurons was the mGFP reporter mouse containing the enhanced green fluorescent protein (eGFP) gene under the control of the Tau-promoter. Timed pregnant mice carrying the appropriate genotypes (Figure 5.27) were treated with 4-

hydroxytamoxifen (OHT) at E9.5. Here, the concentration of OHT lay between 2µg to 40µg per gram body weight. After preparation of the embryos at E12.5, 50µm thick sagittal cryosections were produced and immunostained with a rabbit antibody against GFP (Figure 5.31).

The recombination efficiency of the mGFP reporter was directly proportional to the amount of OHT administered. In the heterozygous Npr2 mouse ($Npr2^{CreERT2/+}mGFP$) administration of OHT at a concentration of 40µg per gram body weight led to a large number of recombination events in Npr2-positive cells and consequently to labeling of a vast number of cranial sensory neurons (Figure 5.31A). After titration of the OHT concentration to 10µg per gram body weight, the number of cells and their central projections recombinantly expressing mGFP could be reduced as visualized by immunostaining. A small number of single axons could be observed at higher magnification, also enabling the detection of cranial sensory axon bifurcation of the gV (Figure 5.31B, lower panel). To refine the resolution of single axons, the concentration of OHT was further titrated to 2µg per gram body weight. As illustrated in Figure 5.31C, this concentration was ideal to induce recombination in only a few cells. In the Npr2 knockout mouse ($Npr2^{CreERT2/cn}mGFP$), usage of 2µg OHT per gram body weight enabled visualization of the defective axon bifurcation upon entry of the cranial sensory axons into the hindbrain (Figure 5.31C, lower panel).
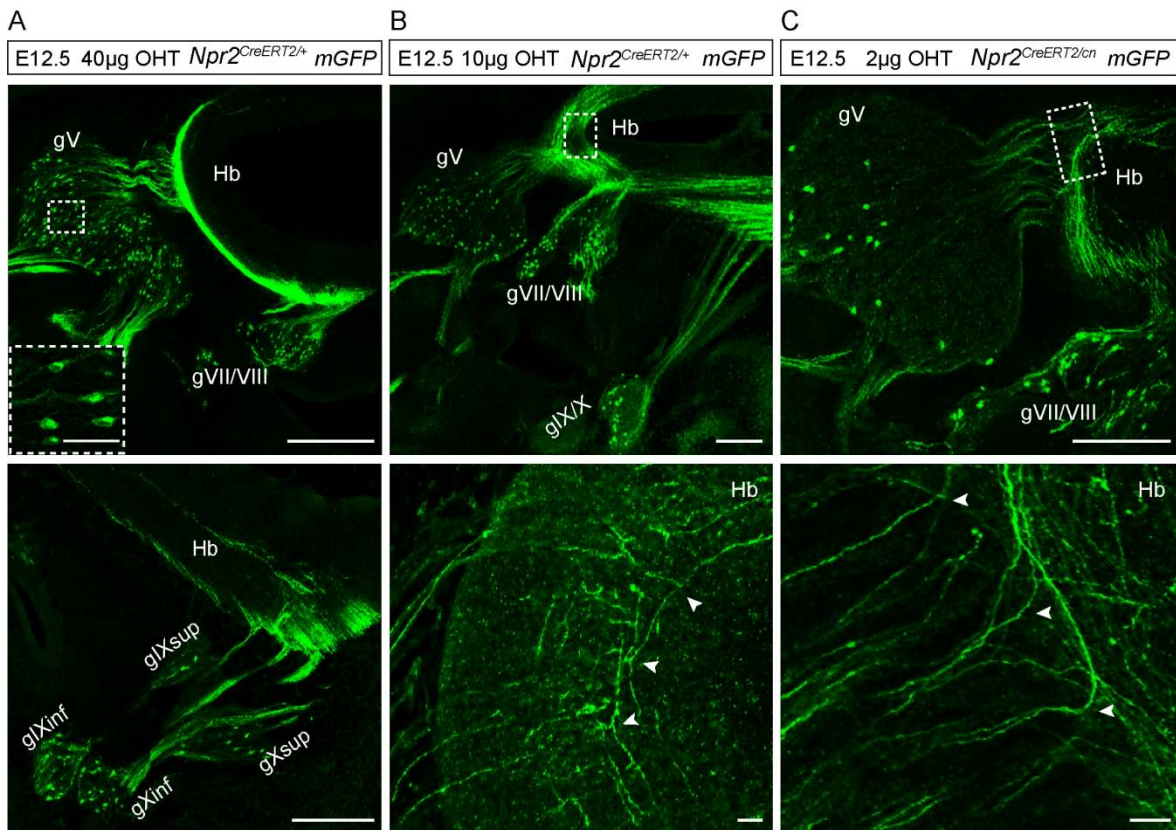
Fig 5.31: Visualization of central projections of cranial sensory neurons using the mGFP reporter line and titrating the concentration of 4-hydroxytamoxifen (OHT). **(A)** At an OHT concentration of 40µg/g body weight a high recombination efficiency of the mGFP reporter line was observed in the heterozygous Npr2 mice (*Npr2^{CreERT2/+}mGFP*). Numerous Npr2-expressing sensory axons were stained in all cranial sensory ganglia. Scale bar 100µm. **(B, C)** At OHT concentrations of 10 and 2µg/g body weight, respectively, only a small number of axons was stained in heterozygous Npr2 (*Npr2^{CreERT2/+}mGFP*) and Npr2 knockout (*Npr2^{CreERT2/cn}mGFP*) mice. Images at higher magnification revealed the bifurcation in the heterozygous and the turn in the Npr2 knockout mice. Scale bars 100µm and 10µm for respective lower and higher magnification images.

Thus, similar to the Z/AP reporter line the mGFP reporter line proved to be a suitable tool to visualize and analyze single Npr2-positive sensory axons.

5.9.3 Quantification of bifurcation errors of cranial sensory axons

The bifurcation of cranial sensory neurons was quantified by counting single axonal projections of each cranial sensory ganglion labeled by either AP or mGFP. Heterozygous Npr2 and Npr2 knockout mice at E12.5 or E13.5 were compared. As illustrated in Figure 5.32A, in the absence of Npr2 the cranial sensory axons did not bifurcate but only turned in either caudal or rostral direction with a slight preference to the caudal direction. In the heterozygous mouse all cranial sensory axons bifurcated except for the sensory axons of the trigeminal (gV) ganglion where some axons (9%) entered the hindbrain without bifurcation.
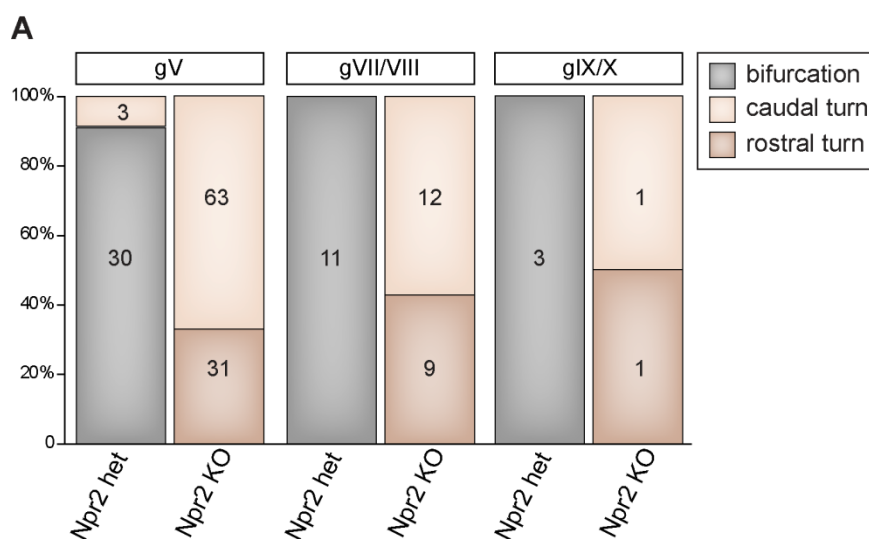
	genotypes	# of embryos
Npr2 het	*Npr2^{CreERT2/+} Z/AP*	13
	Npr2^{CreERT2/+} mGFP	1
Npr2 KO	*Npr2^{CreERT2/cn} Z/AP*	12
	Npr2^{CreERT2/cn} mGFP	3

Figure 5.32: Quantification of the bifurcation of cranial sensory axons in heterozygous Npr2 (Npr2 het) and Npr2 knockout (KO) mice at E12.5 and E13.5. **(A)** The numbers of counted single axons from each cranial ganglion (gV, gVII/VIII, gIX/X) using both Z/AP and mGFP reporter lines are given in the balks. The turning direction of cranial sensory axons (rostral or caudal) is indicated in different colors. In the Npr2 KO mice the cranial sensory axons from all cranial sensory ganglia showed bifurcation failure. In the heterozygous mice the cranial sensory axons from all cranial sensory ganglia bifurcated, except for some trigeminal (gV). 9% of the central projections of sensory axons did not bifurcate upon entering the hindbrain. **(B)** A summary of prepared embryos per genotype and reporter lines in which either AP- or GFP-labeled single axons were detected.

Thus, this genetic approach for the visualization of single Npr2-positive axons is a powerful tool to analyze the bifurcation of axons and to examine the effects of impaired cGMP signaling on axonal branching.

5.10 Analysis of phosphorylation targets of cGKIα

So far three components have been identified to be implicated in axon bifurcation: the ligand CNP, the receptor guanylyl cyclase Npr2 and the cGMP-dependent kinase Iα (cGKIα). To get mechanistic insights into the process of axonal bifurcation, it is essential to identify events downstream of the cGKIα.

To identify proteins that get phosphorylated by cGKIα, protein lysates from mouse embryonic DRG treated with either 8-pCPT-cGMP or CNP-22 ("stimulated", chapter 4.7) were examined by Western blot. Therefore, candidate proteins were analyzed by Western blot to investigate whether they get phosphorylated upon activation of cGKIα. Antibodies were (i) phospho-specific to detect phosphorylated proteins in the "stimulated" versus "non-stimulated" control material, (ii) non-phospho-specific to recognize a shift in the band size of distinct proteins due to phosphorylation in the "stimulated" material compared to the "non-stimulated" control, (iii) phospho-motif specific to detect the consensus phosphorylation site of cGKI (K/RK/RXpS/pT). All antibodies are listed in Table 10.7 in the appendix.

To monitor the activation of cGKIα in "stimulated" DRG material, an antibody against the known cGKIα-target VASP (Vasodilator stimulated phosphoprotein) was used (Halbrugge and Walter 1989) as a positive control. Phosphorylation of VASP by cGKIα results in a band-shift from 46kDa to 50kDa (Schäffer 2006; Stonkute 2010) (Figure 5.33A). A non-phospho-specific antibody recognizing Tau, a microtubule-associated protein, showed a slight band shift after stimulation with the cGMP analogue 8-pCPT-cGMP by Western blot analysis (Figure 5.33B). The band shift was indicative for Tau phosphorylation by cGKIα and its role in bifurcation of DRG sensory neurons.
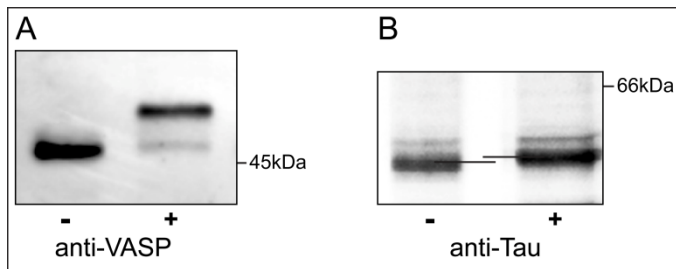
Figure 5.33: Western blot analysis of protein lysates from embryonic DRG after stimulation of cGKIα with 8-pCPT-cGMP. **(A)** The activation of cGKIα in "stimulated" material (labeled as **+**) compared to the "non-stimulated" material (labeled as **-**) was confirmed by a band-shift from 46kDa to 50kDa using an anti-VASP antibody. **(B)** Using an anti-Tau antibody a minimal band shift was detectable in the "stimulated" versus "non-stimulated" material. 6 DRG per lane were applied to SDS-PAGEs.

To study the implication of Tau in the bifurcation of DRG sensory neurons, Tau knockout mouse model (Hundelt et al. 2011) was examined using DiI-labeling (Figure 5.34).There was no bifurcation error in the Tau knockout mouse, indicating that Tau is not implicated in the CNP-Npr2-cGKIα signaling pathway.
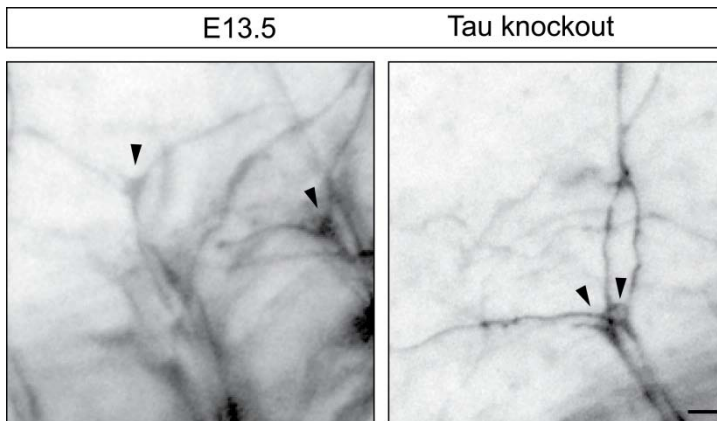
Figure 5.34: DiI-labeling analysis of DRG sensory axons in the Tau knockout mouse at E13.5. The sensory axons bifurcate at the DREZ as indicated by arrowheads. Scale bar 10µm.

Known proteins being phosphorylated by cGKI in DRG are Mena (mammalian enabled Ena/VASP family member) and VASP. Although both proteins are phosphorylated by cGKI, neither VASP knockout mice nor Mena/Vasp double knockout mice showed a bifurcation failure (Stonkute 2010). Hence, they are not components of the CNP-Npr2-cGKIα signaling pathway that controls bifurcation of sensory axons both at the DREZ and hindbrain entry zones. Therefore, besides the accurate search for phosphorylation targets of cGKIα by Western blot analysis, the involvement of a specific protein in the CNP-Npr2-cGKIα signaling pathway needs to be validated at the genetic level by investigating the bifurcation of sensory axons in respective mutant mouse models.

6. Discussion

This study addressed the question whether the cGMP signaling pathway that was previously identified to be responsible for the bifurcation of central axon projections of DRG neurons (Schmidt et al. 2009; Schmidt et al. 2007; Schmidt et al. 2002), is also involved in the bifurcation of other neuronal subpopulations.

The results presented here provide evidence at the single neuron level that in absence of Npr2 the central projections of cranial sensory axons are not able to bifurcate at the hindbrain entry zone. In the Npr2 knockout embryos the central projections of cranial sensory axons grew toward the hindbrain and instead of bifurcating, axons extended either an ascending or a descending arm into the hindbrain (Figure 6.1). Histological studies using heterozygous embryos of the newly generated Npr2LacZ mouse line uncovered a prominent Npr2 expression as well as a co-localization of Npr2 and cGKIα in cranial sensory ganglia. Co-localization of two proteins was also observed in the mesencephalic trigemical nucleus (MTN) and in a neuronal subpopulation in the dorsal part of rhombomere 1 (summarized in Table 6.1).

Neuronal subpopulations	Co-localization of Npr2 and cGKIα	Bifurcation phenotype of sensory neurons		Embryonic origin of neurons*
		in wildtype	Failure in Npr2 KO	
Spinal cord				
Dorsal root ganglia	✓	✓	✓	Neural crest
Cranial sensory ganglia				
Trigeminal (gV)	✓	✓	✓	Neural crest Placode
Geniculate (gVII)	✓	✓	✓	Neural crest
Vestibular (gVIII)	✓	✓	✓	Placode
Cochlear (gVIII)	✓	✓	✓	Placode
Superior (gIX$_{sup}$)	✓	✓	✓	Neural crest
Petrosal (gIX$_{inf}$)	✓	✓	✓	Placode
Jugular (gX$_{sup}$)	✓	✓	✓	Neural crest
Nodose (gX$_{inf}$)	✓	✓	✓	Placode
Mesencephalon				
Mesencephalic trigeminal nucleus (MTN)	✓	Luo et al. 1991, Shiganga et al. 1988	not yet defined	Neural crest Placode or Neural tube?
Hindbrain				
Rhombomere 1	✓	not yet defined	not yet defined	Neural tube
Olfactory system				
Olfactory epithelium	✓ Schäffer 2006	not yet defined	not yet defined	Placode

Table 6.1: Summary of neuronal subpopulations showing a co-localization of Npr2 and cGKIα. The central axonal projections of these neuronal subpopulations exhibit a bifurcation mode of axonal branching, which is failed in the absence of Npr2 (Npr2 KO). ✓, findings in this study; *, (Ayer-Le Lievre and Le Douarin 1982; D'Amico-Martel and Noden 1983; Narayanan and Narayanan 1980).
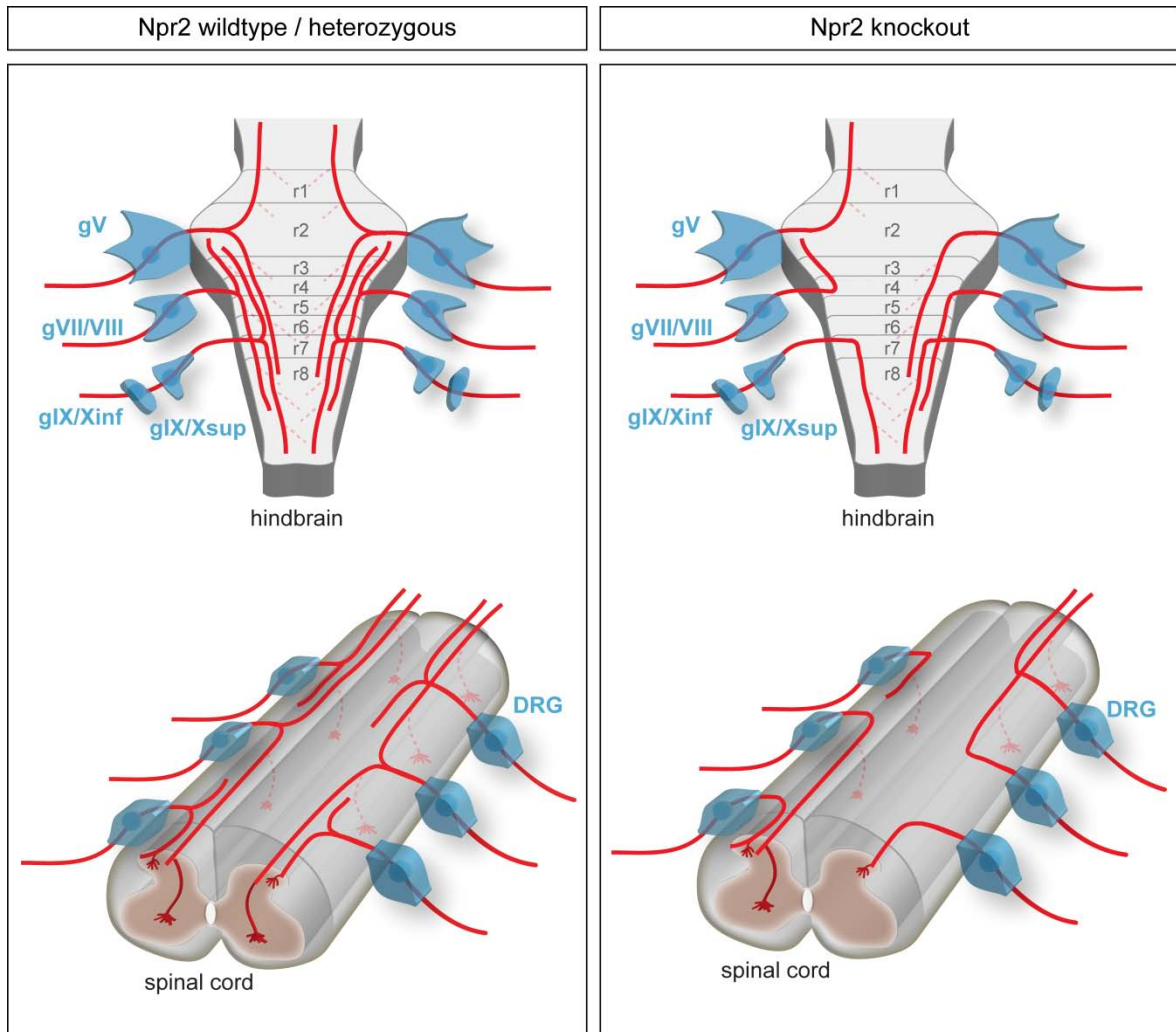
Figure 6.1: Schematic representation of the mouse embryonic hindbrain and spinal cord with cranial sensory ganglia (gV, gVII/VIII, gIX/X$_{inf}$, gIX/X$_{sup}$) and DRG, respectively (dorsal view). In heterozygous and wildtype Npr2 mice the central projections of both cranial and DRG sensory neurons bifurcate at the respective hindbrain and dorsal root entry zone extending arms in both caudal and rostral directions. In the Npr2 knockout mice the central projections of sensory neurons fail to bifurcate and only turn in either caudal or rostral direction. The dotted lines represent corresponding collaterals growing into the hindbrain or spinal cord. The schematic representation of hindbrain is based on an illustration in (Cordes 2001) while the representation of spinal cord is adapted from (Ter-Avetisyan et al. 2012). DRG, dorsal root ganglion; g, ganglion; r, rhombomere.

These findings resemble previous studies examining the role of the CNP-Npr2-cGKIα signaling pathway in the axonal bifurcation of DRG neurons (Schmidt et al. 2009; Schmidt et al. 2007; Schmidt et al. 2002; Zhao and Ma 2009; Zhao et al. 2009). The effect of impaired cGMP signaling on the bifurcation of central projections of cranial sensory neurons was analyzed by a newly generated Npr2CreERT2 mouse model. This model provided a genetic tool for sparse labeling of Npr2-positive neurons. Tamoxifen-inducible AP or GFP reporter gene expression allowed the detailed analysis of single axonal trajectories of cranial sensory neurons in Npr2 heterozygous and knockout embryos.

6.1 Identification of neuronal subpopulations with a co-localization of Npr2 and cGKIα

During development of the nervous system, axons form branches that navigate to distinct targets establishing a unique pattern of circuitry. The formation of functional neuronal circuits relies on the precise pathfinding of axonal branches that convey the sensory information to the CNS. During the last decades, many extracellular and intracellular molecules controlling axonal branching in specific neuronal populations have been identified *in vivo* and *in vitro* (Acebes and Ferrus 2000; Gallo 2011; Gibson and Ma 2011; Schmidt and Rathjen 2010; Tessier-Lavigne and Goodman 1996). However, the molecular mechanisms regulating axonal branch formation are still largely unknown.

A great obstacle for the analysis of regulatory mechanisms of axonal branching is the complexity and limited accessibility of axonal branching patterns. However, in the spinal cord the central projections of DRG neurons have been shown to represent a simple and accessible neuronal system that allows analysis of axonal branching and its regulatory mechanisms.

In the developing mouse nervous system, three patterns of branch formation can be classified in DRG neurons: (i) bifurcation at the DREZ, starting from E10 when the central projections of DRG sensory neurons grow toward the spinal cord: upon arriving at the DREZ their growth cones split, extending branches in caudal and rostral directions without entering the dorsal mantle layer, (ii) collateral or interstitial branching: after a waiting period, collaterals sprout from the branched arms and penetrate the dorsal mantle layer growing into the dorsal and ventral horn and (iii) branching at the termination zone: the collaterals terminate in distinct laminae and branch out further to establish synaptic contacts (Ozaki and Snider 1997).

The accessibility of the spatially and temporally separated axonal branching modes of developing DRG sensory neurons enabled the identification of a cGMP signaling pathway regulating the bifurcation of axons. The cGMP signaling pathway comprises the C-type natriuretic peptide (CNP), natriuretic pepitde receptor 2 (Npr2) and cGMP-dependent kinase Iα (cGKIα) (Schmidt et al. 2009; Schmidt et al. 2007; Schmidt et al. 2002; Zhao and Ma 2009; Zhao et al. 2009). By performing DiI-labeling of embryonic whole mount spinal cords and using Npr2 loss-of-function as well as cGKI- and CNP- deficient mice, it was revealed that in the absence of one of these pathway components axons of developing DRG neurons are not able to bifurcate at the DREZ (Schmidt and Rathjen 2011). In the absence of one of the three proteins, the sensory axons arrive at the DREZ but only turn either in caudal or rostral direction. By *in situ* hybridization and immunohistochemical analysis it was shown that Npr2 and cGKIα are specifically

expressed in the sensory neurons of developing DRG, while CNP expression was located in the dorsal horn of the embryonic spinal cord in CNPLacZ mice (Schmidt et al. 2009; Schmidt et al. 2007; Schmidt et al. 2002). Thus, the ligand CNP that induces axonal bifurcation via activation of the receptor Npr2 and cGKIα, is expressed at the bifurcation zone, complementary to Npr2 and cGKIα which are expressed in the incoming axon.

These findings raise the question whether the CNP-Npr2-cGKIα signaling pathway also regulates the bifurcation of axons in neuronal subpopulations other than DRG neurons.

To address this question, first, the localization of Npr2 and cGKIα was defined by histological examinations using heterozygous Npr2LacZ embryos.

Heterozygous Npr2LacZ mice, which expressed β-gal in the nucleus under the control of the Npr2 promoter, provided a useful tool to identify Npr2-positive neuronal subpopulations in the heterozygous state. X-Gal staining of whole mount embryos and subsequent clearing procedures gave an overview of Npr2-positive cell populations in the developing mouse. Besides the expected expression in DRG, X-Gal staining of E9.5-E13.5 whole mount embryos also revealed a prominent Npr2 expression in cranial sensory ganglia beginning from E10.5. At this stage of development, when the central projections of DRG neurons started to bifurcate at the DREZ, X-Gal staining was also detected in subpopulations of neurons both in the mesencephalon and rhombomere 1 (Liu et al. 2010; Zervas et al. 2004). Furthermore, X-Gal staining on cryosections also enabled the observation of nuclear β-gal (Npr2) expression at a single cell level in cranial sensory ganglia, the mesencephalon, rhomobomere 1 and olfactory epithelium. To analyze the co-localization of Npr2 and cGKIα in the identified Npr2-positive cell populations, immunohistochemical analyses were performed on cryosections of E11.5 heterozygous Npr2LacZ mice using antibodies against β-gal and cGKIα. Co-localization of β-gal in nuclei and cGKIα in cytoplasm was observed in all cranial sensory ganglia as well as in a subpopulation of the mesencephalon and rhombomere 1. In addition to the immunostainings using anti-β-gal and anti-cGKIα antibodies, cryosections of E11.5 heterozygous Npr2LacZ mice were also stained with antibodies against neurofilament-M (NF-M) and neuronal nuclei (NeuN). The triple immunostainings combining antibodies against β-gal, cGKIα and either NF-M or NeuN revealed a specific co-expression of Npr2 and cGKIα in neurons of cranial sensory ganglia of the developing mouse. Furthermore, the Npr2-positive cells in mesencephalon and rhombomere 1 that showed a co-localization of Npr2 and cGKIα were identified as neuronal cells by the immunostainings using antibodies against NF-M and NeuN. On the basis of the localization of the Npr2-positive cells in the dorsal mesencephalon, this group was considered as mesencephalic trigeminal nuclei (MTN) neurons (Chedotal et al. 1995; Hunter et al. 2001; Lazarov 2007).

The third component of the CNP-Npr2-cGKIα signaling pathway that regulates bifurcation of sensory axons at the DREZ is the ligand CNP. Using the CNPLacZ mouse model Schmidt et al. have shown that CNP is not only expressed in the dorsal spinal cord but also in the hindbrain (Schmidt et al. 2009). Since all cranial sensory neurons project their central axons towards the hindbrain, CNP expression in this region from E9.5 onwards indicates an expression of CNP complementary to the expression of Npr2 and cGKIα in cranial sensory neurons. This complementary expression pattern within the hindbrain is similar to that of the spinal cord: hereto project DRG sensory axons and bifurcate at the DREZ.

Thus, co-localized expression of Npr2 and cGKIα in the cranial sensory neurons and CNP expression within the hindbrain indicate that cranial sensory axons may bifurcate at the hindbrain entry zone. This was further examined at the single neuron level.

6.2 Analyzing the central projections of Npr2-positive cranial sensory neurons by a genetic approach at a single neuron level

The plant enzyme horseradish peroxidase (HRP) was the first neuroanatomical tracer used for retrograde axonal tracing (Kobbert et al. 2000). Visualization of HRP is achieved through the histochemical detection of its enzymatic activity using 3,3'-diaminobenzidine (DAB) as a chromogen. The tracing method utilizing wheat germ agglutinin (WGA)-coupled HRP allowed retrogradely, anterogradely and transsynaptically tracing (Gerfen et al. 1982; Herzog and Kummel 2000). A disadvantage of WGA-HRP tracing is, however, that the staining doesn't allow a cell type-specific labeling of axonal projections in spatially distinct regions.

Classical tracers of axonal projections allowing for labeling and analysis of axon arbors are the fluorescent lipophilic carbocyanine dyes such as DiI and DiO (Honig and Hume 1989; Mufson et al. 1990). Although DiI-tracing has proven very useful for visualization of axonal trajectories, a disadvantage of this technique is its direct application on the tissue of interest. This can be problematic in less accessible neuronal systems such as developing cranial sensory ganglia. Additionally, in complex neuronal circuits such as the central projections of cranial sensory axons within the hindbrain, DiI-tracing is not suitable for an accurate labeling of single axonal trajectories. Therefore, in this study a genetic approach was developed that allowed a specific and sparse labeling of neurons in distinct neuronal subpopulations.

In recent years, sparse labeling of neurons based on a genetic strategy has become a powerful tool to visualize and study individual neurons and their branching patterns in

more detail (Badea et al. 2009; Badea and Nathans 2004; Badea et al. 2003; Koundakjian et al. 2004; Li et al. 2010; Madisen et al. 2010; Miyoshi et al. 2010; Rotolo et al. 2008; Young et al. 2008). Such a genetic strategy includes the expression of a reporter gene (LacZ, AP or GFP) mediated by the Cre/loxP recombination system under the control of a promoter of interest. Making use of an inducible Cre recombinase variant as for example CreERT2, which only gains access to the nucleus after exposure to tamoxifen or 4-hydroxytamoxifen (OHT), ensures a controlled Cre-mediated recombination and thus reporter gene expression in a dose-dependent manner.

Taking advantage of this genetic strategy for sparse labeling of neurons, an Npr2CreERT2 mouse model was generated for specific and accurate labeling of Npr2-expressing neurons. This mouse model was then employed to address the question whether and how Npr2 is affecting the branching pattern of cranial sensory axons during development. Therefore, two reporter lines were used: a ubiquitously expressed reporter line Z/AP carrying an enzymatic AP reporter cassette (Lobe et al. 1999; Young et al. 2008) and a mGFP reporter line carrying a fluorescent GFP reporter cassette under the control of murine Tau promoter (Hippenmeyer et al. 2005; Young et al. 2008).

To visualize the axonal projections of Npr2-expressing neurons in heterozygous Npr2 mice, the reporter gene was expressed by inducing the Cre recombinase (CreERT2), which is expressed under the control of the Npr2 promoter. To visualize the axonal projections of Npr2-expressing neurons in Npr2 knockout mice, in addition to the described expression an Npr2 loss-of-function allele (*cn*) was introduced. The usage of the Npr2 loss-of-function mutation to gain an Npr2 knockout is based on the idea of avoiding a difference in CreERT2 expression levels between the heterozygous Npr2 and Npr2 knockout mice. Through introduction of the silent reporter gene (AP or GFP) into the Npr2 heterozygous/knockout, axons could be labeled after tamoxifen/OHT administration and subsequent reporter gene activation. A visualization of central projections at a single axon level was achieved by titrating the concentration of tamoxifen or its active metabolite OHT.

The suitability of the mouse for the intended genetic approach was verified using DRG sensory axons – a well-established system to analyze the role of the CNP-Npr2-cGKIα signaling pathway in axon bifurcation. Whole mount spinal cords with DRG were prepared using mouse embryos at E12.5 or E13.5 that carried the genotypes of interest: (i) Npr2 heterozygous expressing heterozygous CreERT2 and an AP-reporter gene, (ii) Npr2 knockout expressing heterozygous CreERT2 as well as an AP-reporter gene and carrying a loss-of-function Npr2 mutation. The AP-staining of whole mount spinal cords with DRG visualized single DRG sensory axons and confirmed previous findings that in the absence of Npr2, DRG sensory axons lack the bifurcation at the DREZ (Schmidt et al. 2007).

Quantification of the bifurcation and its failure showed that in the presence of Npr2 all DRG sensory axons bifurcate at the DREZ, while in the absence of Npr2 all DRG sensory axons turn but do not bifurcate. A slight preference for turning in the rostral direction was observed. Thus, the Npr2CreERT2 mouse model and the genetic strategy proved to be useful to analyze the branching of Npr2- positive neurons.

To examine single cranial sensory axons in $Npr2^{CreERT2/+}Z/AP$ mice, a BABB clearing method was applied on NBT/BCIP-stained vibratome sections. This allowed the observation of central projections on a clear background. In case of $Npr2^{CreERT2/+}mGFP$ mice, immunostaining against GFP was used to visualize single axons. In both cases single central projections were then analyzed by confocal fluorescence microscopy. Thus, the sophisticated genetic approach as well as the accurate detection techniques allowed a precise visualization of single cranial sensory axons projecting to the hindbrain.

In heterozygous Npr2 mice, cranial sensory axons grew from the corresponding cranial ganglia towards the hindbrain and upon entering the hindbrain bifurcated extending an ascending and a descending arm. In Npr2 knockout mice, the central projections of cranial sensory axons arrived at the hindbrain but instead of bifurcating they only sent an ascending or a descending arm into the hindbrain.

The quantification of genetically labeled Npr2-positive single axonal projections showed that the great majority of central projections of cranial sensory axons bifurcate upon entering the hindbrain. However, when regarding the central projections of trigeminal neurons, 9% of the counted axons exhibited a turn and no bifurcation, when they entered the hindbrain. These data contradict previous studies on axonal bifurcation using HRP-labeling or the Golgi technique to visualize central projections of the trigeminal sensory neurons (Tsuru et al. 1989; Windle 1926). Employing the Golgi technique to label the central projections of trigeminal neurons, Windle found a 1:1 ratio of bifurcating vs. non-bifurcating fibers. Later on, Tsuru and co-workers described a 3:1 ratio of bifurcating vs. non-bifurcating fibers of trigeminal sensory neurons using HRP-labeling. In the present study, the central projections of cranial sensory axons were visualized using sparse axon labeling, which enabled detection of axonal projections independently of dye application. This discrepancy is due the fact, that trigeminal motor neurons exit the hindbrain through the trigeminal ganglion. This means that motor neurons, which do not bifurcate and no expression of Npr2 was observed, can be labeled by HRP- or DiI-tracing and misleadingly can be considered as non-bifurcating sensory fibers.

Quantitative analysis of axonal bifurcation in Npr2 knockout mice further supported a role of Npr2 in the bifurcational branching of developing cranial sensory axons. A preference for turning in the caudal direction upon entry into the hindbrain was observed.

In summary, during mice embryonic development Npr2 is essential for the bifurcation of central projections of both DRG and cranial sensory neurons.

6.3 The Npr2-positive MTN neurons and neuronal cells in the rhombomere 1

The mesencephalic trigeminal nucleus (MTN) is a unique sector of the CNS, where the cell bodies of MTN neurons reside (Lazarov 2007). The MTN is the only known nucleus situated within the CNS that contains the cell bodies of primary sensory neurons (Lazarov 2002). The embryonic origin of the MTN neurons is not clear: whereas transplantation studies in birds suggested that they are neural crest-derived (Narayanan and Narayanan 1978), studies in chick embryos using neural crest markers indicated that they are not neural crest-derived (Hunter et al. 2001).

Investigations of chick MTN neurons during early development have shown that the first MTN neurons arise at stage 14 (corresponds to mouse embryonic days 9.5-10 (Wessels and Markwald 2000)) and extend their axons circumferentially away from the dorsal midline at stage 15. Arriving at the sulcus limitans, the MTN axons make a 90° turn and project caudally to cross the isthmus (midbrain-hindbrain boundary) in the hindbrain (Hunter et al. 2001; Molle et al. 2004). Studies using HRP-labeling to analyze the morphology of MTN neurons in cat have revealed that MTN axons bifurcate into peripheral and central axons extending towards the trigeminal sensory/motor tract or descending caudally within Probst's tract (Shigenaga et al. 1989; Shigenaga et al. 1988). Further morphological analyses on MTN neurons in rat have shown that like DRG and cranial sensory ganglia neurons these are pseudounipolar (Luo et al. 1991; Shigenaga et al. 1988).

In this study, Npr2 expression was also detected in a subpopulation of cells of rhombomere 1 using X-Gal staining on whole mount embryos and cryosections of heterozygous Npr2LacZ mice. In this neuronal subpopulation β-gal (Npr2) expression was observed from E10.5 onwards. Immunohistochemical analyses using antibodies against β-gal, cGKIα and NF-M on cryosections of E11.5 heterozygous Npr2LacZ mice revealed a co-localization of Npr2 and cGKIα in this neuronal subpopulation. However, the neuronal subpopulation in rhombomere 1 is not yet defined.

6.4 Expression of Npr2 in cranial sensory ganglia of dual origin

Cranial sensory ganglia, the cranial equivalents to DRG, are the place where the cell bodies of cranial sensory neurons reside. The cranial sensory ganglia and DRG differ in their gangliogenesis: whereas DRG exclusively contain neural crest-derived cells, cranial sensory ganglia are of dual origin arising from both neural crest- and neurogenic placode-derived cells (Ayer-Le Lievre and Le Douarin 1982; D'Amico-Martel and Noden 1983). Although both cell types originate from the neural plate border (Schloser 2008), they have unique characteristics: the neurogenic placodes are focal thickenings of the embryonic ectoderm exclusively situated in the head of vertebrates. In contrast, neural crest cells are not restricted to the head region and arise from the entire length of the neural tube (Baker and Bronner-Fraser 2001; Graham and Begbie 2000; Graham et al. 2004; Webb and Noden 1993). Studies in chick revealed that cranial neural crest cells contribute to cranial gangliogenesis by organizing the placode-derived sensory neurons (Begbie and Graham 2001).

Contrary to the contribution of neural crest and neurogenic placode to development and formation of cranial sensory ganglia, the neurons arising from a particular ganglion are not derived uniformly from both neural crest and neurogenic placode, as shown by studies in the developing chick cranial sensory system (Ayer-Le Lievre and Le Douarin 1982; D'Amico-Martel and Noden 1983; Narayanan and Narayanan 1980). While the neurons of trigeminal (gV), vestibular (gVIII), superior (gIXsup) and jugular (gXsup) ganglia arise from both structures, the neurons of geniculate (gVII), cochlear (gVIII), petrose (gIXinf) and nodose (gXinf) ganglia arise from neurogenic placode only. In general, the non-neuronal cells in the cranial sensory ganglia arise from neural crest (D'Amico-Martel and Noden 1983; Davies and Lindsay 1985).

The findings shown in this study demonstrate that Npr2 is expressed in neuronal cells of all cranial sensory ganglia (gV, gVII/VIII, gIX/X_{sup}, gIX/X_{inf}). Histological studies on both whole mount embryos and cryosections of E11.5 heterozygous Npr2LacZ mice allowed a detailed analysis of Npr2 expression. These results suggest that Npr2 is expressed in cranial sensory ganglia derived from both neural crest and/or placode without distinguishing between their origins.

6.5 The physiological role of CNP-Npr2 signaling and involvement of Npr2 in a human disease

In the nervous system the absence of one of the pathway components results in an impaired bifurcation mode of axon branching at the DREZ. This was analyzed by an *in vitro* spinal cord preparation to measure the integrated ventral root potential and by patch clamp recordings on slices of dorsal horn neurons. After application of capsaicin – a compound preferentially selective for polymodal nociceptor cells in the dorsal horn – the fraction of neurons responding to capsaicin and their frequency of miniature excitatory postsynaptic currents was reduced in the absence of cGMP signaling. Both methods support the anatomical results of impaired axonal branching and indicate a reduced connectivity between sensory axons and neurons of the dorsal horn of the spinal cord (Schmidt et al. 2009; Schmidt et al. 2007; Schmidt et al. 2002). Using nociceptor-specific knockout mice lacking cGKI, it has been shown that cGKI plays an important role in spinal synaptic potentiation and pain hypersensitivity (Luo et al. 2012). This demonstrates a significant function of cGMP signaling in the processing of sensory information.

Outside the nervous system, mutations in the genes of CNP, Npr2 and cGKII, but not cGKI, impair the induction of long bone growth as demonstrated in respective mouse models. Inactivation of CNP or Npr2 in mice results in dwarfism, whereas overexpression of CNP or reduced clearance of CNP causes skeletal overgrowth (Chusho et al. 2001; Geister et al. 2012; Jaubert et al. 1999; Kake et al. 2009; Matsukawa et al. 1999; Sogawa et al. 2007; Suda et al. 1998; Tamura et al. 2004; Tsuji and Kunieda 2005; Yasoda et al. 2009; Yasoda et al. 2004). Similar defects have been observed in cGKII-deficient mice and rats, suggesting that CNP activates Npr2 on chondrocytes to generate cGMP, which in turn activates cGKII to induce endochondral ossification (Chikuda et al. 2004; Miyazawa et al. 2002). A recent study has shown that loss of Npr2 in mice causes a reduction in the hypertrophic and proliferative zones of the growth plate due to elevated phosphorylated ERK1/2 (extracellular signal-regulated protein kinase 1/2) (Geister et al. 2012). Here, the elucidated signaling pathway includes activation of cGKII and generation of cGMP upon binding of the ligand CNP to its receptor Npr2. Subsequently, cGKII inhibits the activation of MEK1/2 (mitogen-activated protein kinase kinase)-/ERK1/2 by inhibiting RAF-1 (rapidly accelerated fibrosarcoma 1) activation. Thus, Npr2 signaling is required for the inhibition of the MEK/ERK pathway. In respect of cGKII, the cGMP signaling cascade in chondrocytes differs from that in DRG and cranial ganglia sensory neurons.

The absence of Npr2 also causes defects in oocyte maturation (Geister et al. 2012; Zhang et al. 2011; Zhang et al. 2010), cardiac growth (Langenickel et al. 2006) and gastrointestinal function (Sogawa et al. 2010).

In humans, homozygous mutations in the NPR2 gene have been reported to cause one form of human skeletal dysplasia: acromesomelic dysplasia type Maroteaux (AMDM; OMIM602875) (Bartels et al. 2004; Khan et al. 2012). AMDM is a rare autosomal-recessive genetic disorder with a prevalence of approximately 1/1.000.000. This skeletal dysplasia is characterized by an extremely short stature, misshapen bones in the limbs and spine and body disproportion. Point mutations leading to single amino acid exchanges were found in the ligand binding, the kinase homology and the guanylyl cyclase domain (Bartels et al. 2004). In another study, a homozygous missense mutation in the kinase homology domain of NPR2 has been demonstrated to result in an impaired guanylyl cyclase activity without affecting ligand binding (Hachiya et al. 2007). Data from heterozygous carriers furthermore indicated that they were shorter than population-matched controls. Additional studies confirmed that heterozygous mutations in the NPR2 gene are linked with a shortened stature (Bartels et al. 2004).

Whether the CNP–Npr2–cGKIα signaling pathway is implicated in human neurological diseases has not been investigated so far. To characterize neurological consequences resulting from impaired sensory axon bifurcation in rodents, conditional mouse mutants of CNP, Npr2 or cGKIα, which are not impaired in bone growth, are required. It remains to be elucidated whether the absence of the cGMP signaling pathway causes branching errors of sensory axons in the developing human spinal cord.

6.6 Quest for phosphorylation target(s) of the CNP-Npr2-cGKIα pathway

A missing link in the CNP-Npr2-cGKIα pathway is the target substrate(s) of cGKIα that mediates axon bifurcation of DRG sensory neurons at the DREZ and - from the findings of this study - also of cranial sensory neurons at the hindbrain entry zone.

An *in vitro* study has demonstrated that GSK-3 can be phosphorylated by cGKI (Zhao et al. 2009). A double knockin mouse model preventing the phosphorylation of GSK-3 has been studied for its role in branching morphogenesis (McManus et al. 2005). Here, Ser21 of GSK-3α and Ser9 of GSK-3β were exchanged to alanine. No obvious deficits in dendritic or axonal projections have been observed in this double knockin mouse, suggesting that other phosphorylation targets of cGKIα are relevant for sensory axon branching (Gartner et al. 2006; McManus et al. 2005).

Studies dealing intensively with the identification and analysis of cGKIα target substrate(s) have identified putative cGKIα phosphorylation targets using mass spectrometry and 2D-electrophoresis (Schäffer 2006; Stonkute 2010). The implication of distinct proteins in the bifurcation mode of axonal branching was analyzed using mutant mouse models and DiI-

labeling to visualize DRG sensory axons and their branching pattern. Although these studies did identify proteins, which are phosphorylated by cGKIα, the downstream target of cGKIα mediating axonal bifurcation could not be identified.

Here, in order to identify phosphorylation targets of cGKIα, the kinase was activated in embryonic DRG samples employing either the cGMP analogouse 8-pCPT-cGMP or CNP-22. DRG lysates were then analyzed by Western blot, taking non-activated DRG samples as negative controls. Used antibodies were against phospho-specific sequences of a certain protein or against the consensus phospho-motif of cGKI. This aimed to detect specific phospho-bands or a band shift following activation of cGKIα.

Using this approach, an antibody against the cytoskeletal protein Tau detected a band shift in the treated DRG samples compared to the non-treated samples. Consequently, the bifurcation of DRG sensory axons was analyzed in Tau knockout embryos by DiI-labeling. The bifurcation of DRG sensory axons was not affected in the absence of Tau, suggesting that Tau is not involved in the bifurcation mode of axon branching. Thus, the phosphorylation target(s) of cGKIα, which mediates the bifurcation of DRG sensory axons remains to be identified.

The difficulties in the identification of cGKI target protein(s) are (i) material limitation: the CNP-Npr2-cGKIα cascade is established in embryonic DRG, which are dissected at E12.5 or E13.5 and (ii) availability of mutated mouse models of distinct proteins to analyze their influence on axon branching behavior.

7. Future Perspectives

- A major breakthrough in the research of axonal bifurcation would be the live imaging of single axon branching. Therefore, further efforts should be undertaken to visualize splitting of the growth cone *in vivo*. Sparse labeling of Npr2-positive neurons (Npr2CreERT2 mouse model) in combination with an endogenously expressed reporter gene would allow the detection of the bifurcating growth cone.

- It is also important to investigate whether and/or to what extent bifurcation impairment affects neurological functions. Behavioral measurements of nociception using CNP/Npr2/cGKI conditional mutant mouse models could shed light on the physiological role of the signaling pathway.

- In order to gain mechanistic insight into the bifurcation process, future work should furthermore concentrate on the search of downstream component(s) of the CNP-Npr2-cGKIα signaling pathway regulating the bifurcation mode of axonal branching (e.g. dynamic reorganization of actin filaments and microtubules).

- Additionally, it seems reasonable to identify upstream component(s) of the signaling pathway that either interact with or affect secretion of the ligand CNP.

- The influence of transcription factors on the regulation of distinct pathway components would be another interesting issue to follow up. Therefore, it is important to study the axonal bifurcation phenotype in transcription factor-deficient mice.

- In this study, β-gal expression revealed Npr2-positive cells in primary olfactory epithelium. Furthermore, it was shown that cGKIα and Npr2 are co-localized in MTN neurons. Therefore, future studies should examine the branching pattern of single axons projecting into the glomerulus during mouse development. In this context, the branching pattern of MTN neurons as well as the role of CNP-Npr2-cGKIα in the bifurcation of MTN neurons would be of primary interest.

8. Reference List

Acebes, A., Ferrus, A.: Cellular and molecular features of axon collaterals and dendrites. Trends Neurosci., 23: 557-565, 2000.

Ayer-Le Lievre, C.S., Le Douarin, N.M.: The early development of cranial sensory ganglia and the potentialities of their component cells studied in quail-chick chimeras. Dev. Biol., 94: 291-310, 1982.

Baas, P.W., Vidya, N.C., Myers, K.A.: Axonal transport of microtubules: the long and short of it. Traffic., 7: 490-498, 2006.

Babineau, D., Vetter, D., Andrews, B.J., Gronostajski, R.M., Proteau, G.A., Beatty, L.G., Sadowski, P.D.: The FLP protein of the 2-micron plasmid of yeast. Purification of the protein from Escherichia coli cells expressing the cloned FLP gene. J. Biol. Chem., 260: 12313-12319, 1985.

Badea, T.C., Hua, Z.L., Smallwood, P.M., Williams, J., Rotolo, T., Ye, X., Nathans, J.: New mouse lines for the analysis of neuronal morphology using CreER(T)/loxP-directed sparse labeling. PLoS. One., 4: e7859, 2009.

Badea, T.C., Nathans, J.: Quantitative analysis of neuronal morphologies in the mouse retina visualized by using a genetically directed reporter. J. Comp Neurol., 480: 331-351, 2004.

Badea, T.C., Wang, Y., Nathans, J.: A noninvasive genetic/pharmacologic strategy for visualizing cell morphology and clonal relationships in the mouse. J. Neurosci., 23: 2314-2322, 2003.

Bagri, A., Cheng, H.J., Yaron, A., Pleasure, S.J., Tessier-Lavigne, M.: Stereotyped pruning of long hippocampal axon branches triggered by retraction inducers of the semaphorin family. Cell, 113: 285-299, 2003.

Baker, C.V., Bronner-Fraser, M.: Vertebrate cranial placodes I. Embryonic induction. Dev. Biol., 232: 1-61, 2001.

Bartels, C.F., Bukulmez, H., Padayatti, P., Rhee, D.K., van Ravenswaaij-Arts, C., Pauli, R.M., Mundlos, S., Chitayat, D., Shih, L.Y., Al-Gazali, L.I., Kant, S., Cole, T., Morton, J., Cormier-Daire, V., Faivre, L., Lees, M., Kirk, J., Mortier, G.R., Leroy, J., Zabel, B., Kim, C.A., Crow, Y., Braverman, N.E., van den Akker, F., Warman, M.L.: Mutations in the transmembrane natriuretic peptide receptor NPR-B impair skeletal growth and cause acromesomelic dysplasia, type Maroteaux. Am. J. Hum. Genet., 75: 27-34, 2004.

Bastmeyer, M., O'Leary, D.D.: Dynamics of target recognition by interstitial axon branching along developing cortical axons. J. Neurosci., 16: 1450-1459, 1996.

Begbie, J., Graham, A.: Integration between the epibranchial placodes and the hindbrain. Science, 294: 595-598, 2001.

Birling, M.C., Gofflot, F., Warot, X.: Site-specific recombinases for manipulation of the mouse genome. Methods Mol. Biol., 561: 245-263, 2009.

Bodmer, D., Levine-Wilkinson, S., Richmond, A., Hirsh, S., Kuruvilla, R.: Wnt5a mediates nerve growth factor-dependent axonal branching and growth in developing sympathetic neurons. J. Neurosci., 29: 7569-7581, 2009.

Bouquet, C., Soares, S., von, B.Y., Ravaille-Veron, M., Propst, F., Nothias, F.: Microtubule-associated protein 1B controls directionality of growth cone migration and axonal branching in regeneration of adult dorsal root ganglia neurons. J. Neurosci., 24: 7204-7213, 2004.

Branda, C.S., Dymecki, S.M.: Talking about a revolution: The impact of site-specific recombinases on genetic analyses in mice. Dev. Cell, 6: 7-28, 2004.

Brocard, J., Feil, R., Chambon, P., Metzger, D.: A chimeric Cre recombinase inducible by synthetic,but not by natural ligands of the glucocorticoid receptor. Nucleic Acids Res., 26: 4086-4090, 1998.

Buffelli, M., Burgess, R.W., Feng, G., Lobe, C.G., Lichtman, J.W., Sanes, J.R.: Genetic evidence that relative synaptic efficacy biases the outcome of synaptic competition. Nature, 424: 430-434, 2003.

Bunting, M., Bernstein, K.E., Greer, J.M., Capecchi, M.R., Thomas, K.R.: Targeting genes for self-excision in the germ line. Genes Dev., 13: 1524-1528, 1999.

Chedotal, A., Pourquie, O., Sotelo, C.: Initial tract formation in the brain of the chick embryo: selective expression of the BEN/SC1/DM-GRASP cell adhesion molecule. Eur. J. Neurosci., 7: 198-212, 1995.

Chikuda, H., Kugimiya, F., Hoshi, K., Ikeda, T., Ogasawara, T., Shimoaka, T., Kawano, H., Kamekura, S., Tsuchida, A., Yokoi, N., Nakamura, K., Komeda, K., Chung, U.I., Kawaguchi, H.: Cyclic GMP-dependent protein kinase II is a molecular switch from proliferation to hypertrophic differentiation of chondrocytes. Genes Dev., 18: 2418-2429, 2004.

Chusho, H., Tamura, N., Ogawa, Y., Yasoda, A., Suda, M., Miyazawa, T., Nakamura, K., Nakao, K., Kurihara, T., Komatsu, Y., Itoh, H., Tanaka, K., Saito, Y., Katsuki, M., Nakao, K.: Dwarfism and early death in mice lacking C-type natriuretic peptide. Proc. Natl. Acad. Sci. U. S. A, 98: 4016-4021, 2001.

Cohen-Cory, S., Fraser, S.E.: Effects of brain-derived neurotrophic factor on optic axon branching and remodelling in vivo. Nature, 378: 192-196, 1995.

Colamarino, S.A., Tessier-Lavigne, M.: The axonal chemoattractant netrin-1 is also a chemorepellent for trochlear motor axons. Cell, 81: 621-629, 1995.

Colavita, A., Tessier-Lavigne, M.: A Neurexin-related protein, BAM-2, terminates axonal branches in C. elegans. Science, 302: 293-296, 2003.

Copeland, N.G., Jenkins, N.A., Court DL: Recombineering: a powerful new tool for mouse functional genomics. Nat. Rev. Genet., 2: 769-779, 2001.

Cordes, S.P.: Molecular genetics of cranial nerve development in mouse. Nat. Rev. Neurosci., 2: 611-623, 2001.

Court DL, Swaminathan, S., Yu, D., Wilson, H., Baker, T., Bubunenko, M., Sawitzke, J., Sharan, S.K.: Mini-lambda: a tractable system for chromosome and BAC engineering. Gene, 315: 63-69, 2003.

D'Amico-Martel, A., Noden, D.M.: Contributions of placodal and neural crest cells to avian cranial peripheral ganglia. Am. J. Anat., 166: 445-468, 1983.

Dancause, N., Barbay, S., Frost, S.B., Plautz, E.J., Chen, D., Zoubina, E.V., Stowe, A.M., Nudo, R.J.: Extensive cortical rewiring after brain injury. J. Neurosci., 25: 10167-10179, 2005.

Danielian, P.S., Muccino, D., Rowitch, D.H., Michael, S.K., McMahon, A.P.: Modification of gene activity in mouse embryos in utero by a tamoxifen-inducible form of Cre recombinase. Curr. Biol., 8: 1323-1326, 1998.

Dasen, J.S.: Transcriptional networks in the early development of sensory-motor circuits. Curr. Top. Dev. Biol., 87: 119-148, 2009.

Davies, A.M., Lindsay, R.M.: The Cranial Sensory Ganglia in Culture: Differences in the Response of Placode-Derived and Neural Crest-Derived Neurons to Nerve Growth Factor. Developmental Biology, 111: 62-72, 1985.

Dent, E.W., Gertler, F.B.: Cytoskeletal dynamics and transport in growth cone motility and axon guidance. Neuron, 40: 209-227, 2003.

Dent, E.W., Kalil, K.: Axon branching requires interactions between dynamic microtubules and actin filaments. J. Neurosci., 21: 9757-9769, 2001.

Drinjakovic, J., Jung, H., Campbell, D.S., Strochlic, L., Dwivedy, A., Holt, C.E.: E3 ligase Nedd4 promotes axon branching by downregulating PTEN. Neuron, 65: 341-357, 2010.

Dymecki, S.M., Kim, J.C.: Molecular neuroanatomy's "Three Gs": a primer. Neuron, 54: 17-34, 2007.

Feil, R.: Conditional somatic mutagenesis in the mouse using site-specific recombinases. Handb. Exp. Pharmacol.: 3-28, 2007.

Feil, R., Brocard, J., Mascrez, B., LeMeur, M., Metzger, D., Chambon, P.: Ligand-activated site-specific recombination in mice. Proc. Natl. Acad. Sci. U. S. A, 93: 10887-10890, 1996.

Feil, R., Wagner, J., Metzger, D., Chambon, P.: Regulation of Cre recombinase activity by mutated estrogen receptor ligand-binding domains. Biochem. Biophys. Res. Commun., 237: 752-757, 1997.

Gallo, G.: The cytoskeletal and signaling mechanisms of axon collateral branching. Dev. Neurobiol., 71: 201-220, 2011.

Garcia-Marin, V., Garcia-Lopez, P., Freire, M.: The growth cone as seen through Cajal's original histological preparations and publications. J. Hist Neurosci., 18: 197-210, 2009.

Garrido, J.J., Simon, D., Varea, O., Wandosell, F.: GSK3 alpha and GSK3 beta are necessary for axon formation. FEBS Lett., 581: 1579-1586, 2007.

Gartner, A., Huang, X., Hall, A.: Neuronal polarity is regulated by glycogen synthase kinase-3 (GSK-3beta) independently of Akt/PKB serine phosphorylation. J. Cell Sci., 119: 3927-3934, 2006.

Gaveriaux-Ruff, C., Kieffer, B.L.: Conditional gene targeting in the mouse nervous system: Insights into brain function and diseases. Pharmacol. Ther., 113: 619-634, 2007.

Geister, K.A., Brinkmeier, M.L., Hsieh, M., Faust, S.M., Karolyi, I.J., Perosky, J.E., Kozloff, K.M., Conti, M., Camper, S.A.: A novel loss-of-function mutation in Npr2 clarifies primary role in female reproduction and reveals a potential therapy for acromesomelic dysplasia, Maroteaux type. Hum. Mol. Genet., 2012.

Gerfen, C.R., O'Leary, D.D., Cowan, W.M.: A note on the transneuronal transport of wheat germ agglutinin-conjugated horseradish peroxidase in the avian and rodent visual systems. Exp. Brain Res., 48: 443-448, 1982.

Gianola, S., de, C.F., Rossi, F.: Anosmin-1 stimulates outgrowth and branching of developing Purkinje axons. Neuroscience, 158: 570-584, 2009.

Gibson, D.A., Ma, L.: Developmental regulation of axon branching in the vertebrate nervous system. Development, 138: 183-195, 2011.

Govek, E.E., Hatten, M.E., Van, A.L.: The role of Rho GTPase proteins in CNS neuronal migration. Dev. Neurobiol., 71: 528-553, 2011.

Graham, A., Begbie, J.: Neurogenic placodes: a common front. Trends Neurosci., 23: 313-316, 2000.

Graham, A., Begbie, J., McGonnell, I.: Significance of the cranial neural crest. Dev. Dyn., 229: 5-13, 2004.

Hachiya, R., Ohashi, Y., Kamei, Y., Suganami, T., Mochizuki, H., Mitsui, N., Saitoh, M., Sakuragi, M., Nishimura, G., Ohashi, H., Hasegawa, T., Ogawa, Y.: Intact kinase homology domain of natriuretic peptide receptor-B is essential for skeletal development. J. Clin. Endocrinol. Metab, 92: 4009-4014, 2007.

Halbrugge, M., Walter, U.: Purification of a vasodilator-regulated phosphoprotein from human platelets. Eur. J. Biochem., 185: 41-50, 1989.

Hall, A., Lalli, G.: Rho and Ras GTPases in axon growth, guidance, and branching. Cold Spring Harb. Perspect. Biol., 2: a001818, 2010.

Hayashi, S., McMahon, A.P.: Efficient recombination in diverse tissues by a tamoxifen-inducible form of Cre: a tool for temporally regulated gene activation/inactivation in the mouse. Dev. Biol., 244: 305-318, 2002.

Heffner, C.D., Lumsden, A.G., O'Leary, D.D.: Target control of collateral extension and directional axon growth in the mammalian brain. Science, 247: 217-220, 1990.

Herzog, J., Kummel, H.: Fixation of transsynaptically transported WGA-HRP and fluorescent dyes used in combination. J. Neurosci. Methods, 101: 149-156, 2000.

Hippenmeyer, S., Vrieseling, E., Sigrist, M., Portmann, T., Laengle, C., Ladle, D.R., Arber, S.: A developmental switch in the response of DRG neurons to ETS transcription factor signaling. PLoS. Biol., 3: e159, 2005.

Hofmann, F., Bernhard, D., Lukowski, R., Weinmeister, P.: cGMP regulated protein kinases (cGK). Handb. Exp. Pharmacol.: 137-162, 2009.

Homma, N., Takei, Y., Tanaka, Y., Nakata, T., Terada, S., Kikkawa, M., Noda, Y., Hirokawa, N.: Kinesin superfamily protein 2A (KIF2A) functions in suppression of collateral branch extension. Cell, 114: 229-239, 2003.

Honig, M.G., Hume, R.I.: Carbocyanine dyes. Novel markers for labelling neurons. Trends Neurosci., 12: 336-338, 1989.

Huber, A.B., Kolodkin, A.L., Ginty, D.D., Cloutier, J.F.: Signaling at the growth cone: ligand-receptor complexes and the control of axon growth and guidance. Annu. Rev. Neurosci., 26: 509-563, 2003.

Hundelt, M., Fath, T., Selle, K., Oesterwind, J., Jordan, C., Schultz, C., Götz, J., von Engelhardt, J., Monyer, H., Lewejohann, L., Sachser, N., Bakota, L., Brandt, R.: Altered phosphorylation but no neurodegeneration in a mouse model of tau hyperphosphorylation. Neurobiol. Aging, 32: 991-1006, 2011.

Hunter, E., Begbie, J., Mason, I., Graham, A.: Early development of the mesencephalic trigeminal nucleus. Dev. Dyn., 222: 484-493, 2001.

Hur, E.M., Zhou, F.Q.: GSK3 signalling in neural development. Nat. Rev. Neurosci., 11: 539-551, 2010.

Indra, A.K., Warot, X., Brocard, J., Bornert, J.M., Xiao, J.H., Chambon, P., Metzger, D.: Temporally-controlled site-specific mutagenesis in the basal layer of the epidermis: comparison of the recombinase activity of the tamoxifen-inducible Cre-ER(T) and Cre-ER(T2) recombinases. Nucleic Acids Res., 27: 4324-4327, 1999.

Jaubert, J., Jaubert, F., Martin, N., Washburn, L.L., Lee, B.K., Eicher, E.M., Guenet, J.L.: Three new allelic mouse mutations that cause skeletal overgrowth involve the natriuretic peptide receptor C gene (Npr3). Proc. Natl. Acad. Sci. U. S. A, 96: 10278-10283, 1999.

Joyner A.L.: Gene targeting: a practical appoach. Oxford University Press, 1993.

Kake, T., Kitamura, H., Adachi, Y., Yoshioka, T., Watanabe, T., Matsushita, H., Fujii, T., Kondo, E., Tachibe, T., Kawase, Y., Jishage, K., Yasoda, A., Mukoyama, M., Nakao, K.: Chronically elevated plasma C-type natriuretic peptide level stimulates skeletal growth in transgenic mice. Am. J. Physiol Endocrinol. Metab, 297: E1339-E1348, 2009.

Kawabe, H., Neeb, A., Dimova, K., Young, S.M., Jr., Takeda, M., Katsurabayashi, S., Mitkovski, M., Malakhova, O.A., Zhang, D.E., Umikawa, M., Kariya, K., Goebbels, S., Nave, K.A., Rosenmund, C., Jahn, O., Rhee, J., Brose, N.: Regulation of Rap2A by the ubiquitin ligase Nedd4-1 controls neurite development. Neuron, 65: 358-372, 2010.

Kennedy, T.E., Serafini, T., de la Torre, J.R., Tessier-Lavigne, M.: Netrins are diffusible chemotropic factors for commissural axons in the embryonic spinal cord. Cell, 78: 425-435, 1994.

Khan, S., Hussain, A.R., Abbasi, S., Nawaz, M., Muhammad, N., Ahmad, W.: Novel mutations in natriuretic peptide receptor-2 gene underlie acromesomelic dysplasia, type maroteaux. BMC. Med. Genet., 13: 44, 2012.

Kim, W.Y., Zhou, F.Q., Zhou, J., Yokota, Y., Wang, Y.M., Yoshimura, T., Kaibuchi, K., Woodgett, J.R., Anton, E.S., Snider, W.D.: Essential roles for GSK-3s and GSK-3-primed substrates in neurotrophin-induced and hippocampal axon growth. Neuron, 52: 981-996, 2006.

Kim, Y.T., Hur, E.M., Snider, W.D., Zhou, F.Q.: Role of GSK3 Signaling in Neuronal Morphogenesis. Front Mol. Neurosci., 4: 48, 2011.

Kobbert, C., Apps, R., Bechmann, I., Lanciego, J.L., Mey, J., Thanos, S.: Current concepts in neuroanatomical tracing. Prog. Neurobiol., 62: 327-351, 2000.

Koundakjian, E.J., Cowan, D.M., Hardy, R.W., Becker, A.H.: The Zuker collection: a resource for the analysis of autosomal gene function in Drosophila melanogaster. Genetics, 167: 203-206, 2004.

Kuhn, R., Schwenk, F., Aguet, M., Rajewsky, K.: Inducible gene targeting in mice. Science, 269: 1427-1429, 1995.

Kumar, P., Lyle, K.S., Gierke, S., Matov, A., Danuser, G., Wittmann, T.: GSK3beta phosphorylation modulates CLASP-microtubule association and lamella microtubule attachment. J. Cell Biol., 184: 895-908, 2009.

Langenickel, T.H., Buttgereit, J., Pagel-Langenickel, I., Lindner, M., Monti, J., Beuerlein, K., Al-Saadi, N., Plehm, R., Popova, E., Tank, J., Dietz, R., Willenbrock, R., Bader, M.: Cardiac hypertrophy in transgenic rats expressing a dominant-negative mutant of the natriuretic peptide receptor B. Proc. Natl. Acad. Sci. U. S. A, 103: 4735-4740, 2006.

Lazarov, N.E.: Comparative analysis of the chemical neuroanatomy of the mammalian trigeminal ganglion and mesencephalic trigeminal nucleus. Prog. Neurobiol., 66: 19-59, 2002.

Lazarov, N.E.: Neurobiology of orofacial proprioception. Brain Res. Rev., 56: 362-383, 2007.

Li, L., Tasic, B., Micheva, K.D., Ivanov, V.M., Spletter, M.L., Smith, S.J., Luo, L.: Visualizing the distribution of synapses from individual neurons in the mouse brain. PLoS. One., 5: e11503, 2010.

Liu, Z.R., Shi, M., Hu, Z.L., Zheng, M.H., Du, F., Zhao, G., Ding, Y.Q.: A refined map of early gene expression in the dorsal rhombomere 1 of mouse embryos. Brain Res. Bull., 82: 74-82, 2010.

Lobe, C.G., Koop, K.E., Kreppner, W., Lomeli, H., Gertsenstein, M., Nagy, A.: Z/AP, a double reporter for cre-mediated recombination. Dev. Biol., 208: 281-292, 1999.

Lowery, L.A., Van, V.D.: The trip of the tip: understanding the growth cone machinery. Nat. Rev. Mol. Cell Biol., 10: 332-343, 2009.

Lucas, K.A., Pitari, G.M., Kazerounian, S., Ruiz-Stewart, I., Park, J., Schulz, S., Chepenik, K.P., Waldman, S.A.: Guanylyl cyclases and signaling by cyclic GMP. Pharmacol. Rev., 52: 375-414, 2000.

Luo, C., Gangadharan, V., Bali, K.K., Xie, R.G., Agarwal, N., Kurejova, M., Tappe-Theodor, A., Tegeder, I., Feil, S., Lewin, G., Polgar, E., Todd, A.J., Schlossmann, J., Hofmann, F., Liu, D.L., Hu, S.J., Feil, R., Kuner, T., Kuner, R.: Presynaptically localized cyclic GMP-dependent protein kinase 1 is a key determinant of spinal synaptic potentiation and pain hypersensitivity. PLoS. Biol., 10: e1001283, 2012.

Luo, P.F., Wang, B.R., Peng, Z.Z., Li, J.S.: Morphological characteristics and terminating patterns of masseteric neurons of the mesencephalic trigeminal nucleus in the rat: an intracellular horseradish peroxidase labeling study. J. Comp Neurol., 303: 286-299, 1991.

Madisen, L., Zwingman, T.A., Sunkin, S.M., Oh, S.W., Zariwala, H.A., Gu, H., Ng, L.L., Palmiter, R.D., Hawrylycz, M.J., Jones, A.R., Lein, E.S., Zeng, H.: A robust and high-throughput Cre reporting and characterization system for the whole mouse brain. Nat. Neurosci., 13: 133-140, 2010.

Marmigere, F., Ernfors, P.: Specification and connectivity of neuronal subtypes in the sensory lineage. Nat. Rev. Neurosci., 8: 114-127, 2007.

Matsukawa, N., Grzesik, W.J., Takahashi, N., Pandey, K.N., Pang, S., Yamauchi, M., Smithies, O.: The natriuretic peptide clearance receptor locally modulates the physiological effects of the natriuretic peptide system. Proc. Natl. Acad. Sci. U. S. A, 96: 7403-7408, 1999.

McManus, E.J., Sakamoto, K., Armit, L.J., Ronaldson, L., Shpiro, N., Marquez, R., Alessi, D.R.: Role that phosphorylation of GSK3 plays in insulin and Wnt signalling defined by knockin analysis. EMBO J., 24: 1571-1583, 2005.

Metzger, D., Chambon, P.: Site- and time-specific gene targeting in the mouse. Methods, 24: 71-80, 2001.

Metzger, D., Clifford, J., Chiba, H., Chambon, P.: Conditional site-specific recombination in mammalian cells using a ligand-dependent chimeric Cre recombinase. Proc. Natl. Acad. Sci. U. S. A, 92: 6991-6995, 1995.

Metzger, D., Feil, R.: Engineering the mouse genome by site-specific recombination. Curr. Opin. Biotechnol., 10: 470-476, 1999.

Miyazawa, T., Ogawa, Y., Chusho, H., Yasoda, A., Tamura, N., Komatsu, Y., Pfeifer, A., Hofmann, F., Nakao, K.: Cyclic GMP-dependent protein kinase II plays a critical role in C-type natriuretic peptide-mediated endochondral ossification. Endocrinology, 143: 3604-3610, 2002.

Miyoshi, G., Hjerling-Leffler, J., Karayannis, T., Sousa, V.H., Butt, S.J., Battiste, J., Johnson, J.E., Machold, R.P., Fishell, G.: Genetic fate mapping reveals that the caudal ganglionic eminence produces a large and diverse population of superficial cortical interneurons. J. Neurosci., 30: 1582-1594, 2010.

Molle, K.D., Chedotal, A., Rao, Y., Lumsden, A., Wizenmann, A.: Local inhibition guides the trajectory of early longitudinal tracts in the developing chick brain. Mech. Dev., 121: 143-156, 2004.

Moreno, F.J., Avila, J.: Phosphorylation of stathmin modulates its function as a microtubule depolymerizing factor. Mol. Cell Biochem., 183: 201-209, 1998.

Mufson, E.J., Brady, D.R., Kordower, J.H.: Tracing neuronal connections in postmortem human hippocampal complex with the carbocyanine dye DiI. Neurobiol. Aging, 11: 649-653, 1990.

Nagy, A.: Cre recombinase: the universal reagent for genome tailoring. Genesis., 26: 99-109, 2000.

Nagy, A., Gertsenstein, M., Vintersten, K., Behringer, R.: Manipulating the Mouse Embryo: A Laboratory Manual. 2002.

Narayanan, C.H., Narayanan, Y.: Determination of the embryonic origin of the mesencephalic nucleus of the trigeminal nerve in birds. J. Embryol. Exp. Morphol., 43: 85-105, 1978.

Narayanan, C.H., Narayanan, Y.: Neural crest and placodal contributions in the development of the glossopharyngeal-vagal complex in the chick. Anat. Rec., 196: 71-82, 1980.

O'Leary, D.D., Terashima, T.: Cortical axons branch to multiple subcortical targets by interstitial axon budding: implications for target recognition and "waiting periods". Neuron, 1: 901-910, 1988.

Ozaki, S., Snider, W.D.: Initial trajectories of sensory axons toward laminar targets in the developing mouse spinal cord. J. Comp Neurol., 380: 215-229, 1997.

Pagel-Langenickel, I., Buttgereit, J., Bader, M., Langenickel, T.H.: Natriuretic peptide receptor B signaling in the cardiovascular system: protection from cardiac hypertrophy. J. Mol. Med. (Berl), 85: 797-810, 2007.

Portera-Cailliau, C., Weimer, R.M., De, P., V, Caroni, P., Svoboda, K.: Diverse modes of axon elaboration in the developing neocortex. PLoS. Biol., 3: e272, 2005.

Potter, L.R.: Guanylyl cyclase structure, function and regulation. Cell Signal., 23: 1921-1926, 2011.

Potter, L.R., Abbey-Hosch, S., Dickey, D.M.: Natriuretic peptides, their receptors, and cyclic guanosine monophosphate-dependent signaling functions. Endocr. Rev., 27: 47-72, 2006.

Potter, L.R., Yoder, A.R., Flora, D.R., Antos, L.K., Dickey, D.M.: Natriuretic peptides: their structures, receptors, physiologic functions and therapeutic applications. Handb. Exp. Pharmacol.: 341-366, 2009.

Rodriguez, C.I., Buchholz, F., Galloway, J., Sequerra, R., Kasper, J., Ayala, R., Stewart, A.F., Dymecki, S.M.: High-efficiency deleter mice show that FLPe is an alternative to Cre-loxP. Nat. Genet., 25: 139-140, 2000.

Rotolo, T., Smallwood, P.M., Williams, J., Nathans, J.: Genetically-directed, cell type-specific sparse labeling for the analysis of neuronal morphology. PLoS. One., 3: e4099, 2008.

Ruthazer, E.S., Akerman, C.J., Cline, H.T.: Control of axon branch dynamics by correlated activity in vivo. Science, 301: 66-70, 2003.

Sadowski, P.D.: The Flp recombinase of the 2-microns plasmid of Saccharomyces cerevisiae. Prog. Nucleic Acid Res. Mol. Biol., 51: 53-91, 1995.

Sambrook J.: Molecular cloning: A Laboratory Manual. 2001.

Sauer, B., Henderson, N.: Site-specific DNA recombination in mammalian cells by the Cre recombinase of bacteriophage P1. Proc. Natl. Acad. Sci. U. S. A, 85: 5166-5170, 1988.

Schäffer, S.: Investigations about the function of the cGMP-dependent kinase I alpha during the development of the nervous system. 2006.

Schambra, U.B., Lauder, J.M., Silver, J.: Atlas of the prenatal mouse brain. 1992.

Schlosser, G.: Do vertebrate neural crest and cranial placodes have a common evolutionary origin? Bioessays, 30: 659-672, 2008.

Schmidt, H., Rathjen, F.G.: Signalling mechanisms regulating axonal branching in vivo. Bioessays, 32: 977-985, 2010.

Schmidt, H., Rathjen, F.G.: DiI-labeling of DRG neurons to study axonal branching in a whole mount preparation of mouse embryonic spinal cord. J. Vis. Exp., 2011.

Schmidt, H., Stonkute, A., Juttner, R., Koesling, D., Friebe, A., Rathjen, F.G.: C-type natriuretic peptide (CNP) is a bifurcation factor for sensory neurons. Proc. Natl. Acad. Sci. U. S. A, 106: 16847-16852, 2009.

Schmidt, H., Stonkute, A., Juttner, R., Schaffer, S., Buttgereit, J., Feil, R., Hofmann, F., Rathjen, F.G.: The receptor guanylyl cyclase Npr2 is essential for sensory axon bifurcation within the spinal cord. J. Cell Biol., 179: 331-340, 2007.

Schmidt, H., Werner, M., Heppenstall, P.A., Henning, M., More, M.I., Kuhbandner, S., Lewin, G.R., Hofmann, F., Feil, R., Rathjen, F.G.: cGMP-mediated signaling via cGKIalpha is required for the guidance and connectivity of sensory axons. J. Cell Biol., 159: 489-498, 2002.

Shigenaga, Y., Doe, K., Suemune, S., Mitsuhiro, Y., Tsuru, K., Otani, K., Shirana, Y., Hosoi, M., Yoshida, A., Kagawa, K.: Physiological and morphological characteristics of periodontal mesencephalic trigeminal neurons in the cat--intra-axonal staining with HRP. Brain Res., 505: 91-110, 1989.

Shigenaga, Y., Mitsuhiro, Y., Yoshida, A., Cao, C.Q., Tsuru, H.: Morphology of single mesencephalic trigeminal neurons innervating masseter muscle of the cat. Brain Res., 445: 392-399, 1988.

Sogawa, C., Abe, A., Tsuji, T., Koizumi, M., Saga, T., Kunieda, T.: Gastrointestinal tract disorder in natriuretic peptide receptor B gene mutant mice. Am. J. Pathol., 177: 822-828, 2010.

Sogawa, C., Tsuji, T., Shinkai, Y., Katayama, K., Kunieda, T.: Short-limbed dwarfism: slw is a new allele of Npr2 causing chondrodysplasia. J. Hered., 98: 575-580, 2007.

Stonkute, A.: cGMP signalling via CNP-NPR2-cGKI, and its role in axonal branching during embryonic development. 2010.

Suda, M., Ogawa, Y., Tanaka, K., Tamura, N., Yasoda, A., Takigawa, T., Uehira, M., Nishimoto, H., Itoh, H., Saito, Y., Shiota, K., Nakao, K.: Skeletal overgrowth in transgenic mice that overexpress brain natriuretic peptide. Proc. Natl. Acad. Sci. U. S. A, 95: 2337-2342, 1998.

Tamura, N., Doolittle, L.K., Hammer, R.E., Shelton, J.M., Richardson, J.A., Garbers, D.L.: Critical roles of the guanylyl cyclase B receptor in endochondral ossification and development of female reproductive organs. Proc. Natl. Acad. Sci. U. S. A, 101: 17300-17305, 2004.

Ter-Avetisyan, G., Tröster, P., Schmidt, H., Rathjen, F.G.: cGMP signaling and branching of sensory axons in the spinal cord. Future Neurology, 7: 639-651, 2012.

Tessier-Lavigne, M., Goodman, C.S.: The molecular biology of axon guidance. Science, 274: 1123-1133, 1996.

Tessier-Lavigne, M., Placzek, M., Lumsden, A.G., Dodd, J., Jessell, T.M.: Chemotropic guidance of developing axons in the mammalian central nervous system. Nature, 336: 775-778, 1988.

Torres, R.M., Kuhn, R.: Laboratory Protocols for Conditional Gene Targeting. 1997.

Tsuji, T., Kunieda, T.: A loss-of-function mutation in natriuretic peptide receptor 2 (Npr2) gene is responsible for disproportionate dwarfism in cn/cn mouse. J. Biol. Chem., 280: 14288-14292, 2005.

Tsuru, K., Otani, K., Kajiyama, K., Suemune, S., Shigenaga, Y.: Central terminations of periodontal mechanoreceptive and tooth pulp afferents in the trigeminal principal and oral nuclei of the cat. Brain Res., 485: 29-61, 1989.

Wang, K.H., Brose, K., Arnott, D., Kidd, T., Goodman, C.S., Henzel, W., Tessier-Lavigne, M.: Biochemical purification of a mammalian slit protein as a positive regulator of sensory axon elongation and branching. Cell, 96: 771-784, 1999.

Webb, J.F., Noden, D.M.: Ectodermal Placodes: Contributions to the Development of the Vertebrate Head. Integrative and Comparative Biology, 33: 434-447, 1993.

Wessels, A., Markwald, R.: Cardiac morphogenesis and dysmorphogenesis. I. Normal development. Methods Mol. Biol., 136: 239-259, 2000.

Windle, F.W.: Non-bifurcating nerve fibers of the trigeminal nerve. The Journal of Comparative Neurology, 1926.

Yasoda, A., Kitamura, H., Fujii, T., Kondo, E., Murao, N., Miura, M., Kanamoto, N., Komatsu, Y., Arai, H., Nakao, K.: Systemic administration of C-type natriuretic peptide as a novel therapeutic strategy for skeletal dysplasias. Endocrinology, 150: 3138-3144, 2009.

Yasoda, A., Komatsu, Y., Chusho, H., Miyazawa, T., Ozasa, A., Miura, M., Kurihara, T., Rogi, T., Tanaka, S., Suda, M., Tamura, N., Ogawa, Y., Nakao, K.: Overexpression of CNP in chondrocytes rescues achondroplasia through a MAPK-dependent pathway. Nat. Med., 10: 80-86, 2004.

Young, P., Qiu, L., Wang, D., Zhao, S., Gross, J., Feng, G.: Single-neuron labeling with inducible Cre-mediated knockout in transgenic mice. Nat. Neurosci., 11: 721-728, 2008.

Zervas, M., Millet, S., Ahn, S., Joyner, A.L.: Cell behaviors and genetic lineages of the mesencephalon and rhombomere 1. Neuron, 43: 345-357, 2004.

Zhang, M., Su, Y.Q., Sugiura, K., Wigglesworth, K., Xia, G., Eppig, J.J.: Estradiol promotes and maintains cumulus cell expression of natriuretic peptide receptor 2 (NPR2) and meiotic arrest in mouse oocytes in vitro. Endocrinology, 152: 4377-4385, 2011.

Zhang, M., Su, Y.Q., Sugiura, K., Xia, G., Eppig, J.J.: Granulosa cell ligand NPPC and its receptor NPR2 maintain meiotic arrest in mouse oocytes. Science, 330: 366-369, 2010.

Zhao, Z., Ma, L.: Regulation of axonal development by natriuretic peptide hormones. Proc. Natl. Acad. Sci. U. S. A, 106: 18016-18021, 2009.

Zhao, Z., Wang, Z., Gu, Y., Feil, R., Hofmann, F., Ma, L.: Regulate axon branching by the cyclic GMP pathway via inhibition of glycogen synthase kinase 3 in dorsal root ganglion sensory neurons. J. Neurosci., 29: 1350-1360, 2009.

Zhu, H., Luo, L.: Diverse functions of N-cadherin in dendritic and axonal terminal arborization of olfactory projection neurons. Neuron, 42: 63-75, 2004.

9. Curriculum Vitae

For privacy reasons the curriculum vitae is not included in the online version of this dissertation.

Publications:

- *cGMP signaling and branching of sensory axons in the spinal cord.*
  Gohar Ter-Avetisyan, Philip Tröster, Hannes Schmidt, Fritz G. Rathjen
  Future Neurology, Sept 2012; 7; 5: 639-651

- *Bifurcation of axons from cranial sensory ganglia is impaired in the absence of cGMP signalling involving the guanylyl cyclase receptor Npr2.*
  Gohar Ter-Avetisyan, Fritz G. Rathjen, Hannes Schmidt
  In preparation

- *A genetic strategy for the analysis of individual axon morphologies in cGMP signalling mutant mice.*
  Hannes Schmidt, **Gohar Ter-Avetisyan,** Fritz G. Rathjen
  Methods in Molecular Biology, 2013; 1020: 193-204

- *Cell entry of arginine-rich peptides is independent of endocytosis.*
  Gohar Ter-Avetisyan, Gisela Tünnemann, Danny Nowak, Matthias Nitschke, Andreas Herrmann, Marek Drab, M. Cristina Cardoso
  J. Biol. Chem., Feb 2009; 284: 3370 – 3378

- *Live-cell analysis of cell penetration ability and toxicity of oligo-arginines.*
  Gisela Tünnemann, **Gohar Ter-Avetisyan**, Robert M. Martin, Martin Stöckl, Andreas Herrmann, M. Cristina Cardoso
  J. Pept. Sci. 2008; 14: 469-476

- *Equine arteritis virus is delivered to an acidic compartment of host cells via clathrin-dependent endocytosis.*
  Matthias Nitschke, Thomas Korte, Claudia Tielesch, **Gohar Ter-Avetisyan**, Gisela Tünnemann, M. Cristina Cardoso, Michael Veit, Andreas Herrmann
  Virology 2008, 377, 248-254

Oral presentations:

- *A cGMP signaling pathway that triggers bifurcation of DRG axons is also an essential regulator for the arborization of central afferents from cranial sensory ganglia.*
  Gohar Ter-Avetisyan, Fritz G. Rathjen and Hannes Schmidt
  Axon Guidance, Synapse Formation and Regeneration
  Cold Spring Harbor Laboratory, *September 18-22, 2012, New York, USA*

- *A cGMP signaling pathway that triggers bifurcation of DRG axons is also an essential regulator for the arborization of central afferents from cranial sensory ganglia.*
  Gohar Ter-Avetisyan, Fritz G. Rathjen and Hannes Schmidt
  PhD retreat, *August 30–Septmeber 01, 2012, Brandenburg, Germany*

Posters:

- *Expression of the natriuretic peptide receptor 2 (Npr2) and its role in axonal branching.*
  Gohar Ter-Avetisyan, René Jüttner, Hannes Schmidt and Fritz G. Rathjen
  Developmental Disturbances in the Nervous System,
  SFB665 International Symposium, *October 27-29, 2011, Berlin, Germany*

- *Expression of the natriuretic peptide receptor 2 (Npr2) and its role in axonal branching.*
  Gohar Ter-Avetisyan, Agne Stonkute, Renè Jüttner, Hannes Schmidt and Fritz G. Rathjen
  Cell Biology of the Neuron: Polarity, Plasticity and Regeneration
  EMBO workshop, *May 07-10, 2011, Heraklion, Greece*

- *Genetic mouse models to analyze the function of natriuretic peptide receptor 2 in axonal branching and pathfinding.*
  Gohar Ter-Avetisyan, Hannes Schmidt and Fritz G. Rathjen
  PhD retreat, *September 09-11, 2010, Rheinsberg, Germany*

Honour:

- The 59th Nobel Laureates Meeting, June 28-03 July, 2009, Lindau, Germany

10. Appendix

10.1 Cloning plasmids

Some of the cloning plasmids used in this study were provided by Dr. Hagen Wende, AG Birchmeier-Kohler (Table 10.1). The amplified DNA fragments were cloned into the pBluescript II SK+ vector (denoted by pBlu[ ]), analyzed by restriction enzyme digestion and sequenced by MWG Operon. The oligonucleotides used for fragment amplification (primer pairs are denoted (f) for forward primer and (r) for reverse primer) and for sequencing (some standard primers were provided by MWG Operon) are listed in the appropriate tables. The primers were diluted to a final concentration of 50pmol/μl.

Table 10.1

Provided plasmids	Application
pBluescript II SK+	Backbone for amplified DNA fragments and mini-targeting vectors.
pDTA	Was provided with homology arms to recombine first the Npr2 gene locus, then the mini-targeting vector resulting in a final targeting vector.
pHW025	Contains the sequence [loxP-FRT-Neo-FRT-loxP] on the pBluescript backbone and was used to gain the final sequence of [FRT-Neo-FRT] in the plasmid pBlu[5'arm-FRT-Neo-FRT-3'arm].
pHW032	Contains the mini-λ plasmid; was used to amplify and make Maxi prep.
pBlu[Cre-Neo/Kan]	Was provided with 3'arms and ligated with the pBlu[5'arm-NLSLacZpolyA].
pBlu[Zero-Cre-polyA]	Amplification of the polyA-sequence to clone into the plasmid pBlu[5'arm-CreERT2-FRT-Neo-FRT-3'arm].
pBlu[CreERT2-w/o polyA]	Gaining of CreERT2-cassette to clone into the plasmid pBlu[5'arm-pHW025-3'arm].
pBlu[NLSLacZ-polyA]	Was provided with 5'arms and ligated with the pBlu[Cre-Neo/Kan-3'arm].

Table 10.2

Common plasmids for Npr2LacZ and Npr2CreERT2	Amplification primers
[5'probe]	(f) TCATTTAATTTTGCTGACTG (r) TTACTTGTTTAGAAACAGG
[3'probe]	(f) GTAAGCCAAGAAAGTGGGG (r) GCAGACAGAGAGAAGGCATAG
[gSC-armA]	(f)GGGCTCGAGGTCGTGTCTTTTTCATATTG (r) CGCGGATCCGCTGGAACACGAAAGAAGC
[gSC-armB]	(f)GCGGGATCCCCGAGAACCCCCAAATCCTG (r) CCCACTAGTGTCCCCACGCCTCCCCAC
[5'arm]	(f) GGGCTCGAGCGTTAGTCCAGGCAGGAGC (r) CCGCCATGGGGATAGAGCAGCTG
[3'arm]	(f) GCGGAATTTGTGTGGCCCGGGCTGTTTTAG (r) CCCGCGGCCGCTGTCCTCAAAAGTTCCTCC

Table 10.3

Common plasmids for Npr2LacZ and Npr2CreERT2	Description	Sequencing primers
pBlu[5'probe]	A unique sequence amplified from the BAC DNA and used for the recognition of the targeted DNA mutation at the 5'end by radiolabeling.	T7
pBlu[3'probe]	A unique sequence amplified from the BAC DNA and used for the recognition of the targeted DNA mutation at the 3'end by radiolabeling,	T7, M13Rev(-29)
pBlu[gSC-armA]	A 5'end homology arm sequence amplified from the BAC DNA to recombine the Npr2 gene locus.	T3
pBlu[gSC-armB]	A 3'end homology arm sequence amplified from the BAC DNA to recombine the Npr2 gene locus	T3
pDTA[gSC-armA-armB]	Plasmid with homology arms used for the recombination of the Npr2 gene locus between exon1 and exon3 by min-λ-recombination system.	T3
pBlu[5'arm]	A 5'end homology arm sequence amplified from the BAC DNA for the recombination of the mutated Npr2 gene locus into the ES cells.	T7, M13Uni(-21)
pBlu[3'arm]	A 3'end homology arm sequence amplified from the BAC DNA for the recombination of the mutated Npr2 gene locus into the ES cells.	T7

Table 10.4

Plasmids for the targeting vector of Npr2LacZ	Description	Sequencing primers
pBlu[5'arm-NLSLacZpolyA]	Plasmid after cloning the 5'arm into the plasmid pBlu[NLSLacZ-polyA].	M13Uni(-43)
pBlu[Cre-Neo/Kan-3'arm]	Plasmid after cloning the 3'arm into the plasmid pBlu[Cre-Neo/Kan].	M13Rev(-49)
pBlu[5'arm-NLSLacZpolyA-Cre-Neo/Kan-3'arm]	The mini-targeting vector after ligating the pBlu[5'arm-NLSLacZ-polyA] and pBlu[Cre-Neo/Kan-3'arm]; was recombined into the Npr2 gene locus by the mini-λ-recombination system.	M13Rev(-49)
Npr2NLSLacZ	The targeting vector with the mutated Npr2 locus; for the recombination into ES cells	See Fig. A.3

| primer	sequence	sequenced region
P1 (T7)	TAATACGACTCACTATAGGG	680 - 1510
P2	GCTTCTTTCGTGTTCCAGC	1310 - 2055
P3	GTCGTGTCTTTTTCATATTG	1820 - 2560
P4	CATAGCTGTTCCCTTTGCA	3370 - 3930
P5	TTCCTGGCCCTCTTCCCCAG	3930 - 4800
P6	ATGGCTCCAAAAAAGAAGAG	4040 - 5110
P7	GGAAATTGCATCGCATTGTC	7270 - 8190
P8	GGGGAGGATTGGGAAGACAAT	7350 - 8360
P9	TTCGCAAGAACCTGATGGA	8240 - 9160
P10	CTCTGGTGTAGCTGATGA	8840 - 9850
P11	GGAGGAACTTTTGAGGACA	10360 - 11440
P12	GTGTGGCCCGGGCTGTTTTAG	11380 - 12150
P13	GGGCTCGAGCGTTAGTCCAGGC	14260 - 15120
P14	GTGGGGAGGCGTGGGGAC	18480 - 18890
P15	CCGAGAACCCCCAAATCCTG	18680 - 19600

Figure10.1: Illustration of the sequenced targeting vector Npr2NLSLacZ and binding sites of the primers P1 to P15 (regions that were not sequenced are marked red). The sequences of the primers and the sequenced regions of the targeting vector are listed in the right table.

Table 10.5

Plasmids for the targeting vector of Npr2CreERT2	Description	Sequencing primers
pBlu[NotI-pHW025]	An inserted NotI restriction site into the pHW025;	T7
pBlu[5'arm-pHW025]	Plasmid after cloning the 5'arm into the pHW025.	M13Uni(-43)
pBlu[5'arm-pHW025-3'arm]	Plasmid after cloning the 3'arm into the pBlu[5'arm-pHW025]	M13Rev(-49)
pBlu[5'arm-CreERT2-FRT-Neo-FRT-3'arm]	The CreERT2-cassette is cloned into the pBlu[5'arm-pHW025-3'arm]	T7, AAGTTCGGGTGAAGGCCCAG, TTCCTGGCCCTCTTCCCCAG
pBlu[polyA] (Sauer and Henderson 1988)	The polyA-sequence amplified from the pHW032 to insert after the CreERT2-cassette.	M13Uni(-43)
pBlu[5'arm-CreERT2-polyA-FRT-Neo-FRT-3'arm]	The mini-targeting vector after cloning the polyA- sequence into the pBlu[5'arm-CreERT2-FRT-Neo-FRT-3'arm]; recombined into the Npr2 gene locus by the mini-λ-recombination system.	AAGTTCGGGTGAAGGCCCAG
pDTA[gNpr2-CreERT2]	The targeting vector with the mutated Npr2 locus; for the recombination into ES cells.	See Fig.A.4

Table 10.6

Plasmids for the targeting vector of Npr2CreERT2	Amplification primers
pBlu[NotI-pHW025]	AGCGGCCGCTTGCA
pBlu[polyA]	(f) GCGGGGCCCTGTGCCTTCTAGTTGCCAGC (r) CCCGCGGCCGCGGCCCTCTAGATGCATGCTC

| primer	sequence	sequenced region
P1 (T7)	TAATACGACTCACTATAGGG	680 - 1510
P2	ATGGAATCTACATAACCAG	1440 - 2400
P3	CTTTTTGCTTCCTCTTGCA	1710 - 2440
P4	CATAGCTGTTCCCTTTGCA	2400 - 3140
P5	CCGTGGGTCAGCTGCTCTAT	2970 - 3940
P6	GGCAGCGGCGGGCAGCGC	3320 - 4340
P7	CTCTGGTGTAGCTGATGA	4720 - 5480
P8	AGCTGGTTCACATGATCA	5280 - 6140
P9	ACGCCCACCGCCTACATG	5860 - 6700
P10	CAGCTTGATGAAGATCTGA	6010 - 6870
P11	GGAGGAACTTTTGAGGACA	7310 - 8290
P12	AGCTGGTTCACATGATCA	8230 - 9250
P13	AGGAAGGGAAAGACCTGA	9370 - 10430
P14	GAAACAACCAGCTCACCTG	10650 - 11650
P15	TACAGTGGATCGTCTTAG	11930 - 12930
P16	TGAACACTTTCTAGACACT	13300 - 13500
P17	AACAGAGACATGTTGATTC	13470 - 14490
P18	TTTCCTATGGTGGTCCTT	14520 - 15380
P19 (T3)	CCCTTTAGTGAGGGTTAATT	15190 - 15830

Figure 10.2: Illustration of the sequenced targeting vector pDTA[gNpr2-CreERT2] and binding sites of the primers P1 to P19 (the regions that were not sequenced are marked red). The sequences of the primers and the sequenced regions of the targeting vector are listed in the right table.

10.2 Antibodies used for Western blots of DRG

Table 10.7

Name	Used dilution	Company
CDK5	1:1000	Cell Signaling
CLIP170	1:1000	Sigma-Aldrich
GAP-43	1:1000	Chemicon
KIF2A	1:1000	LifeSpan Biosciences
goat anti-Lis1	1:100	Santa Cruz
Nudel	1:2000	Abcam
Nde1	1:2000	Proteintech Europe
OP-18/Stathmin	1:1000	Sigma-Aldrich
Phospho-PKC (pan) (βII Ser660)	1:1000	Cell Signaling
Phospho-PKCα/β II (Thr638/641)	1:1000	Cell Signaling
Phospho-PKCδ (Thr505)	1:1000	Cell Signaling
Phospho-PKD/PKCμ (Ser916)	1:1000	Cell Signaling
Phospho-PKD/PKCμ (Ser744/748)	1:1000	Cell Signaling
Phospho-PKCδ/θ (Ser643/676)	1:1000	Cell Signaling
PKD/PKCμ	1:1000	Cell Signaling
Phospho-PKCθ (Thr538)	1:1000	Cell Signaling
Phospho-PKCζ/λ (Thr410/403)	1:1000	Cell Signaling
Phospho-Akt (Thr308)	1:1000	Cell Signaling
Phospho-Akt (Ser473)	1:1000	Cell Signaling
Phospho-(Ser/Thr) Akt Substrate	1:1000	Cell Signaling
Phospho-PTEN (Ser380)	1:1000	Cell Signaling
Phospho-PDK1 (Ser241)	1:1000	Cell Signaling
Phospho-c-Raf (Ser259)	1:1000	Cell Signaling
Phospho-c-Raf (Ser338) (56A6)	1:1000	Cell Signaling
Phospho-MEK1/2 (Ser217/221)	1:1000	Cell Signaling
Phospho-p44/42 MAPK (Erk1/2) (Thr202/Tyr204)	1:1000	Cell Signaling
Phospho-p90RSK (Ser380)	1:1000	Cell Signaling
Phospho-Elk-1 (Ser383)	1:1000	Cell Signaling
Phospho-p44/42 MAPK (Erk1/2) (Thr202/Tyr204)	1:1000	Cell Signaling
Phospho-44/42 MAPK (Erk1/2)	1:1000	Cell Signaling
SAPK/JNK (56G8)	1:1000	Cell Signaling
Phospho-38 MAPK	1:1000	Cell Signaling
Phospho-BAD	1:1000	Cell Signaling
Phospho-35/25	1:1000	Cell Signaling
Phospho-Stathmin	1:1000	Cell Signaling
Phospho-RhoA	1:1000	Calbiochem
RKVpS	1:2000	GenScript
Stathmin	1:1000	Cell Signaling
Tau	5μg/ml	Millipore
mAB 4G10 Phosphotyrosin	1:1000	Millipore
chicken anti-β-Galactosidase	1:1000	Jackson ImmunoResearch
mouse-anti-γ-Tubulin	1:25.000	Sigam-Aldrich
mouse anti-Mena	1:10	F.B. Gertler
guinapig-anti-Npr2	1:1000	AG Rathjen
14-3-3-E	1:2000	Epitomics
14-3-3 pan	1:2000	Santa Cruz
VASP	1:1000	Abcam